POLITECNICO DI MILANO
Corso di Laurea Triennale in Ingegneria Biomedica
Dipartimento di Elettronica, Informazione e Bioingegneria

Atrial Fibrillation detection in PPG signal recorded through a wristband device

Relatore: Prof. Luca Mainardi

Tesi di Laurea di:
Lorenzo Ferranti, matricola 814878
Rita Laureanti, matricola 816759

Anno Accademico 2014-2015

Summary

A Introduction

Atrial fibrillation (AF) is a very common heart arrhythmia: this condition causes a pathological atrial function, with a rapid, uncoordinated heart rate. AF can lead to many collateral effects, such as fatigue, dizziness and chest pain and increase the risk of myocardial infarction [32], heart failure [6] and stroke [39]. Furthermore, if untreated, the arrhythmia roots its mechanism into the subject's heart, becoming increasingly persistent [38], therefore an early diagnosis is fundamental to counteract its impact.

One of the main problems with AF identification is that this arrhythmia can be paroxysmal, meaning it can occur episodically and terminate spontaneously; in such cases it is very hard to identify the pathology, because clinical analyses carried out in a normal sinus rhythm (NSR) period don't show the presence of AF [22]. Furthermore, there are many undiagnosed subjects who present asymptomatic AF, often diagnosed by chance during electrocardiograph control for other clinical reasons; these subjects show a possibly large under-representation of the effective prevalence of AF. Undiagnosed AF patients are an important bulk of patients with high risk of cardioembolic stroke or other complications associated with AF that could lead to a potential loss of lives and higher costs related to health care resources utilization.

A screening of the general population would answer the issue of the paroxysmal and asymptomatic nature of AF. A monitoring device able to oversee the patient's condition such as a wristband for blood volume pulse (BVP) recording could be useful and answer the developing trust in m-Health. Therefore there is a pressing need to develop methods for accurate AF detection and monitoring in order to improve patient care and reduce healthcare costs associated with complications from AF. Such method would have important clinical and research applications for AF screening as well as in assessing treatment response.

The aim of this thesis is the development of a decision-making system trained on AF detection in the BVP signal, acquired through non-invasive instrumentation.

B Methods

The starting point of this work was to recover biosignals through the Empatica E4 wristband [40]. For all subjects, we acquired 10 minutes long BVP signals, measured while the patient laid relaxed in a steady state. This kind of acquisition, recorded by a photoplethysmographic system, answers the non-invasivity requirement for a screening device used 24/7 in a non hospital contest and exploits the spreading of smart devices able to embed such systems.

B.1 Study population

We recorded the BVP signals of subjects of known health state to extract features able to discriminate between three target classes: AF patients, NSR subjects and patients suffering from other arrhythmias.

We acquired a total of 70 BVP signals from distinct subjects, recruited among hospitalized patients at Ospedale Maggiore Policlinico in Milan, Italy; after the acquisition, every subject was classified into one of the three target classes by expert cardiologists: 30 of the recorded patients were affected by atrial fibrillation, 31 were healthy subjects and 9 suffered from other arrhythmias. As for the gender of the subjects, 36 recorded patients were male and 34 were female; the age of recorded patients ranged from 21 to 93 years.

B.2 BVP preprocessing

The signal was preprocessed to remove noise distortions and to highlight important features. In order to cancel noise interference, which is mainly caused by movement artifacts, accelerometric data collected by the Empatica E4 wristband were analyzed, synchronously with the BVP signal acquisition; it was decided that, when the accelerometers recorded a differential acceleration higher that an empirically set threshold, that is $0.07g$, the signal interval was labeled as noisy and not considered for successive analysis.

In a following phase, the signal was searched in order to automatically identify characteristic features, such as diastolic minima and systolic max-

ima, which represent significant point in time of the cardiac cycle; by studying the timing and the values at those instants, it was possible to obtain a surrogate of the pulse pressure of each beat and to calculate the inter-systolic and inter-diastolic intervals, thus deriving the heart rate; all such parameters were later used to study the regularity of the sequence of the heart cycles.

B.3 Diagnostic indexes

We computed 16 diagnostic indexes out of the preprocessed BVP signal, in order to be used by a decision making system to classify the patient's health status.

B.3.1 Spectral analysis

Two indexes represented the spectral behavior of both the BVP signal and the inter-diastolic intervals.

The first index, called peak density (PD), expressed the concentration of the BVP power spectrum and was calculated as the integral of the BVP power spectral density (PSD) in a 12 mHz region around the heart rate, divided by the integral of the PSD between 0 Hz and the sampling frequency; the PD was higher for healthy subjects and lowest for AF patients, because their BVP was more chaotic and therefore bore a wider power spectrum, less concentrated around the main heart rate.

The power spectral density of the inter-diastolic intervals (PSDsum) provided an evaluation of the variance of the series, distributed along the frequency spectrum. After calculating the PSD of the intervals sequence, the integral sum of it (i.e. the total power) was computed; this quantity was bigger for arrhythmic subjects, in particular AF patients, and lesser for NSR subjects.

B.3.2 Time domain indexes

Six diagnostic indexes were used to assess heart rate variability during the 10 minutes of the acquisition, because the presence of arrhythmia is correlated to a more chaotic organization of the heart rhythm.

All time domain indexes were calculated on the series of inter-diastolic intervals: we computed the standard deviation (SD), the root mean square of successive differences (RMSSD), the normalized RMSSD (nRMSSD) and the coefficient of variation (CV) of the intervals; we also evaluated the percentage of successive interval differences greater than 50 ms (pNN50).

Finally we computed the AF evidence index. This diagnostic index was originally proposed by Sarkar et al. [30] and exploits the Lorenz plot distribution of subsequent interval deltas to assess the presence of AF. The version we employed was slightly different from the original, mainly because we needed to adapt this index, originally conceived for ECG analysis, to the BVP signal; the working principle, however, is the same; this index assumed higher values for AF patients and low, generally negative values for NSR subjects, while subjects with other arrhythmias had values in between.

B.3.3 Nonlinear indexes

In the category of nonlinear indexes we included the sample entropy and normalized Shannon entropy.

Sample entropy (SampEn) [29] is a modified version of approximate entropy. Our analysis evaluated the sample entropy of the intervals, as an index of the complexity of their distribution. The values of this index were lowest for the other arrhythmia class and higher for the AF and NSR classes.

Shannon entropy (ShEn) [24] characterizes the uncertainty of a statistical distribution and increases proportionally to the presence of randomness sources, therefore it is a good indicator of the chaotic nature of the statistical distribution of the intervals. The Shannon entropy index was normalized (nShEn) by dividing it by the logarithm of the number of intervals detected; this was performed since Shannon entropy tends to increase with the dimension of the the dataset of variables. As can be expected, values were lowest for healthy subjects and higher for all the classes of arrhythmic patients.

B.3.4 Shape analysis

Other than the indexes focused on the variability of time intervals, we also evaluated a category of indexes based on the morphology of the BVP: the normalized wave deviation, the detection of multi-peak waves and two-peak waves and the shape similarity index.

The wave deviation (WD) was calculated as the median absolute deviation of the excursions between the values of the systolic peak and of the diastolic minimum. Since the overall signal amplitude can change during different acquisition, even for the same subject, we provided a normalized index of wave excursion (nWD), obtained as the WD divided by the median excursion of the signal. The normalized wave deviation assumed slightly higher values for arrhythmic subjects in comparison with NSR subjects.

The multi-peak waves and two-peak waves represented two peculiar wave shapes which were noticed during the analysis of the BVP of AF subjects

(Figure 1); since their manifestation was observed more frequently for this class of patients, it was decided to implement an algorithm for their detection, which allowed us to quantify the percentage of such waves on the total number of waves. This percentage constituted the final index of multi-peak waves (MPW) and two-peak waves (TPW). It was observed that both MPW and TPW percentages were higher in AF subjects and in subjects affected by other arrhythmias with respect to NSR subjects.

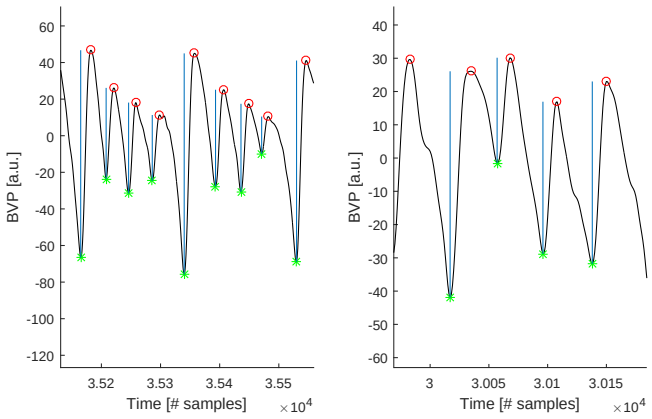

Figure 1: ***Multi-peak wave and two-peak wave shapes.*** *The shape of a typical multi-peak wave (left) and of a two-peak wave (right).*

The last shape analysis index was the *shape similarity* [14]; this index measured the similitude of all the BVP waves by comparing them with one another; the similarity was expected to be higher for subjects with normal sinus rhythm, since their cardiac output is physiologically more regular. The *shape similarity* calculation was obtained by performing the dot product between the arrays of the t values composing each wave in the acquisition. The dot product between t-dimensional vectors is proportional to the moduli of the vectors and to the cosine of the angle between them; in this calculation each wave vector was normalized by dividing it by its norm, therefore this calculation provided higher values for similar wave shapes, thus quantifying their respective resemblance. The final *shape similarity* was obtained as the percentage of waves in the acquisition which were more similar than an empirical threshold, which was established to maximize index differences between target classes. The values obtained for this index were, as expected, higher for NSR subjects, lower for subjects affected by other arrhythmias and lowest for AF patients. To obtain a more comprehensive examination from this analysis, two more indexes were computed: the median (*MedianArc*)

and the mode (*ModeArc*) of the angle of the dot product, calculated for all waves. This values were instead higher for patients suffering from AF and lower for subjects with normal sinus rhythm.

B.4 Analysis

We performed a preliminary univariate analysis by observing the values assumed by each index in the three different target classes: in every case an overlap was present, precluding the possibility of using only one index to accurately separate the subjects.

We then decided to carry out a multivariate analysis by training a support vector machine (SVM) and evaluating its performance through a *leave one out* cross-validation method. To decrease the dataset dimension, a reduction in the number of indexes was performed, simplifying the analysis and potentially improving the final separation accuracy. Two different methods were used: principal components analysis (PCA) and wrapper method.

C Results

C.1 PCA

The PCA was performed on the full dataset of subjects and indexes. The performance of the classifier was evaluated for different numbers of principal components, from 1 to 16. In Table 1 the classification accuracy obtained for different numbers of principal components taken into account is displayed, together with the relative percentage of explained variance. The best accuracy was 90% and occurred when the first 12 principal components were considered, for an explained variance of 99.91%.

# PCs	1	2	3	4	5	6	7	8
Acc [%]	50	48.57	75.71	84.29	87.14	82.86	81.43	81.43
I_q[%]	50.61	76.36	82.71	87.72	91.37	94.52	96.72	98.21
# PCs	9	10	11	12	13	14	15	16
Acc [%]	85.71	87.14	85.71	90	84.29	85.71	82.86	81.43
I_q[%]	98.80	99.34	99.71	99.91	99.98	99.99	100	100

Table 1: ***Classification accuracy for number of principal components included.*** *The classification accuracy obtained through a* leave one out *procedure is displayed for an increasing number of principal components considered and their relative percentage of explained variance.*

C.2 Wrapper method

A selection of the most relevant indexes was performed through the wrapper method. We tested all the possible sets of indexes, thus, for 16 indexes, $2^{16} - 1$ combinations.

The distribution of SVM classification performance for all the combinations of indexes is shown in Figure 2.

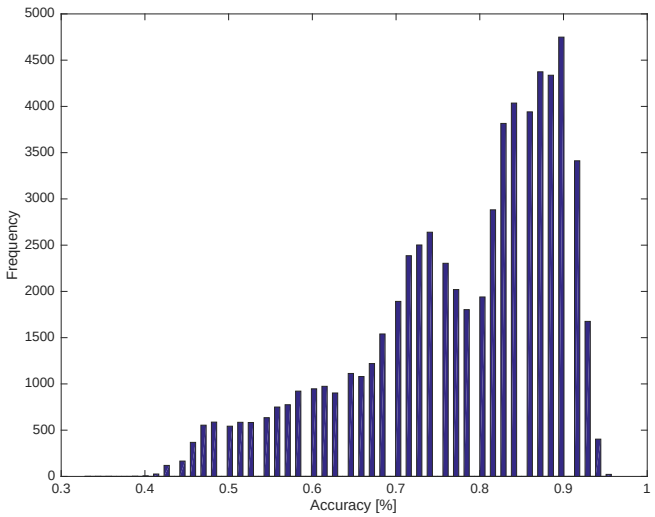

Figure 2: ***Distribution of SVM classification accuracy.*** *The hystogram displays the classification accuracies obtained using different combinations of indexes.*

As can be seen, the results of the SVM could vary greatly depending on

the indexes it was trained on, going from a minimum accuracy of 32.86% of one case to the maximum of 95.71% obtained by 22 combinations; as for the statistical distribution of the accuracy, the median was equal to 81.43%, with a mean of 77.65% and a mode of 90%. Out of the 22 combinations providing the best accuracy, we selected 16 cases that also provided the best value of sensitivity to the AF class, 96.67%.

The sets of indexes that achieved the best performance are reported in Table 2.

																% Ind
SD	1	1	1				1	1	1			1		1		1	56.25
RMSSD		1				1	1	1			1	1	1	1	1	1	62.5
nRMMSD	1	1		1		1	1	1			1	1	1	1	1	1	75
pNN50	1	1	1	1	1	1	1	1	1	1	1	1	1	1	1	1	100
CV					1	1	1			1			1	1	1	1	50
SampEn	1	1	1	1	1	1	1	1	1	1	1	1	1	1	1	1	100
nShEn	1	1	1	1	1	1	1	1	1	1	1	1	1	1	1	1	100
ShapeSim	1																6.25
MedianArc		1				1	1	1			1	1	1	1	1	1	62.5
ModeArc			1	1	1				1	1							31.25
AF evidence	1	1	1	1	1	1	1	1	1	1	1	1	1	1	1	1	100
PD																	0
nWD											1	1	1	1			25
MPW						1	1								1	1	25
TPW																	0
PSDsum								1	1	1	1	1	1	1	1	1	56.25
Tot Ind	7	8	6	6	6	9	10	9	7	7	9	10	10	11	10	11	

Table 2: ***Sets of indexes with best classification accuracy and sensitivity.*** *This table shows the best 16 combinations of indexes (columns). For each combination, the indexes (rows) taken into account are marked with 1 in the correspondent box. At the end of each column the number of indexes considered for each combination is specified. At the end of each row the frequency of appearance for each index in all the 16 combinations is indicated.*

These 16 combinations used from 6 to 11 different indexes simultaneously. Four indexes appeared in all the 16 combinations: the percentage of differences of successive intervals greater than 50 ms (pNN50), the sample entropy (SampEn), the normalized Shannon entropy (nShEn) and the AF evidence, constituting an essential set of indexes for a good classification performance. Aside from these always present indexes, every combination

featured a morphology based parameter and another index of heart variability in the time domain.

For each combination, we analyzed the confusion matrix obtained at the end of the *leave one out* method. The columns of the matrix indicate the true health status of every subject, while the rows indicate the category in which the patient is classified by the SVM; therefore, the diagonal elements represent correct classifications. For the 16 best combinations, two typologies of confusion matrix were obtained multiple times, displayed in Table 3 and Table 4.

	NSR	Other	AF
NSR	31	1	0
Other	0	7	1
AF	0	1	29

Table 3: ***Confusion matrix A.*** *Confusion matrix obtained in 10 of the 16 best combinations of indexes. NSR=normal sinus rhythm, AF=atrial fibrillation and "other" stands for other typologies of arrhythmia. The columns of the matrix indicate the true health status of every subject, while the rows indicate the category in which the patient is classified by the SVM.*

	NSR	Other	AF
NSR	30	1	0
Other	1	8	1
AF	0	0	29

Table 4: ***Confusion matrix B.*** *Confusion matrix obtained in 6 of the 16 best combinations of indexes. NSR=normal sinus rhythm, AF=atrial fibrillation and "other" stands for other typologies of arrhythmia. The columns of the matrix indicate the true health status of every subject, while the rows indicate the category in which the patient is classified by the SVM.*

In all the matrices the sensitivity, that is the ratio between the number of AF identified by the SVM and the total number of AF subjects, was 96.67%, while the specificity to NSR class was 100% in ten cases and 96.77% in the other combinations; specificity to "other arrhythmia" class was 77.78% in ten cases and 88.89% for the remaining six combinations.

Sommario

A Introduzione

La fibrillazione atriale (*atrial fibrillation*, AF) è un'aritmia cardiaca piuttosto diffusa: questa condizione causa un'attività atriale patologica, caratterizzata da una frequenza cardiaca elevata e caotica. La AF può causare molti effetti collaterali come affaticamento, vertigini e dolori al petto, ed aumenta il rischio di infarto cardiaco [32], arresto cardiaco [6] e ictus [39]. Inoltre, se non trattata, l'aritmia consolida il proprio meccanismo nel cuore del soggetto, diventando progressivamente persistente [38], dunque una diagnosi tempestiva è fondamentale per fermarne l'avanzamento.

Uno dei motivi per i quali è complicato diagnosticare la AF è che questa aritmia può essere parossistica, ossia può manifestarsi occasionalmente e terminare spontaneamente; in queste condizioni essa diviene molto difficile da identificare poiché, se durante le analisi cliniche il soggetto è in un periodo di ritmo sinusale (*normal sinus rhythm*, NSR), le tecniche diagnostiche non sono in grado di rilevare in alcun modo la presenza della AF. Inoltre, ci sono alcuni soggetti in cui la malattia si presenta in forma asintomatica, che sfuggono alla diagnosi e che sono spesso individuati solo per caso durante controlli cardiaci per altri problemi; ciò mostra una possibile sottostima della prevalenza effettiva della AF. Pazienti non diagnosticati presentano, inoltre, un alto rischio di cardioembolia o di altre complicanze associate alla fibrillazione atriale che possono comportare perdite di vite e costi elevati per la sanità.

Uno screening della popolazione risponderebbe al problema della natura a volte parossistica o asintomatica della AF. Un dispositivo di monitoraggio capace di supervisionare la condizione del paziente, come un braccialetto per la registrazione del *blood volume pulse* (BVP), può essere utile in questo contesto e risponderebbe alla fiducia crescente verso la "mobile health" (m-Health). C'è quindi una notevole richiesta di sviluppare metodi per un accurato riconoscimento di episodi di AF e per il monitoraggio cardiaco,

nel tentativo di migliorare la cura dei pazienti e ridurre i costi della sanità associate alle complicanze dovute ad AF. Tali metodi avrebbero importanti applicazioni cliniche e di ricerca, favorendo sia lo screening che la valutazione della risposta clinica al trattamento.

L'obiettivo di questa tesi è lo sviluppo di un sistema di decision-making addestrato per il riconoscimento di AF in segnali BVP acquisiti tramite dispositivi non invasivi.

B Metodi

Il punto iniziale di questa tesi è stato il recupero di biosegnali attraverso il braccialetto Empatica E4. Per tutti i soggetti abbiamo acquisito segnali BVP di 10 minuti registrati con il paziente supino e rilassato. Questo tipo di segnale, registrato da un sistema fotoplestismografico, risponde all'esigenza di non invasività richiesta da un dispositivo di screening usato 24/7 in un contesto non ospedaliero e sfrutta la crescente diffusione di dispositivi smart capaci di integrare tali sistemi.

B.1 Popolazione in studio

Abbiamo registrato i segnali BVP di soggetti dallo stato di salute noto per estrarne le caratteristiche in grado di discriminare fra tre classi target: pazienti con AF, soggetti NSR e pazienti con altre aritmie.

Abbiamo acquisito 70 segnali BVP da soggetti distinti, reclutati tra i pazienti ricoverati all'Ospedale Maggiore Policlinico di Milano, Italia; dopo l'acquisizione, ogni soggetto è stato assegnato ad una classe target da un cardiologo esperto: 30 dei soggetti erano affetti da AF, 31 erano sani e 9 soffrivano di altre aritmie. Per quanto riguarda il sesso dei pazienti, 36 erano maschi e 34 femmine; l'età variava dai 21 ai 93 anni.

B.2 Preprocessing del segnale BVP

Abbiamo fatto un preprocessing del segnale per rimuovere il rumore ed evidenziare importanti caratteristiche. Per eliminare il rumore, principalmente causato da artefatti di movimento, abbiamo analizzato i dati accelerometrici acquisiti dal braccialetto Empatica E4 in modo sincrono al BVP; è stato deciso che, quando l'accelerometro registrava un'accelerazione differenziale maggiore di una certa soglia, fissata a $0.07g$, il segmento di segnale era etichettato come rumoroso e non veniva considerato nelle successive analisi.

Successivamente, si è implementata una ricerca automatica sul segnale per identificarne alcune caratteristiche, come i minimi diastolici e i massimi

sistolici, che rappresentano punti significativi del ciclo cardiaco; studiando la tempistica e i valori assunti dal segnale in questi istanti, è stato possibile ottenere un surrogato della pressione pulsatile di ogni battito e calcolare gli intervalli inter-sistolici e inter-diastolici, derivando la frequenza cardiaca; tutti questi parametri sono stati in seguito usati per studiare la regolarità della sequenza dei cicli cardiaci.

B.3 Indici diagnostici

Abbiamo calcolato 16 indici diagnostici sul segnale BVP ottenuto dopo la fase di preprocessing, su cui basare un sistema di decision-making in grado di classificare lo stato di salute del paziente.

B.3.1 Analisi spettrale

Due indici sono stati usati per esprimere il comportamento spettrale del segnale BVP e degli intervalli inter-diastolici.

Il primo indice, chiamato peak density (PD), rappresentante la concentrazione dello spettro di potenza del BVP, è stato calcolato come l'integrale della power spectral density (PSD) in una regione di 12 mHz intorno alla frequenza cardiaca, diviso per l'integrale della PSD tra 0 Hz e la frequenza di campionamento; PD è risultato più elevato per soggetti sani ed inferiore per pazienti AF, perché il loro BVP è più caotico e quindi presenta uno spettro di potenza più largo, meno concentrato intorno al picco principale di frequenza cardiaca.

La PSD degli intervalli inter-diastolici (PSDsum) è servita per stimare la varianza della serie, distribuita sulle frequenze dello spettro. Dopo il calcolo della PSD della serie di intervalli, la sua somma integrale (ossia la potenza totale) è stata calcolata; questo indice ha presentato valori maggiori per i soggetti aritmici, in particolare per i pazienti AF, e minori per i soggetti NSR.

B.3.2 Indici nel dominio del tempo

Sei indici diagnostici sono stati usati per valutare la variabilità cardiaca durante i 10 minuti di registrazione, in quanto la presenza di aritmia comporta un'organizzazione più caotica del ritmo cardiaco.

Tutti gli indici nel dominio del tempo sono stati calcolati sulla serie di intervalli inter-diastolici: abbiamo calcolato la deviazione standard (SD), la radice quadrata della media delle differenze al quadrato di intervalli successivi (RMSSD), la RMSSD normalizzata (nRMSSD) e il coefficiente di

variazione (CV) degli intervalli; abbiamo anche valutato la percentuale di differenze di intervalli successivi maggiori di 50 ms, (pNN50).

Infine abbiamo calcolato l'indice AF evidence. Questo indice diagnostico è stato originariamente proposto da Sarkar et al. [30] e sfrutta la distribuzione dei delta tra intervalli successivi sul diagramma di Lorenz per valutare la presenza di AF. La versione da noi implementata è leggermente diversa dall'originale, soprattutto perché abbiamo avuto bisogno di adattare quest'indice, originariamente pensato per l'analisi dell'ECG, all'analisi del BVP; il principio operativo, comunque, è lo stesso; questo indice ha assunto valori più elevati per i pazienti AF ed inferiori, generalmente negativi, per i soggetti NSR, mentre i soggetti con altre aritmie presentavano valori intermedi.

B.3.3 Indici non lineari

Nella categoria degli indici non lineari abbiamo incluso la sample entropy e la Shannon entropy normalizzata.

La sample entropy (SampEn) [29] è una versione modificata della approximate entropy. La nostra analisi ha stimato la sample entropy degli intervalli come un indice della casualità della loro distribuzione. I valori di questo indice erano molto bassi per la classe di altre aritmie e più alti per le classi AF e NSR.

La Shannon entropy (ShEn) [24] esprime l'incertezza di una distribuzione statistica ed è un buon indicatore della natura caotica della serie temporale di intervalli. L'indice della Shannon entropy è stato normalizzato (nShEn) dividendolo per il logaritmo del numero di intervalli rilevati; questa operazione è stata svolta perché la Shannon entropy tende ad aumentare proporzionalmente alle dimensioni del dataset di variabili. Come atteso, i valori minimi di questo indice sono stati ottenuti per i pazienti sani mentre valori maggiori appartengono alla classe dei pazienti aritmici.

B.3.4 Analisi morfologica

Oltre agli indici della variabilità degli intervalli temporali, abbiamo anche calcolato un'altra categoria di indici basati sulla morfologia del segnale BVP: la wave deviation normalizzata, le percentuali di multi-peak waves e di two-peak waves e la shape similarity.

La wave deviation (WD) è stata calcolata come la deviazione mediana assoluta dell'escursione del BVP tra il picco sistolico ed il minimo diastolico. Dal momento che l'ampiezza globale del segnale può cambiare durante acquisizioni differenti, anche per lo stesso soggetto, abbiamo generato un

indice dell'escursione di ogni onda (nWD) calcolato come la WD divisa per l'escursione mediana del segnale. La wave deviation così normalizzata assume valori leggermente maggiori per i soggetti aritmici in confronto con i soggetti NSR.

Le multi-peak waves e le two-peak waves rappresentano due peculiari forme d'onda che sono state osservate durante l'analisi del BVP di soggetti AF (Figura 3); dal momento che la loro apparizione è stata osservata più frequentemente per questa classe di soggetti, è stato deciso di implementare un algoritmo per la loro identificazione, che ci ha permesso di quantificare la percentuale di tali onde sul numero totale di cicli cardiaci dell'acquisizione. Questa percentuale ha costituito l'indice finale delle multi-peak waves (MPW) e delle two-peak waves (TPW). Si è osservato che sia le MPW che le TPW presentavano una percentuale maggiore nei soggetti AF e nei soggetti affetti da altre aritmie in confronto ai soggetti NSR.

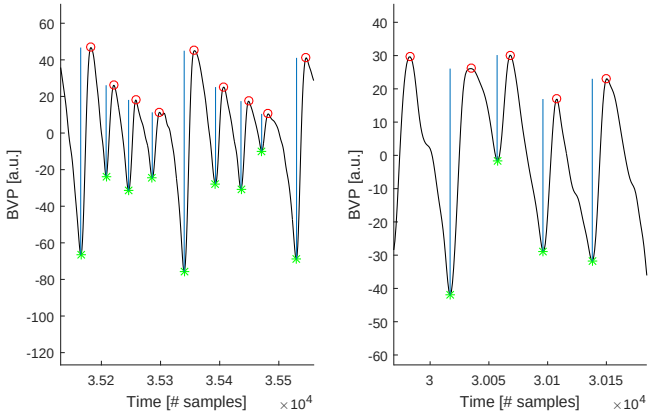

Figura 3: ***Forma di multi-peak wave e di two-peak wave.*** *La forma tipica di una multi-peak wave (sinistra) e di una two-peak wave (destra).*

L'ultimo indice di analisi morfologica è la *shape similarity* [14]; questo indice misura la somiglianza di tutte le onde del BVP paragonandole una ad una; è stata prevista una somiglianza maggiore per i soggetti in ritmo sinusale, dal momento che il loro output cardiaco è fisiologicamente più regolare. Il calcolo della *shape similarity* è ottenuto svolgendo il prodotto scalare tra gli array di t campioni che compongono ogni onda dell'acquisizione. Il prodotto scalare tra due vettori t-dimensionali è proporzionale al modulo dei due vettori e al coseno dell'angolo compreso tra di essi; in questa operazione, il vettore dei campioni di ogni onda è stato normalizzato dividendolo per la norma, di conseguenza questo calcolo fornisce valori più elevati per forme

d'onda simili, quantificandone la somiglianza relativa. L'indice finale di *shape similarity* è stato ottenuto come la percentuale di onde in un'acquisizione che sono più simili di una certa soglia, impostata in modo da massimizzare le differenze di questo indice tra le classi target. I valori ottenuti dall'indice erano, come previsto, maggiori per i soggetti NSR, inferiori per soggetti affetti da altre aritmie e minimi per i soggetti AF. Per ottenere un'analisi più comprensiva, sono stati calcolati altri due indici: la mediana (*MedianArc*) e la moda (*ModeArc*) dell'angolo del prodotto scalare, calcolato per tutte le onde. Questi valori risultavano invece più alti per i pazienti AF ed inferiori per i soggetti NSR.

B.4 Analisi

Abbiamo svolto un'iniziale classificazione univariata osservando i valori assunti da ciascun indice nelle tre classi target: in ogni caso era presente una sovrapposizione di valori, precludendo la possibilità di utilizzare un solo indice per separare i soggetti.

Abbiamo deciso pertanto di svolgere un'analisi multivariata addestrando una support vector machine (SMV) e valutandone l'accuratezza attraverso il metodo di cross-validation *leave one out*. Per ridurre le dimensioni del dataset è stato diminuito il numero di indici impiegati, semplificando l'analisi e potenzialmente migliorando l'accuratezza di classificazione finale. Due metodi diversi sono stati impiegati: l'analisi delle componenti principali (*principal component analysis*, PCA) ed il metodo wrapper.

C Risultati

C.1 PCA

Abbiamo applicato la PCA sull'intero dataset di soggetti e indici. La performance del classificatore è stata valutata per un numero diverso di componenti principali, da 1 a 16. Nella Tabella 5 è mostrata l'accuratezza di classificazione ottenuta per un differente numero di componenti principali prese in considerazione, insieme alla relativa percentuale di varianza spiegata. La migliore accuratezza era 90%, ottenuta considerando le prime 12 componenti principali, per una varianza spiegata del 99.91%.

# PCs	1	2	3	4	5	6	7	8
Acc [%]	50	48.57	75.71	84.29	87.14	82.86	81.43	81.43
I_q[%]	50.61	76.36	82.71	87.72	91.37	94.52	96.72	98.21
# PCs	9	10	11	12	13	14	15	16
Acc [%]	85.71	87.14	85.71	90	84.29	85.71	82.86	81.43
I_q[%]	98.80	99.34	99.71	99.91	99.98	99.99	100	100

Tabella 5: ***Accuratezza di classificazione per numero di componenti principali considerate.*** *L'accuratezza di classificazione ottenuta attraverso una procedura* leave one out *e la percentuale di varianza spiegata sono mostrate per un numero progressivamente maggiore di componenti principali considerate.*

C.2 Metodo wrapper

Una selezione degli indici più rilevanti è stata ottenuta attraverso il metodo wrapper. Abbiamo testato tutte le possibili combinazioni di indici, quindi, per 16 indici, $2^{16} - 1$ opzioni.

La distribuzione di accuratezza di classificazione ottenuta tramite SVM è mostrata in Figura 4.

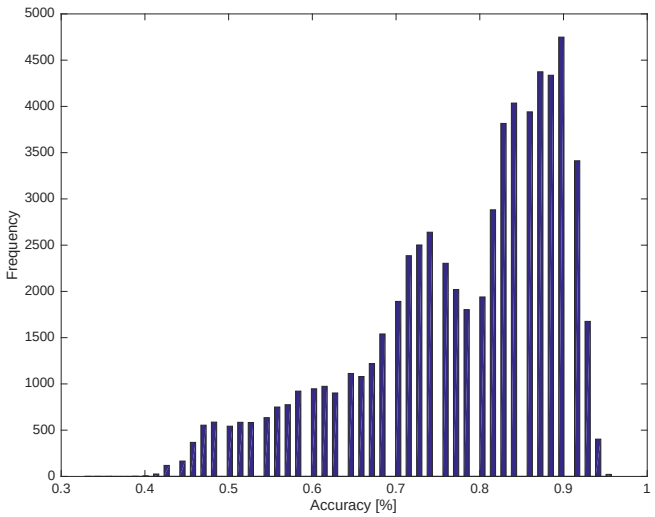

Figura 4: ***Distribuzione della accuratezza di classificazione ottenuta tramite SVM.*** *L'istogramma mostra le accuratezze di classificazione ottenute usando differenti combinazioni di indici.*

Come si può vedere, i risultati della SVM cambiano notevolmente in base agli indici su cui è stata addestrata, andando da un'accuratezza minima di 32.86% ottenuta in un caso, al valore massimo di 95.71% ottenuto per 22 diverse combinazioni; per quanto riguarda la distribuzione statistica dell'accuratezza, la mediana era uguale a 81.43%, con una media di 77.65% e una moda di 90%. Delle 22 migliori opzioni abbiamo selezionato i 16 casi che offrivano anche il miglior valore di sensitività alla classe AF, 96.67%.

Le combinazioni di indici che offrivano la migliore performance sono mostrati in Tabella 6.

																	% Ind
SD	1	1	1				1	1	1			1		1		1	56.25
RMSSD		1				1	1	1			1	1	1	1	1	1	62.5
nRMMSD	1	1		1		1	1	1			1	1	1	1	1	1	75
pNN50	1	1	1	1	1	1	1	1	1	1	1	1	1	1	1	1	100
CV					1	1	1			1			1	1	1	1	50
SampEn	1	1	1	1	1	1	1	1	1	1	1	1	1	1	1	1	100
nShEn	1	1	1	1	1	1	1	1	1	1	1	1	1	1	1	1	100
ShapeSim	1																6.25
MedianArc		1				1	1	1			1	1	1	1	1	1	62.5
ModeArc			1	1	1				1	1							31.25
AF evidence	1	1	1	1	1	1	1	1	1	1	1	1	1	1	1	1	100
PD																	0
nWD											1	1	1	1			25
MPW						1	1								1	1	25
TPW																	0
PSDsum								1	1	1	1	1	1	1	1	1	56.25
Tot Ind	7	8	6	6	6	9	10	9	7	7	9	10	10	11	10	11	

Tabella 6: ***Combinazioni di indici con migliore accuratezza di classificazione e sensitività.*** *La tabella mostra le 16 migliori combinazioni di indici (colonne). Per ogni combinazione, gli indici (righe) presi in considerazioni sono indicati con un 1 nella casella corrispondente. Alla fine di ogni colonna è indicato il numero di indici presi in considerazione in ogni caso. Alla fine di ogni riga è specificata la percentuale di utilizzo di ogni indice in tutte le 16 combinazioni.*

Queste 16 combinazioni erano costituite da un numero di indici variabile da 6 a 11. Quattro di questi indici apparivano in tutti i 16 casi: la percentuale di differenze di intervalli successivi maggiori di 50 ms, (pNN50), la sample entropy (SampEn), la Shannon entropy normalizzata (nShEn) e la AF evidence, che hanno quindi costituito un sottoinsieme di indici fondamentali

per una buona classificazione. A parte questi indici sempre presenti, in ogni combinazione comparivano un parametro morfologico e un altro indice di variabilità cardiaca nel dominio del tempo.

Per ogni combinazione, abbiamo analizzato la matrice di confusione ottenuta alla fine del metodo *leave one out*. Le colonne della matrice indicano il reale stato di salute di ogni soggetto, mentre le righe indicano la categoria nella quale il paziente è classificato dalla SVM; quindi, gli elementi sulla diagonale principale indicano le classificazioni corrette. Per le 16 combinazioni migliori, due tipologie di matrice di confusione sono state ottenute più volte, mostrate in Tabella 7 e Tabella 8.

	NSR	Other	AF
NSR	31	1	0
Other	0	7	1
AF	0	1	29

Tabella 7: ***Matrice di confusione A.*** *Matrice di confusione ottenuta in 10 delle 16 migliori combinazioni di indici. NSR=normal sinus rhythm, AF=atrial fibrillation e "other" indica le altre tipologie di aritmia. Le colonne della matrice indicano il reale stato di salute di ogni soggetto, mentre le righe indicano la categoria nella quale il paziente è classificato dalla SVM.*

	NSR	Other	AF
NSR	30	1	0
Other	1	8	1
AF	0	0	29

Tabella 8: ***Matrice di confusione B.*** *Matrice di confusione ottenuta in 6 delle 16 migliori combinazioni di indici. NSR=normal sinus rhythm, AF=atrial fibrillation e "other" indica le altre tipologie di aritmia. Le colonne della matrice indicano il reale stato di salute di ogni soggetto, mentre le righe indicano la categoria nella quale il paziente è classificato dalla SVM.*

In tutte le matrici la sensitività, che è il rapporto tra il numero di pazienti AF identificati dalla SVM e il numero totale di soggetti AF, era 96.67%, mentre la specificità alla classe NSR era 100% in 10 casi e 96.77% nelle altre combinazioni; la specificità alla classe "altre aritmie" era 77.78% in 10 casi e 88.89% per le rimanenti 6 combinazioni.

Ringraziamenti

Desideriamo esprimere la nostra riconoscenza innanzitutto verso i professori e i collaboratori di questa tesi, il cui apporto è stato fondamentale alla riuscita del nostro lavoro. Ringraziamo il nostro relatore, il Professor Luca Mainardi, che ci ha seguito in ogni aspetto di questo studio, dalla sua ideazione fino al completamento; gli siamo grati per il suo aiuto instancabile e paziente con cui ha sostenuto da vicino i nostri sforzi. Ringraziamo di cuore i medici dell'U.O.C. di Malattie dell'Apparato Cardiovascolare dell'Ospedale Maggiore Policlinico di Milano: il Professor Federico Lombardi per il sostegno alla nostra attività sperimentale e il Dottor Giorgio Scarpini per l'eccezionale operosità e cordialità nel fornirci le misure che sono il fondamento del nostro lavoro scientifico; ulteriormente, vogliamo esprimere la nostra riconoscenza a tutti coloro che si sono prestati a fornire i loro dati biometrici, poiché, pur senza conoscerci personalmente, con il loro apporto hanno fornito le basi dei nostri risultati. Vogliamo esprimere la nostra gratitudine all'azienda Empatica Inc. per averci concesso l'utilizzo del dispositivo Empatica E4 che ha permesso di effettuare le misure sperimentali.

Ringrazio tutti i miei amici che, vicini o lontani che siano, sono sempre vicini nel cuore.

Grazie a Claudia per i suoi pareri, specialmente quelli sugli argomenti più affini alla medicina.

Grazie a Filippo, che mi sopporta sempre e mi sostiene in ogni mia scelta, e a tutta la sua famiglia, che mi ha accolto a braccia aperte sorprendendomi con il calore dimostratomi.

Grazie ai miei genitori e a tutta la mia famiglia che mi è stata accanto in questo lungo periodo di crescita che viene coronato da questa tesi. Siete fantastici e sono fortunata ad avervi.

Last but not least, voglio ringraziare il mio collega Lorenzo. Insieme siamo riusciti a portare a termine questo lavoro e sono orgogliosa di ciò che abbiamo raggiunto. Grazie di essere stato al mio fianco, di avermi suppor-

tato nei momenti difficili e di aver reso possibile tutto ciò, con il tuo lavoro, la tua abnegazione e la tua infinita pazienza, la tua fiducia incrollabile e il tuo dono di dire le parole giuste al momento giusto. Sono felice di poterti chiamare amico oltre che collega.

La prima persona che voglio ringraziare è la mia amica e collega Rita: abbiamo progettato insieme ogni aspetto del lavoro sperimentale ed ogni capitolo di questo testo conclusivo, quindi devo soprattutto a te il raggiungimento di questo traguardo importante. Lavorare a stretto contatto con me per così tanto tempo avrebbe messo alla prova chiunque, invece sei sempre stata disponibile, paziente e soprattutto meticolosa nel lavoro, una qualità che mi auguro ti aiuterà a raggiungere ogni traguardo desideri nella tua futura vita professionale.

Voglio ringraziare tutti i miei amici, siete tanti da elencare ma ricorderò per sempre ognuno di voi. Vi ringrazio per tutte le giornate, le serate ed i momenti passati insieme in questi lunghi anni, sono io ad aver finito questo percorso, ma è grazie a voi se ho qualcuno con cui festeggiare.

Ringrazio la mia famiglia, i miei nonni e gli zii, che mi hanno cresciuto con il loro affetto. Ringrazio i miei genitori, che mi hanno seguito e supportato da più tempo di quanto possa ricordare; ringrazio mia sorella, che spesso mi capisce meglio di chiunque altro, e che è sempre dalla mia parte.

Contents

Summary **I**
A Introduction . . . I
B Methods . . . II
B.1 Study population . . . II
B.2 BVP preprocessing . . . II
B.3 Diagnostic indexes . . . III
B.4 Analysis . . . VI
C Results . . . VI
C.1 PCA . . . VI
C.2 Wrapper method . . . VII

Sommario **X**
A Introduzione . . . X
B Metodi . . . XI
B.1 Popolazione in studio . . . XI
B.2 Preprocessing del segnale BVP . . . XI
B.3 Indici diagnostici . . . XII
B.4 Analisi . . . XV
C Risultati . . . XV
C.1 PCA . . . XV
C.2 Metodo wrapper . . . XVI

1 Introduction **1**

2 Contemporary view on atrial fibrillation **3**
2.1 Introduction . . . 3
2.2 Electrophysiology of the heart . . . 4
2.3 Mechanisms of atrial fibrillation . . . 5
2.4 A clinical view . . . 7
2.4.1 Incidence and risk factors . . . 7

2.4.2 Treatment of atrial fibrillation 10
2.4.3 Identification and diagnosis 11

3 Signals and algorithms for AF detection 13
3.1 Signals 13
3.1.1 Electrocardiogram 13
3.1.2 Intracardiac electrogram 14
3.1.3 Implanted loop recorders 15
3.1.4 Photoplethysmography 16
3.1.5 Comparison 18
3.2 Algorithms 18
3.2.1 The Lorenz plot 19
3.2.2 Time domain parameters 25
3.2.3 Entropy 25
3.2.4 Shannon entropy 28
3.2.5 Morphology-based analysis 28

4 Experimental protocol and signal preprocessing 31
4.1 Study population 31
4.2 Data acquisition protocol 33
4.2.1 Empatica wristband 34
4.3 Signal preprocessing 35
4.3.1 Noise detection 35
4.3.2 Peak detection 37

5 Measures and results 42
5.1 Spectral analysis 42
5.1.1 BVP spectral analysis 42
5.1.2 Intervals spectral analysis 45
5.2 Time domain indexes 48
5.2.1 Standard deviation 48
5.2.2 Root mean square of successive differences 49
5.2.3 Coefficient of variation 50
5.2.4 pNN50 51
5.2.5 AF evidence 52
5.3 Nonlinear indexes 55
5.3.1 Sample entropy 55
5.3.2 Normalized Shannon entropy 56
5.4 Shape analysis 57
5.4.1 Normalized wave deviation 57

5.4.2 Multi-peak waves 59
5.4.3 Two-peak waves 61
5.4.4 Shape similarity 64

6 Classification and results **68**
6.1 Correlation between indexes 68
6.2 Support vector machine 72
6.2.1 Indexes reduction 74

7 Discussion **79**
7.1 Univariate classification 80
7.2 Multivariate classification 81

8 Limitations and future work **83**

Bibliografia **85**

List of Tables

1 Classification accuracy for number of principal components included VII
2 Sets of indexes with best classification accuracy and sensitivity VIII
3 Confusion matrix A IX
4 Confusion matrix B IX
5 Accuratezza di classificazione per numero di componenti principali considerate XVI
6 Combinazioni di indici con migliore accuratezza di classificazione e sensitività XVII
7 Matrice di confusione A XVIII
8 Matrice di confusione B XVIII

3.1 Comparison between heart signals for AF diagnosis 18

6.1 Classification accuracy for number of principal components included 75
6.2 Sets of indexes with best classification accuracy and sensitivity 77
6.3 Confusion matrix A 78
6.4 Confusion matrix B 78

7.1 nRMSSD confusion matrix 80
7.2 RMSSD confusion matrix 81
7.3 CV confusion matrix 81

List of Figures

1 Multi-peak wave and two-peak wave shapes V
2 Distribution of SVM classification accuracy VII
3 Forma di multi-peak wave e di two-peak wave XIV
4 Distribuzione della accuratezza di classificazione ottenuta tramite SVM XVI

2.1 Cardiac conduction system 5
2.2 AF Mechanism 6
2.3 Kaplan-Meier mortality curves 9

3.1 Absorption in PPG signal 16
3.2 PPG systems 17
3.3 Lorenz diagram 20
3.4 Examples of Lorenz plot in AT/AF patients 20
3.5 Lorenz plot 21
3.6 Cardiac rhythm and Lorenz plot 22
3.7 Logic of the Lorenz plot detector 24

4.1 Population gender 32
4.2 Population age 32
4.3 E4 wristband applied 33
4.4 E4 wristband 34
4.5 Phases of signal preprocessing 35
4.6 Disturbed signal 36
4.7 Disturbed signal and accelerometric data 36
4.8 Peak detection 38
4.9 Diastolic minima detection 39
4.10 Variability of the sistolic peak 40
4.11 BVP Characteristics 41

5.1 Signal example 43
5.2 Power spectra comparison 44

5.3 Spectral analysis boxplot 45
5.4 Original intervals sequence and interpolation. 46
5.5 Interval series with empty periods 47
5.6 Intervals spectral analysis boxplot 48
5.7 SD boxplot 49
5.8 RMSSD boxplot 50
5.9 nRMSSD boxplot 50
5.10 CV boxplot 51
5.11 pNN50 boxplot 52
5.12 Lorenz plot distribution 53
5.13 AF evidence boxplot 55
5.14 SampEn boxplot 56
5.15 nShEn boxplot 57
5.16 The R value. 58
5.17 Normalized WD boxplot 59
5.18 Multi-peak waves' identification 60
5.19 MPW boxplot 61
5.20 TPW shape 62
5.21 TPW shape and alpha angle 63
5.22 TPW boxplot 64
5.23 Comparison between different thresholds 65
5.24 Shape similarity boxplot 66
5.25 Boxplot of the median of dot product angle 67
5.26 Boxplot of the mode of dot product angle 67

6.1 Correlation between SD and PSDsum 69
6.2 Correlation between SD and RMSSD 70
6.3 Comparison between nRMSSD and CV 70
6.4 nRMSSD and SampEn comparison 71
6.5 nRMSSD versus shape similarity 72
6.6 SVM classification in 2D space 73
6.7 Distribution of SVM classification accuracy 76

Chapter 1

Introduction

Atrial fibrillation (AF) is a very common heart arrhythmia: this condition causes a pathological atrial function, with a rapid, uncoordinated heart rate.

AF is triggered by pathological activation mechanisms in the cardiac system: the physiological impulses generated in the sinus node undergo the interference of other rapid impulses produced in the atria and adjacent parts; this results in the generation of abnormal activation patterns in the atria, which in turn causes some of the pathological fronts of depolarization to pass through the atrioventricular node, generating chaotic contractions of the ventricles [28].

The disordered stimulation of the myocardium produces uncoordinated contractions of the heart, thereby interfering with the physiological blood flux pumped to the body; the circulatory inefficiency associated can cause severe diseases, such as stroke [11].

One of the main problems with AF identification is that this arrhythmia can be paroxysmal, meaning it can occur episodically and terminate spontaneously; in such cases it is very hard to identify the pathology because clinical analyses carried out in a normal sinus rhythm period don't show the presence of the pathology [22]. Although two thirds of the subjects affected by this arrhythmia report that it is disruptive to their lives, the manifestation of AF can also be asymptomatic [23], yet it is important to intervene as soon as this disease arise to affect the normal sinus rhythm, because if untreated, the arrhythmia roots its mechanism into the subject's heart, becoming increasingly persistent [38].

As a consequence, it is important to provide a rapid diagnosis, and it would be best to perform some sort of screening on the asymptomatic population, in order to treat this pathology from its very beginning, even when

the patient does not suffer its effects yet.

Despite AF mechanisms being caused by electric disturbances, it is possible to witness the presence of this pathology by studying the photoplethysmographic (PPG) signal, since AF patients experience an irregular flow in the blood vessels; using a PPG signal instead of an ECG signal for diagnosis brings the advantage of the non-invasivity and accessibility of this type of measure: nowadays a PPG acquisition can be easily obtained, even by most non-medical smart devices of common use, for example by smartphones with dedicated apps for signal processing [20].

It is possible to apply a PPG sensor on the patient by using a dedicated wristband device, like the Empatica E4; such device can be applied on the patient without causing discomfort even for prolonged acquisitions [40]. The possibility to monitor the blood volume pulse (BVP) continuously for hours or even days allows the diagnosis even for paroxysmal asymptomatic AF: by prolonging the acquisition time, the possibility to analyze a time window affected by AF increases. Furthermore, the spreading of smart devices can help monitoring population with higher patient compliance and less cost for healthcare systems.

The raw photoplethysmographic signal, however, must be analyzed by an expert to reveal the presence of AF; this type of examination would not be practicable for a wide analysis on the asymptomatic population, potentially comprehensive of millions of subjects, hence the need for an automatic form of diagnosis.

In this study, we build a decision-making system trained on AF detection from BVP signal analysis. The aim is an automatic, algorithmic classification of each patient into one of three target classes: healthy subject, subject affected by atrial fibrillation or subject affected by another arrhythmia.

We recorded 70 BVP signals from distinct subjects, recruited among hospitalized patients at Ospedale Maggiore Policlinico in Milan, Italy; after the acquisition, every subject is classified into one of the three target classes by expert cardiologists. All data collected in this phase are employed to train the decision-making algorithm, which bases its analysis on several indexes already present in current clinical practice, along with some new ones proposed by us, obtained from the BVP acquisition; all the indexes' values are finally used by a support vector machine (SVM), which estimates their correlation with the health status of the patient; all the information gathered by the SVM during this training phase is later used in the automatic classification of new subjects.

Chapter 2

Contemporary view on atrial fibrillation

2.1 Introduction

Atrial fibrillation (AF) is the most common chronic arrhythmia of clinical significance [11].

In an AF heart, disordered or rapid electrical signals cause the upper chambers (the atria) to contract too quickly and chaotically (fibrillate). The normal, ordered contraction of the muscle fibers of the atria typically allows the coordinated and complete emptying of blood from the heart's upper chambers into the lower ones. However, in the presence of fibrillation, flow becomes irregular and chaotic, and that can cause blood to pool in the atria without being pumped into the lower chambers of the heart (the ventricles). This leads to a loss of efficiency of the heart and to various diseases [41].

In 2010 the estimated number of individuals with AF worldwide was 33.5 millions, corresponding to the 0.5 percent of the world's population [11]. AF has heterogeneous clinical presentations and is traditionally classified on the basis of the temporal pattern of the arrhythmia [23] [22]:

- Paroxysmal: episodes terminate spontaneously, usually within seven days and mostly in less than 24 hours.
- Persistent: abnormal heart rhythm continues for more than a week, requiring treatment (pharmacological or electrical) for termination.
- Permanent: longstanding (>1 year) AF, where cardioversion is not indicated, has failed or has not been attempted.

Permanent AF is the most frequent form of diagnosed AF (40%-50% of

patients) [44]. Every form of AF can lead to many collateral effects, such as fatigue, dizziness, chest pain and is reported to increase the risk of myocardial infarction [32], heart failure [6] and stroke [39]: therefore an early diagnosis is fundamental to counteract its impact.

2.2 Electrophysiology of the heart

The human heart works physiologically as a functional syncytium: the electrical impulses propagate in every direction, so that the myocardium functions as a single contractile unit. In this manner, the myocardial cells respond to an electrical stimulus in a coordinated way, rapidly diffusing the action potential and leading to an efficiently organized contraction. There are two syncytia: the atrial and the ventricular one, connected by the atrioventricular node.

The cardiac conduction system of the electrical signal is depicted in Figure 2.1. The initiation of the heart contraction takes place in the right atrium where the sinoatrial (SA) node, that is the cardiac pacemaker, spontaneously generates an electrical impulse. The electrical signal stimulates the atria to contract, forcing all the blood still in the atria (up to 30%) into the ventricles during the so called *atrial kick*. At the end of the contraction, the electric signal reaches the atrioventricular (AV) node. The AV node is located in the interatrial septum and it is the only point that electrically connects the atria and the ventricles. After a little delay that allows the atria to complete pumping blood, the action potential goes through the bundles of His in the ventricular septum and through its two bundle branches, the left and right bundles. Finally, the electrical signal reaches the Purkinje fibers, which spread the impulse to the contractile fibers of each ventricle, leading to their efficient and synchronized contraction.

A refractory period occurs after each depolarization, during which a successive action potential cannot be triggered. This characteristic may lead to complex activation patterns in the atria; if action potentials are pathologically too short, reactivation can occur too early, leading to extremely rapid atrial rate, as in AF.

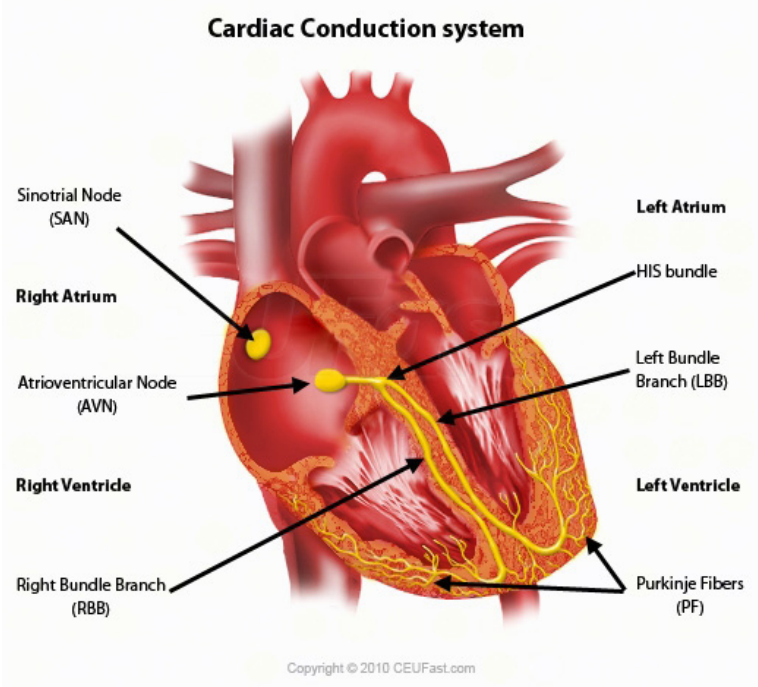

Figure 2.1: ***Cardiac conduction system.*** *The conduction pattern from the sinoatrial node to the final part of the ventricles is depicted in the longitudinal section of the heart (www.ceufast.com/courses/viewcourse.asp?id=239).*

2.3 Mechanisms of atrial fibrillation

Atrial fibrillation has a complex and not completely understood pathophysiology. Many factors contribute to the initiation and maintenance of the fibrillatory process (Figure 2.2) [28].

As reviewed by Jalife et al. [18], historically Winterberg [4] in 1907 considered AF as the effect of rapidly firing foci distributed throughout the atria. In 1914 Mines [25] advanced the theory of reentry (circus movement): the return of the same impulse into a zone of the heart muscle that it has recently activated, sufficiently delayed so that the zone is no longer refractory, could lead to a continuous and disorganized excitation of the atrial cells.

After the publication of the multiple wavelet hypothesis by Moe [27] AF has been seen as the result of the propagation of multiple wavelets across the atria. The number of wavelets depends on the atrial refractory period, mass, and conduction velocity [4]. If the number of the wavelets is high, the statistical probability that they will all extinguish at the same time will be small and atrial fibrillation will persist. On the other hand, when only a small number of wavelets are present, the chance that they will die out

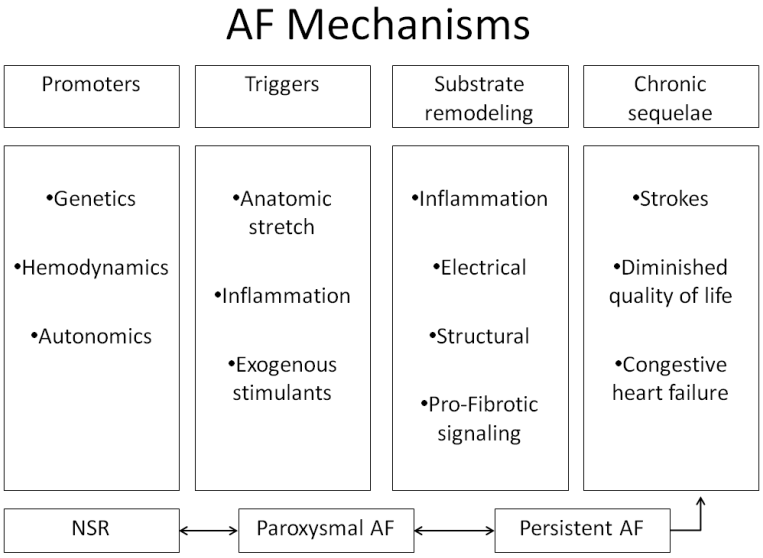

Figure 2.2: ***AF mechanism.*** *An overview of the main causes and consequences of AF.*

simultaneously is higher and atrial fibrillation will self-terminate [38].

Atrial size increasing and refractoriness shortening are likely to promote the generation of multiple reentrant wavelets, by decreasing the atrial wavelength of reentry. The atrial wavelength, a crucial concept in understanding atrial fibrillation, is defined as the product of Effective Refractory Period (ERP) and Conduction Velocity (CV) [22]. In other words, at a given conduction velocity, atrial wavelength represents the distance covered by a depolarization potential in one refractory period [12]. Short wavelength and high atrial size allow more wavelets to coexist, leading to an increase in persistence of AF. Experimental evidence of Moe's multiple wavelet hypothesis is provided by records of the excitation of the atria in AF through a high–resolution electrode mapping system [5]. Allessie et al. showed multiple wavelets wandering around natural anatomic obstacles and functional arcs of conduction block. In some cases, the wavelets appeared to be offspring of a single reentrant circuit [19].

Finally, Haïssaguerre et al. [16] proved that in some cases AF is triggered by ectopic activity arising from the pulmonary vein region.

All these proposed theories are often interlinked with the history of a single patient. Furthermore, it is known that "atrial fibrillation begets atrial fibrillation" [38]: in a 30-year follow up study of 2007 up to 30% of patients with paroxysmal or persistent AF developed permanent AF [2]. A possible explanation is that AF itself causes electrophysiological and/or structural

changes to the atria, which promote its perpetuation. Functional, electrical, structural and biochemical changes occur in the atria remodeling due to AF, such as decreased ERP, poorer ERP rate-adaptation with consequential contractile dysfunction that leads to atrial dilation [12] in a cascade of cause and effect in which the fibrillation interval keeps shortening. As soon as the fibrillation interval passes a critical threshold, AF becomes more stable and its duration increases. This in turn will further shorten the fibrillation interval which will prolong the duration of AF again, etc. following a positive feedback mechanism that will continue until a new steady state is reached in which atrial fibrillation has become the predominant atrial rhythm (domestication of atrial fibrillation) [38]. Remodeling links all the potential AF mechanisms. When paroxysmal AF is initiated by rapid ectopic activity or single-circuit reentry, it causes anatomic and electrical changes, which favor spatially heterogeneous refractoriness shortening. This tends to move AF towards multiple-circuit reentry.

Ectopic activity, as well as an increased vagal tone play a key rule in triggering pathological conditions capable of sustaining AF: heart failure, atrial stretch, age-related development of interstitial fibrosis all provide a prolific substrate for reentry. However, the nature of interaction between triggers and substrate in AF genesis is still not completely understood [12].

2.4 A clinical view

The history of atrial fibrillation in medical science dates back to the nineteenth century; it is one of the most common serious abnormal heart rhythms and, as a consequence, it is one of the oldest and most studied heart diseases, with a wide clinical documentation.

2.4.1 Incidence and risk factors

Atrial fibrillation is becoming one of the most significant public health issues and an important cause of health care costs in the world.
In the review by Zoni-Berisso at al. [44] the prevalence of AF is 0.12%-0.16% in subjects younger than 49 years, 3.7%–4.2% in those aged 60–70 years, and 10%–17% in those aged 80 years or older. Furthermore, AF is more frequent in males, with a male to female ratio of approximately 1.2. The prevalence is continuously increasing, with high rates, such as 0.3% per year in the USA among Medicare beneficiaries older than 65 years. This trend shows an endemic dimension.

AF is often associated with other cardiac diseases such as hypertensive heart disease (present in 22%–36% of a AF patients), coronary heart disease (14%–32%), valvular heart disease (12%–26%), and cardiomyopathy (6%–10%). Furthermore, widespread AF comorbidities are hypertension (67%–76%), heart failure (22%–42%), obesity (20%–35%), diabetes (20%–24%), chronic pulmonary disease (10%–18%), thyroid dysfunction (8%–11%), renal failure (11%–22%), neuropsychiatric disturbances (19%) and stroke/transient ischemic attack (9%–16%).

In particular, one third of AF patients have at least three associated comorbidities; no comorbidity or cardiac disease is present in one fifth and one quarter of patients, respectively. Lone AF (when AF occurs without identifiable etiology in patients with a structurally normal heart [23]) is present in a low proportion of cases, ranging between 2% and 15% [44] [23].

In the Framingham study [9] the impact of AF on the risk of death was assessed in 5209 residents of Framingham, Mass, in 40 years of follow-up. The Kaplan-Meier mortality curves are displayed in Figure 2.3 for the subjects 55 to 74 years of age (top) and the subjects 75 to 94 years of age (bottom).

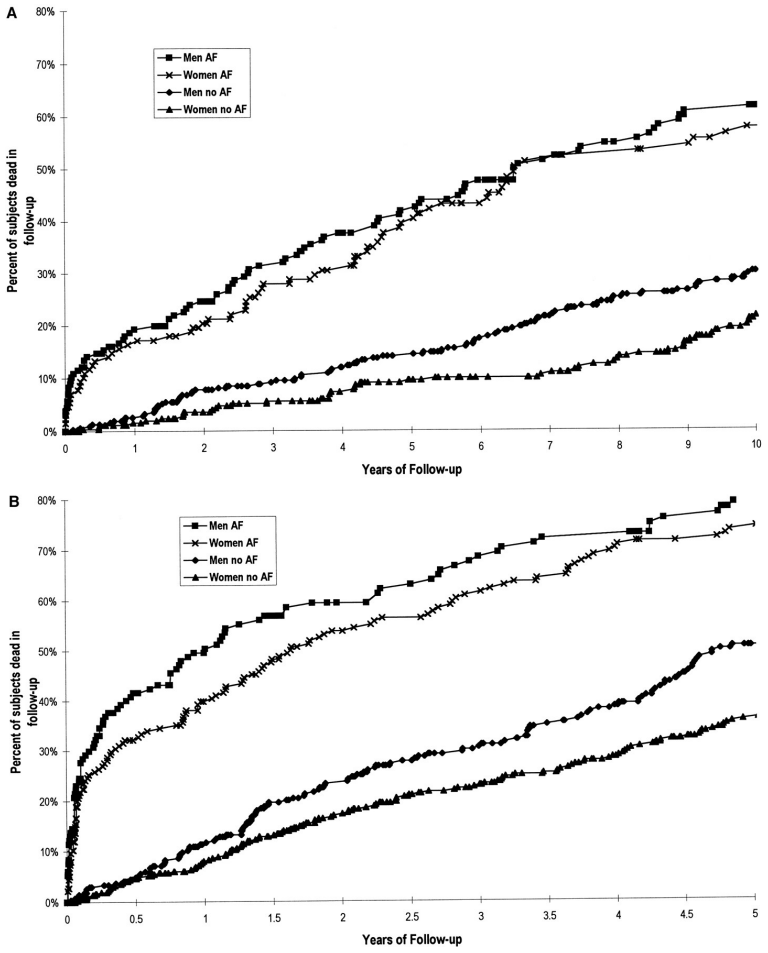

Figure 2.3: ***Kaplan-Meier mortality curves.*** ***A:*** *Kaplan-Meier mortality curves for subjects 55 to 74 years of age. Vertical axis shows the percent of subjects dead at follow-up (*0% *to* 80%*); horizontal axis, up to 10 years of follow-up. Subjects included men with AF (n=159), men without AF (n=318), women with AF (n=133), and women without AF (n=266).* ***B:*** *Kaplan-Meier mortality curves for subjects 75 to 94 years of age. Vertical axis shows the percent of subjects dead at follow-up (*0% *to* 80%*); horizontal axis, up to 5 years of follow-up. Results are shown for men with AF (n=137), men without AF (n=274), women with AF (n=192), and women without AF (n=384) [9].*

In general the mortality of men and women with AF was substantially greater than that of the non-AF subjects (log rank test, all $P<0.0001$). The study demonstrates that AF is an independent risk factor for the risk of death, even after adjustment for coexisting cardiovascular conditions.

Atrial fibrillation is an independent risk for stroke [39] with an age-adjusted incidence of stroke near fivefold in excess when atrial fibrillation

is present ($p<0.001$), making AF responsible for a total of 15%-18% of all strokes [22]. The Framingham study data indicates that atrial fibrillation exerts a significant impact on the risk of stroke that is independent of the often associated cardiovascular abnormalities. Furthermore, other cardiovascular abnormalities have a decreasing influence with age, whereas the impact of atrial fibrillation increases into the ninth decade of life. The dramatic reduction in the incidence of stroke in randomized clinical trials by warfarin anticoagulation and by aspirin strengthens this consideration, because these treatments have no reported effect on the comorbidities typically associated with AF. Although these findings are encouraging, the use of these drugs carries some hazard and substantial side effects.

2.4.2 Treatment of atrial fibrillation

In patients with AF there are three main therapeutic strategies:

- Reduction of thromboembolic risk.
- Restoration and maintenance of sinus rhythm (rhythm control).
- Control of ventricular rate during AF (rate control).

The thromboembolic risk increases significantly when AF duration exceeds 48 hours so anticoagulation therapy is highly recommended, regardless of the arrhythmia pattern or the therapeutic strategy chosen [23]. The timing of anticoagulation is one of the most critical decisions and the great incidence of asymptomatic episodes in paroxysmal AF or of asymptomatic recurrences after cardioversion cast additional doubts on its interruption. Most of the patients with permanent AF have to continue oral anticoagulant therapy for the rest of their lives.

In rate control strategies, the arrhythmia is allowed to continue so symptomatic improvement and better hemodynamic function is achieved solely because of a better control of the ventricular rate. As the atria continue to fibrillate, the risk of thromboembolism persists and ventricular filling occurs only passively, without the active contribution of atrial contraction [23]. Drugs such as β or calcium channel blockers and digoxin are the most commonly applied; sometimes amidarone or AV node ablation with implantation of a permanent pacemaker are indicated in refractory cases [22].

Rhythm control, on the other hand, aims to restore sinus rhythm and thus synchronized atrioventricular contraction. This strategy should also help slow or prevent the progression to permanent AF, reduce symptoms, improve cardiac hemodynamics and reduce the risk of thromboembolism [23].

Sinus rhythm can be restored through pharmacological treatment (class IC or III antiarrhythmic drugs) or by electrical cardioversion (biphasic shock is 98% effective in restoring sinus rhythm [22]). For patients who have to undergo electrical cardioversion, it is recommended a minimum of 3 weeks of therapeutic oral anticoagulant (OAC) prior to the conversion and a minimum of 4 weeks of OAC following cardioversion [28]. Likelihood of successful cardioversion is inversely proportional to duration of AF so it is important to restore sinus rhythm as soon as this is possible and safe [23]. In about 60% of patients with restored sinus rhythm AF recurs within 6-12 months, thus prophylaxis of AF recurrences is an important topic, with a proposal of various novel strategies such as administration of blockade of the renin-angiotensin-aldosterone system or statins [22].

In the last years another strategy is emerging as one of the most promising therapeutic approaches to AF management: ablation of AF triggers and substrates. Since the description of radiofrequency catheter ablation by Haïssaguerre et al. in a study on the proarrhythmic role of pulmonary vein foci in 1997 [16], multiple approaches have been developed with success rates exceeding 80% in patients with paroxysmal AF and 50% in persistent AF [22]. In particular, minimally invasive techniques utilizing microwave, radiofrequency and cryoablation energy sources applied with balloon-based ablation systems and cardiac image integration are possible surgical treatments.

2.4.3 Identification and diagnosis

Atrial fibrillation is often diagnosed through its symptoms. In the ALFA study [21] palpitations were present in 54.1% of patients with AF, dyspnea in 44.4%, fatigue in 14.3%, syncope and dizzy spells in 10.4% and chest pain in 10.1% of cases. In subjects with suspicious clinical setting, the standard techniques for diagnosis are ambulatory ECG, Holter recording of 24-48 hours or event recorders (implantable or not) automatically activated or activated by the subject when symptoms occur.

Unfortunately there are many undiagnosed subjects who present asymptomatic AF. In the ALFA study 11.4% of patients were asymptomatic, with a higher percentage considering only permanent AF (16.2% presented no symptoms). This important share of patients often diagnosed by chance during electrocardiograph control for other clinical reasons shows a possible large under-representation of the effective prevalence of AF. Furthermore, Holter is useless when paroxysmal events occur at intervals larger than 24 hours, leading to an incorrect evaluation of the subject's condition (false neg-

atives). Undiagnosed AF patients are an important bulk of patients with high risk of cardioembolic stroke or other complications associated with AF. Since AF worsens through time and the best prevention of AF or its recurrence is to terminate the arrhythmia as soon as possible [38], this share of undiagnosed people will have medical complications and will raise costs related to health care resources utilization.

The high rates of recurrence, disturbing symptoms, and clinical sequelae (stroke, heart failure, initiation of new antiarrhythmic drugs, drug-related complications, interventional therapy) contribute strongly to the use of health care resources. In Italy, AF is the cause of 1.5% of all emergency room visits [44]; a screening of the general population would answer the issue of paroxysmal and asymptomatic nature of AF, improving outcomes within the screened population and reducing costs. A monitoring device able to oversee the patient's condition such as a wristband for BVP recording could be useful and answer the developing trust in m-Health.

Since significant shares of global healthcare cost are related to cardiac arrhythmias and incidence of atrial fibrillation is destined to raise, m-Health could really meet the needs of governments, private insurers and individuals to prevent and timely treat such debilitating conditions while supporting cost-effective and interoperable ways of delivering health care. According to a global end-user research commissioned by GSMA between March-June 2012 about the perception of m-Health, 89% of caregivers, 75% of patients and 73% of consumers believe that m-Health solutions can convey significant benefits [12].

This work is intended to be a contribution on the path of a more efficient worldwide healthcare in AF identification.

Chapter 3

Signals and algorithms for AF detection

This chapter is divided into two sections: the first section overviews the typologies of signal employed in AF detection, while the second part focuses on the algorithms used to aid the clinicians in AF diagnosis.

3.1 Signals

There are numerous signal techniques for atrial activity analysis, each with different advantages and disadvantages for AF diagnosis and treatment. There are three main aspects to consider when choosing the signal employed to detect and study AF:

- Accuracy of the recording, such as spatial and temporal definition, amplitude and signal-to-noise ratio.
- Invasivity.
- Monitoring capability.

The ideal device would feature a high recording accuracy with 24/7 monitoring time and non-invasivity of the measurement. Unfortunately such device doesn't exist and a trade-off between these characteristics is needed. In this section, four of the most widespread heart signals and their main features are depicted.

3.1.1 Electrocardiogram

The standard 12-lead ECG is the most commonly used non-invasive tool for diagnosing electrical abnormalities like AF. The ECG shows the overall

electrical activity of the heart. During AF the ventricular heart rate results more irregular than in NSR, but less irregular than atrial activity because the atrioventricular node regulates the electrical trigger from atrial to ventricular tissue. The atrial activity is the most interesting for AF study and its waveforms are superimposed on the ventricular signals. Unfortunately, the atrial signals are much smaller (10 times lower in amplitude) than those related to ventricles (QRS complexes), thus the diagnostic applications based on P waves' analysis are compromised and computationally expensive. Furthermore, relying on body surface potential, the electrical image on the body surface is blurred with a low spatial definition in comparison to the potentials recorded inside the atria in an endocardial electrogram [22]. The main disadvantage of the ECG is the low suitability for continuous long-term monitoring. The traditional monitoring and detection of AF relies on intermittent ECG examination during clinical visit, 24-48 h Holter monitoring, several days of monitoring triggered by patients' symptoms or mobile cardiac outpatient telemetry capable of monitoring patient for up to 30 days. Considering the possible paroxysmal behavior of AF, sometimes also asymptomatic, many AF episodes may not be detected. In a study by Ziegler et al. [43] symptom-based and intermittent external monitoring methods were shown to have significantly lower sensitivity (31%-71%) for identification of patient with AT/AF and to significantly underestimate AT/AF burden compared to continuous monitoring. Moreover such external devices can interfere with daily activities like showering and can cause skin irritation over prolonged usage. Consequently, patient compliance with these systems can be quite low [35].

3.1.2 Intracardiac electrogram

Intracardiac electrogram (EGM) is recorded from two electrodes, at least one of which is implanted in the heart. EGMs allow clinicians to record the atrial activity directly *in situ* usually by passing catheter-guided electrodes through one of the major veins into the atria (endocardial signals). While ECG shows the electrical activity of all the heart, EGM records the local wavefronts of depolarization and repolarization that pass below the electrode at the tip of the lead. The amplitude of the recorded electrical signal is 10 times greater than the amplitude of an ECG signal. The amplitude, frequency content and morphology of EGMs depend on the location of the electrodes, the cardiac rhythm, posture, respiration and drugs. The amplitude of the atrial EGM tends to be smaller and/or more spatially and temporally variable during AF than in NSR. Furthermore, the spectral co-

herence of EGMs from two separate atrial sites is highly reduced during AF in comparison to other atrial rhythms. The analysis of EGMs is used in diagnostic procedures as well as for guiding therapeutic interventions [22]. New systems such as the basket catheter or the non-contact catheter provide high-density mapping of the atria in a dramatically reduced time, thanks to the possibility to record from many sites simultaneously. The non-contact system records 64 unipolar floating signals and mathematically reconstructs up to 3360 unipolar endocardial signals [7]. The high level of accuracy, temporal and spatial detail is paid with the elevated invasivity of the recording system.

3.1.3 Implanted loop recorders

Devices like Implanted Loop Recorders (ILRs) are typically inserted subcutaneously for ECG recording through closely spaced electrodes on their surface. ILRs can automatically record asymptomatic brady- and tachyarrhythmia events and patients can manually signal symptomatic events using a handheld activator. ILRs cannot detect AT/AF using P waves because their amplitude tends to be too small, but rely only on the analysis of RR intervals. For space, power and battery constraints algorithms should be computationally simple and the recorded information must be condensed and summarized due to memory size restrictions. Furthermore, a big amount of repetitive or unimportant data can overwhelm the physician and hinder his analysis. Thus this kind of device typically stores extremely detailed information only for a small subset of meaningful episodes, while general information is tabulated across all the episodes. In most implantable devices data is extracted during follow-up visits so the clinician can become aware of the presence of a new onset of AT/AF after potentially 6 months from the time of the first AT/AF occurrence. Some newer devices have wireless alert capabilities which automatically send an alarm to clinicians when an AT/AF burden threshold is exceeded. This can dramatically improve anticoagulation therapy, reducing the risk of stroke in asymptomatic patients. ILR ECG is different from a near-field signal recorded by bipolar electrodes within the heart. The frequency content is lower as is the amplitude of R waves and this, with the higher possibility of noise and artifacts, makes R wave sensing more challenging than with intracardiac signals. On the other hand a subcutaneous device is less invasive than an intracardiac electrogram and causes less discomfort during everyday life compared to constant ECG monitoring [22].

3.1.4 Photoplethysmography

In recent years, a new way of monitoring AF patients is being developed, based on photoplethysmography. A photoplethysmographic system allows the recording of the blood volume pulse (BVP) signal, which is the variation of volume of arterial blood under the skin resulting from the heart cycle. A BVP signal can be obtained from the measurement of the variation of the light absorbed by the skin due to arterial pulse.

Light travelling through the human body can be absorbed by different substances, including bones, tissues and venous and arterial blood (Figure 3.1). The majority of absorption is due to the continuous component, which is the constant absorption due to tissues and venous blood; the alternate component, instead, is caused by the absorption due to the arterial blood vessels that contain more blood volume during the systolic phase of the cardiac cycle than during the diastolic phase.

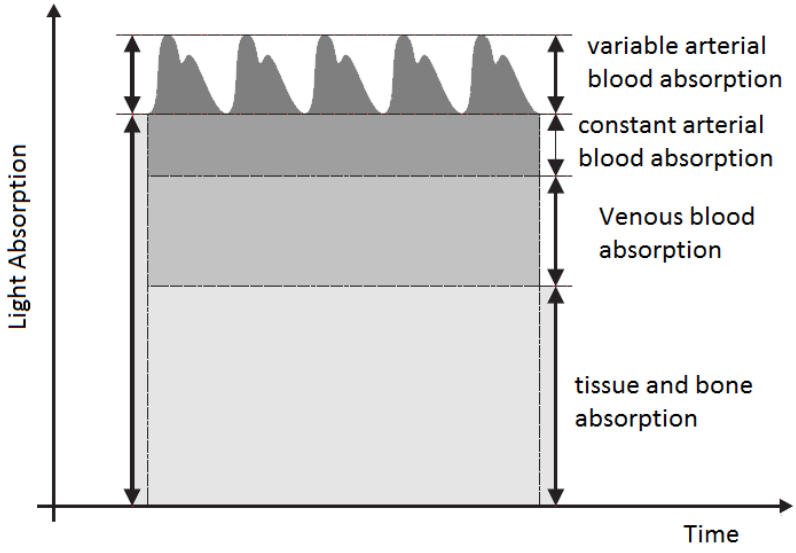

Figure 3.1: ***Absorption in PPG signal.*** *In a transmission system, the majority of the light from the LEDs is absorbed by the intermediate layer before reaching the photodetector. The absorption is divided in constant absorption of bones, tissues, venous blood and variable absorption of arterial blood. Thus the cardiac cycle induces a PPG signal which is variable in time [1].*

Photoplethysmographic (PPG) systems optically detect changes in the blood flow volume (i.e., changes in the detected light intensity due to different concentration of oxygenated hemoglobin). There are two types of system, depicted in Figure 3.2: the transmission system and the reflectance

system. In a transmission system, the light transmitted through the medium is detected by a photodetector (PD) opposite to the LED source, while in a reflectance system, the PD detects light that is back-scattered or reflected from tissue, bone and/or blood vessels [33].

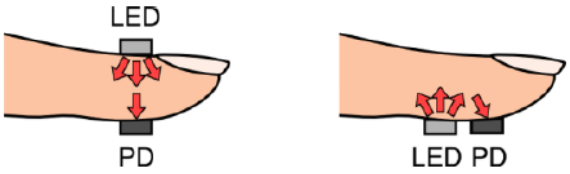

Figure 3.2: ***PPG systems.*** *There are two typologies of PPG system: the transmission system and the reflectance system. In a transmission system (left figure), the light transmitted through the medium is detected by a PD opposite to the LED source, while in a reflectance system (right figure), the PD detects light that is back-scattered or reflected from the tissues, bones and/or blood vessels [33].*

In contrast with ECG, EGM and ILP, that record the electrical activity of the heart, a PPG systems records the mechanical outcome of the ventricular ejection, similarly to a blood pressure signal. Despite the different nature of the signal in comparison with the gold standard in AF detection (ECG) and in spite of being the less spatially and temporally definite signal between the four proposed, due to the distance between the record site and the AF events, a PPG signal allows AF detection studying the waves' morphology and the pulse series extractable from the record. Moreover, the BVP signal is totally non-invasive, because it is recorded on the body surface, typically on the tip of the fingers or on the wrist. Lee et al. [20] proposed a method to detect AF using the camera of an iPhone 4S. They developed an application for the collection of a pulsatile time series followed by real-time detection of AF using the following three statistical methods: RMSSD, Shannon entropy (ShEn) and sample entropy (SampEn). AF detection performance was tested on 25 AF subjects undergoing electrical cardioversion. The beat-by-beat accuracy for each algorithm was 0.9844, 0.8494 and 0.9552, for RMSSD, ShEn and SampEn respectively, and 0.9951 with the three methods combined. Furthermore, considering the clinical objective of detecting the presence of AF episodes from a given dataset, the accuracy was 100% for all three methods. A smartphone based application has the potential to be widely accepted and widespread, thus more easily reaching asymptomatic subjects and providing clinicians with an opportunity to better treat and prevent AF complications.

Given the ever-growing popularity of smartphones, smartwatches and

smart wristbands, similar applications can provide patients and their caregivers with access to an inexpensive and easy-to-use monitor for AF detection outside of the traditional health care establishment.

3.1.5 Comparison

In Table 3.1 the non-invasivity, the accuracy and the monitoring ability of the four illustrated signals are evaluated and compared. Each type of signal (in the rows) has a mark (0=worst, 3=best) for each feature (in the columns). The color highlights the performance of each typology of signal under each aspect.

	Non-invasivity	Accuracy	Monitoring
ECG	2	2	1
EGM	0	3	2
ILR	1	2	3
PPG	3	1	3

Table 3.1: ***Comparison between heart signals for AF diagnosis.*** *In the columns the three main aspects to consider in the choice of the signals are evaluated. Each type of signal (in the rows) has a mark (0=worst, 3=best) for each feature. The color highlights the performance of each typology of signal under each aspect. The acronyms stand for: ECG=electrocardiogram, EGM=intracardiac electrogram, ILR= Implanted Loop Recorder, PPG=photoplethysmography.*

3.2 Algorithms

In literature, there are many algorithms for the detection and analysis of AF. They are divided into two major classes:

- Methods based on atrial activity analysis.
- Methods based on ventricular response analysis.

The source of atrial fibrillation is in the atrial cells and heart conduction pathway, consequently, methods based on atrial activity can convey significant diagnostic information. However, in many recorded cardiac signals, the atrial activity can be disturbed by the presence of the ventricular activity, which has a much larger amplitude, and the presence of potential noise and artifacts superimposed. Standard 12-lead ECG may not be enough to study

atrial activity, because the number of electrodes is too small and their location is not ideal for AF detection. For atrial analysis a stable, high quality signal is required, difficult to obtain in real-time long-term recordings. To conclude, although highly effective, atrial activity analysis is not the most suitable approach for an automatic screening application, since simplicity of use, global acceptance and robustness to noisy tracings are important requirements [12].

Methods based on the ventricular response, instead, are intended to capture the irregular, rapid nature of AF by exploiting the most prominent feature of cardiac signals, such as QRS peaks for ECG and systolic peaks for blood pressure signals. The ventricular response can be easily detected by non-invasive devices applied on the skin, making it a useful tool for long-term monitoring and automatic screening. The present section summarizes the state-of-art in ventricular response analysis during AF. The proposed techniques are: Lorenz plot, time domain heart rate parameters, nonlinear analysis and morphology-based analysis.

3.2.1 The Lorenz plot

The Lorenz plot (also known as Poincaré plot) is a scatter plot in which each RR interval is plotted versus the preceding one. It can distinguish AF from other atrial tachyarrhythmias such as atrial flutter where ventricular response is not as irregular as in AF [22].

Sometimes the Lorenz plot is used as a δRR scatter plot. In this case, the differences of RR intervals are plotted against the previous differences. The advantage of this scatter plot is the independence from heart rate changes. Moreover, this scatter plot takes into account three RR intervals simultaneously [17]. The δRR interval, defined as $\delta\text{RR}(i)=\text{RR}(i)-\text{RR}(i\text{-}1)$ is a measure of irregularity and the Lorenz plot encodes the uncorrelated nature of RR intervals in the direction of change of three consecutive RR intervals [30]. Each point ($\delta\text{RR}(i)$, $\delta\text{RR}(i\text{-}1)$) has magnitude and phase where the magnitude expresses the irregularity and where magnitude and phase together encode the incoherence of changes in RR intervals. Figure 3.3 shows the method to populate the Lorenz plot starting from an ECG signal. The δRR intervals are obtained from the RR intervals derived from the ECG and placed as an appropriate point in the diagram [22].

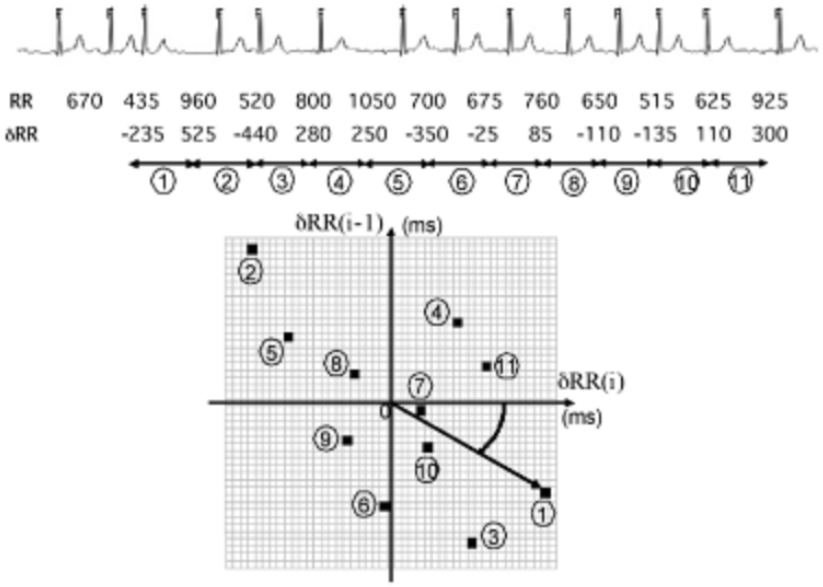

Figure 3.3: ***Lorenz diagram.*** *Illustration showing how δRR intervals are calculated and placed on the Lorenz diagram. Each point has magnitude and phase. The axes of the diagram extend from -600 to +600 ms [22].*

The clusters of points in a Lorenz plot are characteristic signatures of ventricular rhythms. Examples of ECG signals during AF and AT and the respective Lorenz plot are depicted in Figure 3.4 [22, 30].

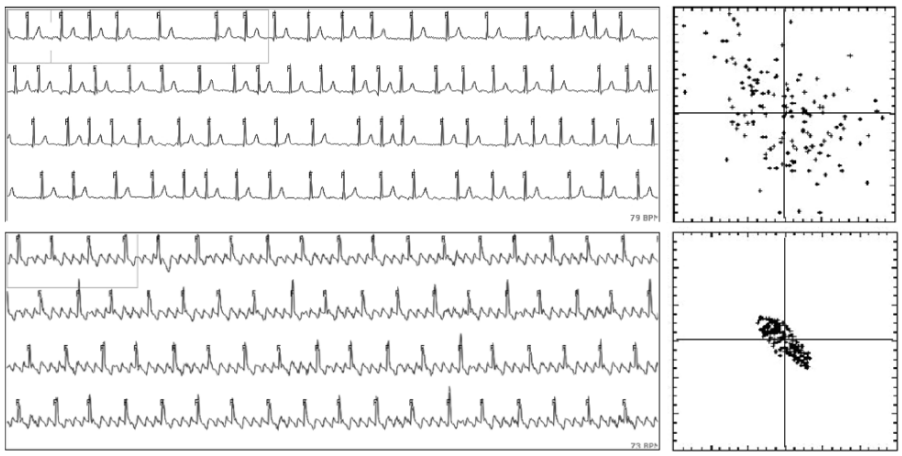

Figure 3.4: ***Examples of Lorenz plot in AT/AF patients.*** *Two ECG examples during AF/AT and the corresponding Lorenz plot of δRR intervals. The first signal shows AF behavior in a 2-minutes segment, the second one the behavior of atrial flutter [30].*

In Figure 3.5(a) the Lorenz plot is illustrated as a two-dimensional his-

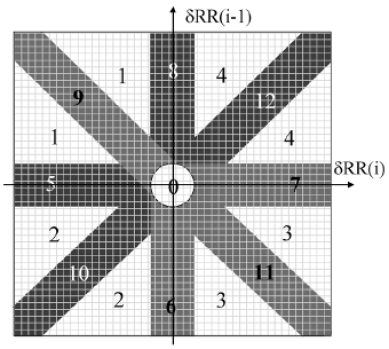

(a)

Segments	Sequence	δRR Values
0	SSS/LLL	$\lvert\delta RR\rvert <$ NSRmask
1	S-L-S	$\lvert\delta RR(i-1)\rvert \neq \lvert\delta RR(i)\rvert$
2	L-M-S	$\lvert\delta RR(i-1)\rvert \neq \lvert\delta RR(i)\rvert$
3	L-S-L	$\lvert\delta RR(i-1)\rvert \neq \lvert\delta RR(i)\rvert$
4	S-M-L	$\lvert\delta RR(i-1)\rvert \neq \lvert\delta RR(i)\rvert$
5	L-L-S	One $\lvert\delta RR\rvert <$ NSRmask
6	L-S-S	One $\lvert\delta RR\rvert <$ NSRmask
7	S-S-L	One $\lvert\delta RR\rvert <$ NSRmask
8	S-L-L	One $\lvert\delta RR\rvert <$ NSRmask
9	S-L-S	$\delta RR(i-1) \cong -\delta RR(i)$
10	L-M-S	$\delta RR(i-1) \cong \delta RR(i)$
11	L-S-L	$\delta RR(i-1) \cong -\delta RR(i)$
12	S-M-L	$\delta RR(i-1) \cong \delta RR(i)$

(b)

Figure 3.5: ***Lorenz plot.*** *(a) The 2-D histogram, a numeric representation of the Lorenz plot of δRR intervals. 13 segments are marked on the plot, denoting regions that would be populated by points for different sequences of RR intervals as tabulated in (b). S, M, L stand for Short, Medium and Long respectively.* NSRmask *is the radius of segment 0 and has a nominal value of 80 ms [30].*

togram. The histogram is divided in 13 segments, populated as shown in Figure 3.5(b). For example, segments 1 and 9 have a RR sequence of a short interval followed by a long interval followed by a short interval (S–L–S). Segment 1 is populated when $|\delta RR(i)| \neq |\delta RR(i-1)|$ whereas segment 9 is populated when $|\delta RR(i)| \approx |\delta RR(i-1)|$ [22, 30]. The width of segment 9, equal to the width of segment 0 defined by the parameter *NSRmask*, accounts for the variation due to autonomic modulation of the AV-node.

In NSR subjects, the majority of points are within segment 0, as depicted in Figure 3.6(a). During AF, instead, the points are randomly distributed across all the segments (Figure 3.6(f)) given the lack of correlation between the current RR interval and the next one. Other rhythms, neither NSR nor AF, exhibit specific signatures in the Lorenz plot as shown in Figure 3.6(b-e). Figure 3.6(b) shows the distribution during a series of premature atrial contractions leading to irregular RR intervals but with a different behavior compared to the AF/AT one. Figure 3.6(c-e) shows different degrees of organization of ventricular response during AT with the most regular in (c), "group beating" in (d), and irregular like AF in (e). During AT, segments 0, 6, 7, 9, and 11 are most often populated [30].

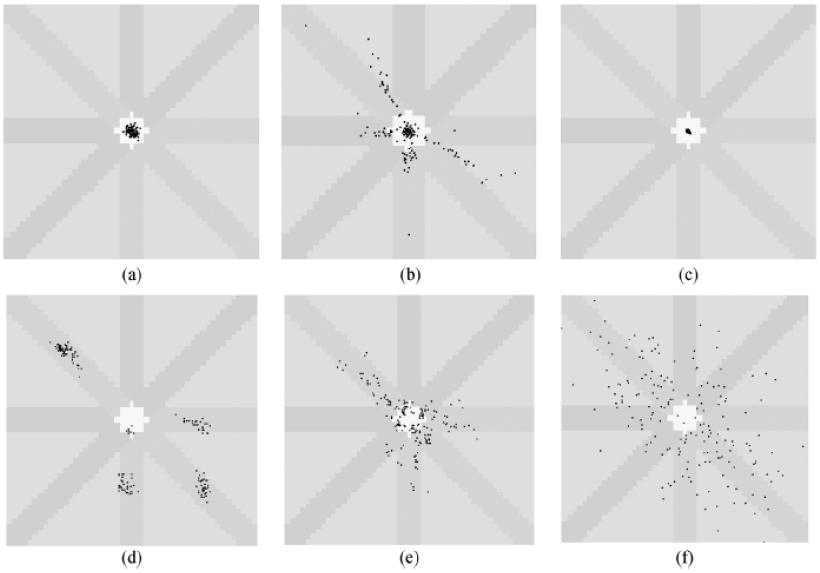

Figure 3.6: ***Cardiac rhythm and Lorenz plot.*** *Lorenz plot of δRR intervals overlaid on the segmented 2-D histogram for 2 minutes of data during (a) normal sinus rhythm, (b) series of premature atrial contractions, (c) atrial tachycardia (AT) with regular ventricular response, (d) AT "group beating", (e) AT with irregular ventricular response, and (f) atrial fibrillation. The plots exhibit various forms of irregularity in ventricular response. The Lorenz plot axes extend from -600 ms to +600 ms and the* NSRmask *value is 80 ms [30].*

The AF/AT detector proposed by Sarkar et al. [30] uses a number of metrics to encode the information regarding patterns in the distribution of (δRR(i), δRR(i-1)) in a Lorenz plot over a period of 2 minutes.

Irregularity evidence (denoted $\mathcal{L}_{IE}$) measures the sparseness of the distribution of (δRR(i), δRR(i-1)) and is defined as

$$\mathcal{L}_{IE} = \sum_{k=1}^{12} B_k \tag{3.1}$$

where B_k denotes the number of histogram bins in segment k of the Lorenz histogram that are populated by at least one point. This metric has higher values during AF (Figure 3.6(f)) and lower values during NSR (Figure 3.6(a)).

Regularity evidence ($\mathcal{L}_{RE}$) is the number of 6-beat and 12-beat RR medians that are not different by more than 10 ms from the RR interval median of the previous 2-minutes period.

Density evidence ($\mathcal{L}_{DE}$) measures the density of (δRR(i), δRR(i-1)) in

a cluster as

$$\mathcal{L}_{DE} = \sum_{k=5}^{12}(P_k - B_k) \tag{3.2}$$

where P_k denotes the number of points that populate segment k. This metric has higher values when multiple points populate the same bin in segments 5-12 as in the case of AT with ventricular "group beating" (Figure 3.6(d)).

Anisotropy evidence ($\mathcal{L}_{AE}$) measures the orientation of the distribution (δRR(i), δRR(i-1)) as

$$\mathcal{L}_{AE} = \left| \sum_{k=9,11} P_k - \sum_{k=10,12} P_k \right| + \left| \sum_{k=6,7} P_k - \sum_{k=5,8} P_k \right| \tag{3.3}$$

This metric has higher values if the points densely populate segments 6, 7, 9 and 11 as in case of AT with irregular ventricular response (Figure 3.6(d-e)).

Premature atrial contraction evidence ($\mathcal{L}_{PE}$) measures the presence of a dense distribution in segments 1-4 which is a characteristic of compensatory pauses,

$$\mathcal{L}_{PE} = \sum_{k=1}^{4}(P_k - B_k) + \sum_{k=5,6,10}(P_k - B_k) - \sum_{k=7,8,12}(P_k - B_k) \tag{3.4}$$

This behavior is illustrated in (Figure 3.6(b)).

AF evidence ($\mathcal{L}_{AFE}$) and *AT evidence* ($\mathcal{L}_{ATE}$) quantify the degree to which the Lorenz plot suggests the presence of AF and AT, respectively, computed as

$$\mathcal{L}_{AFE} = \mathcal{L}_{IE} - \mathcal{O} - 2\mathcal{L}_{PE} \tag{3.5}$$

$$\mathcal{L}_{ATE} = \mathcal{L}_{IE} + \mathcal{L}_{AE} + \mathcal{L}_{DE} + \mathcal{L}_{RE} - 4\mathcal{L}_{PE} \tag{3.6}$$

where $\mathcal{O}$ denotes the number of points in the bin containing the origin.

Organization index ($\mathcal{L}_{OI}$) quantifies the degree of organization in an atrial arrhythmia by evaluating the degree of organization in the ventricular response,

$$\mathcal{L}_{OI} = \mathcal{O} + \mathcal{L}_{RE} + \mathcal{L}_{AE} + \mathcal{L}_{DE} - 2\mathcal{L}_{IE} \tag{3.7}$$

The detector uses these metrics to assess the presence of AT, AF or NSR each 2 minutes. Two modalities are present: "AT/AF mode" which detects AF and AT based on irregular ventricular response by comparing $\mathcal{L}_{AFE}$ to

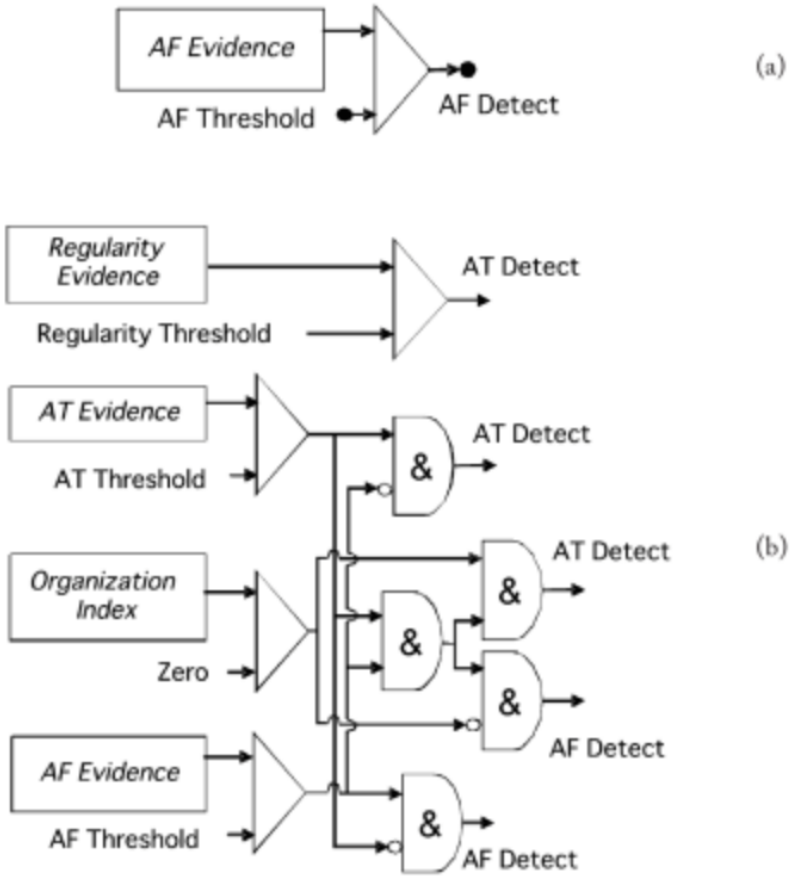

Figure 3.7: ***Logic of the Lorenz plot detector.*** *The logic used to assess the state of the detector over a 2-minutes period in AT/AF mode (a) and supplemental AT detector (b) [22].*

a previously set threshold (Figure 3.7(a)) and the "supplemental AT mode", in which AT and AF are detected with a series of different comparisons with various thresholds (Figure 3.7(b)). This mode allows the detection of AT with "group beating" and regular ventricular response [30, 22].

Sarkar demonstrated that the detector had good performances in AT/AF mode and that it was able to compute AF/AT burden (hours per day) accuracy within 20% of true burden in 96% of patients. The AF/AT detector underestimated AT burden, thus degrading performance, in patients with significant amounts of AT with more regular ventricular response. To improve performance, the supplementary AT detector was introduced, reducing the underestimation of AT while overestimating burden.

This type of detector is computationally simple enough to be easily im-

plemented in an implantable monitoring device for accurate long-term AF monitoring. This allows the continuous evaluation of "rhythm control" strategy, particularly in patients with asymptomatic and paroxysmal AF/AT. Furthermore, efficacy of "rate control" therapies can be measured accurately by evaluating the ventricular rate for the entire duration of AF.

3.2.2 Time domain parameters

Time domain analysis of AF usually includes the standard deviation of RR intervals (SD), the root mean square differences of successive RR intervals (RMSSD), the coefficient of variation (CV) and the percentage of differences of successive RR intervals greater than 50ms (pNN50).

For a RR time series made of N intervals, the standard deviation is defined as:

$$SD = \sqrt{\frac{1}{N-1}\sum_{i=1}^{N}|RR_i - \mu|^2} \tag{3.8}$$

where μ is the mean of the RR series.

SD and RMSSD are time-domain tools used to assess heart rate variability. The root mean square of the successive differences is defined as:

$$RMSSD = \sqrt{\frac{1}{N-1}\sum_{i=2}^{N}|RR_i - RR_{i-1}|^2} \tag{3.9}$$

As subjects have different mean heart rates, RMSSD is usually normalized by the mean value of the RR time series (nRMSSD).

The coefficient of variation (CV), also known as relative standard deviation (RSD), is a standardized measure of dispersion. It is defined as the ratio of the standard deviation divided by the mean μ (or its absolute value, $|\mu|$):

$$CV = \frac{SD}{\mu} \tag{3.10}$$

SD, nRMSSD, CV and pNN50 are used to quantify beat-to-beat variability. Since AF exhibits higher variability than NSR, these metrics can be used to detect AF when higher than a previously fixed threshold [20].

3.2.3 Entropy

Approximate entropy, *ApEn*, is a measure of signal randomness. It represents the likelihood that similar patterns of observations will not be followed by other similar observations. When there are many similar values in a time

series *ApEn* will be small; a less predictable and more complex process has a greater *ApEn*. Given N points, the *ApEn*(m, r, N) is approximately equal to the negative average natural logarithm of the conditional probability that two sequences that are similar for m points remain similar, that is, within a tolerance r, at the next point [29]. *ApEn* is defined as

$$ApEn(m, r, N) = \ln\left[\frac{C_N^m(r)}{C_N^{m+1}(r)}\right] \tag{3.11}$$

where C_N^m expresses the prevalence of repetitive patterns of length m in the series.

ApEn algorithm counts each sequence as matching itself to avoid the occurrence of ln(0) in the calculations. This step has led to the discussion of the bias of *ApEn* [29]. Therefore a new family of statistics, called sample entropy (*SampEn*) has been developed. Theoretically, *SampEn* reduces the bias of *ApEn* by avoiding counting self-matches, it can be used on shorter series and it is more consistent than *ApEn*. Additionally, *SampEn* is easier to compute [3].

Given N points, *SampEn*(m, r, N) is the negative natural logarithm of the conditional probability that two sequences similar for m points remain similar at the next point within a tolerance r, where self-matches are not included in calculating the probability. Therefore a lower value of *SampEn* also indicates more self-similarity in the time series [29].

Formally, given N data points from a time series $\{x(n)\} = x(1), x(2), ..., x(n)$, *SampEn* can be computed as follows [29] [3]:

1. Vector sequences of size m, $\mathbf{X}_m(1), ..., \mathbf{X}_m(N - m - 1)$ are formed, defined by $\mathbf{X}_m(i) = \{x(i), x(i + 1), ..., x(i + m - 1)\}$, for $1 \leq i \leq N - m + 1$. These vectors represent m consecutive x values, starting with the i-th point.

2. The distance between vectors $\mathbf{X}_m(i)$ and $\mathbf{X}_m(j)$, $d[\mathbf{X}_m(i), \mathbf{X}_m(j)]$ is defined as the absolute maximum difference between their scalar components:

$$d[\mathbf{X}_m(i), \mathbf{X}_m(j)] = \max_{k=0,...,m-1}(|x(i + k) - x(j + k)|)$$

3. For a given $\mathbf{X}_m(i)$, the number of $j(1 \leq j \leq N - m, j \neq i)$ is counted and denoted as B_i, such that the distance between $\mathbf{X}_m(i)$ and $\mathbf{X}_m(j)$ is less than or equal to r. Then, for $1 \leq i \leq N - m$:

$$B_i^m(r) = \frac{1}{N-m-1} B_i$$

4. $B^m(r)$ is defined as

$$B^m(r) = \frac{1}{N-m} \sum_{i=1}^{N-m} B_i^m(r)$$

5. The dimension is increased to $m+1$ and A_i is calculated as the number of $\mathbf{X}_{m+1}(i)$ within r of $\mathbf{X}_{m+1}(j)$ where j ranges from 1 to $N-m$ ($j \neq 1$). Then, $A_i^m(r)$ is defined as

$$A_i^m(r) = \frac{1}{N-m-1} A_i$$

6. $A^m(r)$ is set as

$$A^m(r) = \frac{1}{N-m} \sum_{i=1}^{N-m} A_i^m(r)$$

Thus, $B^m(r)$ is the probability that two sequences will match for m points, whereas $A^m(r)$ is the probability that two sequences will match for $m+1$ points. Finally, *SampEn* can be defined as

$$SampEn(m,r) = \lim_{N\to\infty} \left\{ -\ln \left[\frac{A^m(r)}{B^m(r)} \right] \right\} \tag{3.12}$$

which is estimated by the statistic

$$SampEn(m,r,N) = -\ln \left[\frac{A^m(r)}{B^m(r)} \right] \tag{3.13}$$

SampEn or *ApEn* analysis on the RR interval series could be useful to assess randomness of RR time series. AF presents an apparent total irregularity of ventricular rhythm so higher values of entropy could be used to detect AF [20]. Furthermore, a reduction in *ApEn* [29] or *SampEn* [34], indicating a decreased heart rate complexity, is considered a sign of altered heart rate dynamics useful to predict AF episodes: a significant decreasing trend in RR interval entropy over time towards the onset of AF has been observed by Tuzcu et al. [34]. Also *ApEn* has been found to have a prognostic value in patients with chronic AF, with lower values of ventricular irregular response predicting an adverse prognosis for cardiac death, but not fatal stroke [42].

3.2.4 Shannon entropy

Shannon entropy (*ShEn*) is widely used as a measure of dispersion and structure complexity of a series [31]. *ShEn* is formally defined as the average value of the logarithms of the probability density function:

$$ShEn = -\sum_{i=1}^{M} p(i) \ln p(i) \tag{3.14}$$

where M is the number of discrete values the considered variable can assume and $p(i)$ is the probability of assuming the i-th value.

Shannon entropy is conceptually different from measures of variability (as variance) that quantify the magnitude of deviation from a mean value, since it quantifies the intrinsic unpredictability of an event series [24]. *ShEn* has been used to quantify the synchronization of fibrillation signals recorded by a basket catheter in the right atrium [24]. Gokana at al. [15] proposed an AF detection method based on ECG signals composed by three steps: firstly they computed the RMSSD of the RR intervals extracted from a 24 hours ECG recording to find whether an arrhythmia had occurred; secondly they applied the autocorrelation of the squared signal to precisely determine the start time and stop time of the arrhythmic episode; finally, they computed the Shannon entropy from the start to the stop time extracted at the previous step to discern AF from other types of arrhythmia. Since an ECG segment containing AF episodes is expected to have a higher value of *ShEn*, due to the uncertainty to predict the patterns of the signal, they compared the *ShEn* with a previously fixed threshold, detecting AF with up to 99.5% accuracy in time resolution. A similar method has been implemented by Lee et al. [20] using a photoplethysmographic signal.

3.2.5 Morphology-based analysis

Morphological analysis of heart activity during AF could supply significant information about AF organization and the mechanisms behind it. During AF, refractoriness, conduction velocity and atrial tissue heterogeneity cause different kinds of electrical activation that determine variations in the observed morphology. Nevertheless, the majority of the methods do not perform direct analysis of morphologic feature of cardiac activation signal, or perform it after significant manipulation of the signal [22]. The first morphological study of an endocardial recording was performed by Wells et al. [37], and provided qualitative criteria to classify different episodes of arrhythmia through visual electrogram scoring from right atria bipolar electrograms recorded after open-heart surgery. The manual classification

of AF episodes according to Wells' criteria is widely used, in spite of its limitations: it is time consuming and can lead to results neither objective nor reproducible [22]. Barbaro et al. [8] developed an automatic classification scheme in accordance with Well's criteria to obtain more quantitative and objective measures.

Another possible approach to the morphological analysis was provided by Faes et al. [14] evaluating AF organization based on the analysis of the variations in morphology of the atrial activation waves. Faes proposes an algorithm that compares pairs of local activation waves (LAWs) on bipolar electrograms recorded in human atria during AF to compute a regularity index ρ which measures the extent of repetitiveness over time of its consecutive activation waves.

For an atrial recording in which N atrial activations are detected, LAWs are defined as signal windows of p samples centered on the atrial activation instants. To prevent the amplitude of the LAWs from affecting the regularity index, the normalized LAWs are computed and used.

$$\boldsymbol{s}_i = \frac{\boldsymbol{x}_i}{||\boldsymbol{x}_i||} \tag{3.15}$$

Thus the new LAWs $\{\boldsymbol{s}_i, ..., \boldsymbol{s}_N\}$ can be seen as points belonging to the p-dimensional unitary sphere. The morphological dissimilarity between two normalized LAWs can be evaluated by using the standard metric of the sphere to compute their distance:

$$d(\boldsymbol{s}_i, \boldsymbol{s}_j) = arccos(\boldsymbol{s}_i^T \cdot \boldsymbol{s}_j) \tag{3.16}$$

The regularity index, $\rho(r)$, is then defined by calculating the relative number of similar pairs of LAWs in the endocardial recording as:

$$\rho(r) = \frac{2}{N(N-1)} \sum_{i=1}^{N} \sum_{j=i+1}^{N} \Theta(r - d(\boldsymbol{s}_i, \boldsymbol{s}_j)) \tag{3.17}$$

where N is the number of LAWs, Θ the Heaviside function and r a threshold below which two analyzed LAWs are considered similar.

The index proposed by Faes et al. shows maximum regularity ($\rho = 1$) for all atrial flutter episodes and decreases significantly with increasing AF complexity as defined by Wells. The ability to characterize different AF episodes was assessed by designing a classification scheme based on a minimum distance analysis, obtaining an accuracy of 85.5%.

A measure of organization of AF electrograms highly sensitive to changes in wave morphology could help investigate disturbances in the conduction

pattern and, in case of a multi-site evaluation of the spatial distribution of AF organization, it could constitute an effective support to the treatment of AF. Indeed, the real-time evaluation of the spatial distribution of AF regularity may guide the definition of the optimal ablative pathway [14, 22]. Moreover, the ability of the proposed index to evaluate beat-by-beat changes in AF complexity indicates the possibility to follow dynamic changes of AF pattern and to study the atrial remodeling. Such information should be useful to determine the optimal moment for the treatment of AF.

Faes applied this method on bipolar electrograms recorded in human atria, but this kind of evaluation can be implemented also for other typologies of signals, such as ECG (superficial and subcutaneous) or PPG. This because an alteration in wave morphology due to AF can also be witnessed in electrical signals recorded far from the heart and in blood volume pulse signals.

Chapter 4

Experimental protocol and signal preprocessing

4.1 Study population

We recorded 70 subjects, recruited from hospitalized patients at Ospedale Maggiore Policlinico in Milan, Italy. Among the recorded patients, 30 are affected by atrial fibrillation, 31 are healthy subjects and 9 suffer from other arrhythmias; the measurement protocol and classification for all patients has been performed by cardiologists at Ospedale Maggiore Policlinico; all data were recorded between March and November 2015. As for the gender of the subjects, 36 recorded patients are male and 34 are female. The gender distribution for the three classes of patients can be seen in the following bar graph (Figure 4.1).

The age of recorded patients ranges from 21 to 93 years, the statistical distribution is displayed in the following boxplots (Figure 4.2).

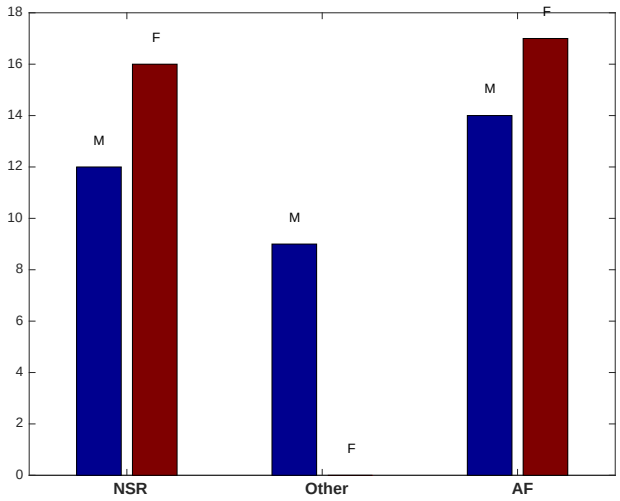

Figure 4.1: ***Population gender.*** *Statistical distribution of the subjects' gender between the AF, NSR and "other arrhythmia" categories.*

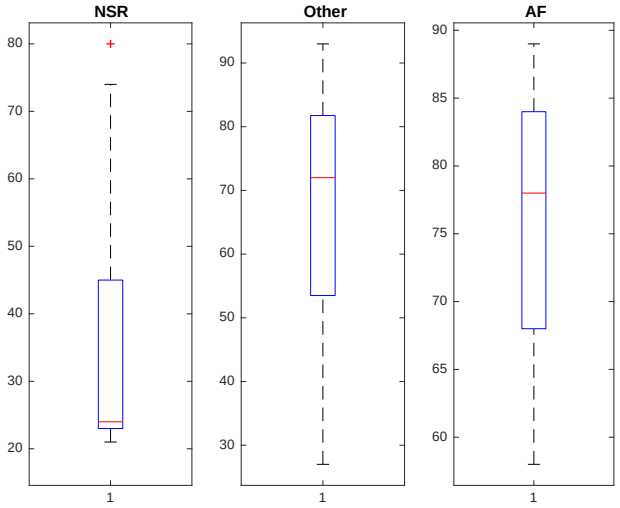

Figure 4.2: ***Population age.*** *Statistical distribution of the subjects' age between the AF, NSR and "other arrhythmia" categories.*

Among recorded patients, one of them displayed a BVP signal with a behavior that changes alternatively between AF and NSR: such patient is said to be in *paroxysmal* AF, a condition in which AF occurs occasionally and then stops, with episodes that can last from minutes to days before

returning to normal sinus rhythm. Such patient was discarded from our analysis because the acquired signal, along with its statistical indexes, is not representative neither of the NSR category nor of the AF class.

4.2 Data acquisition protocol

A standard protocol for data recording was defined; the setting of a uniform acquisition procedure allows us to control the use of the device, ensuring that it is applied in the optimal way to enhance signal quality.

The patient is supposed to remain in steady state for the whole process, in order to reduce motion artifacts as far as possible; to simplify this task, the subject has to lie down on his back during the acquisition, while the physician takes care of the measurements. While the patient lays in a relaxed position, the Empatica E4 wristband is applied on the wrist of the non-dominant arm, with the main part of the device facing upward, in a similar way to a regular wrist watch (Figure 4.3); then, the device is activated, and after a short time required for initialization, it starts collecting data from the patient.

Figure 4.3: ***E4 wristband applied.*** *E4 wristband on the patient's wrist during acquisition.*

Ten minutes after activation, the device is turned off and later removed from the patient; we therefore acquired 10 minute segments for all patients. It was decided to maintain a standard duration for all our measurements,

because some of the indexes evaluated from the signal can vary in relation to this parameter.

Though relatively simple, the correct execution of this protocol, both by the physician and the patient, is a strongly determinant factor for signal quality and, as a consequence, for a correct employment of diagnostic algorithms: an excessive movement of the patient or other procedural errors can induce significant artifacts and distortions in the signal.

4.2.1 Empatica wristband

The Empatica E4 wristband, used to record the BVP signals of the patients, is a wearable wireless device designed for continuous, real-time data acquisition in daily life.

The device is equipped with sensors for the registration of different signals, including bio-signals: an Electrodermal Activity Sensor (EDA), an infrared thermopile, a 3-axis accelerometer and, fundamental to this study, a photoplethysmographyc (PPG) sensor which measures the blood volume pulse (BVP) signal. The BVP is sampled at 64 Hz, with 12-bit resolution. The device is not an invasive instrument, and is worn like a regular wrist watch, without causing discomfort to the patient, not even after prolonged acquisitions [40].

Figure 4.4: ***E4 wristband.*** *The Empatica E4 device*

4.3 Signal preprocessing

The raw photoplethysmographic signal must be preprocessed before it is analyzed by diagnostic algorithms.

The preprocessing of the signal can be divided in two phases: noise detection and peak detection.

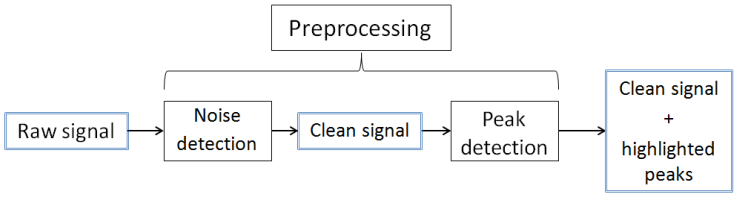

Figure 4.5: ***Phases of signal preprocessing.*** *The preprocessing is divided in noise detection and peak detection; the two phases are sequential. In the end a clean signal and the peaks extracted from it are obtained.*

The first preprocessing phase is the detection and removal of noise: the raw PPG is often disturbed , mainly due to movement artifacts, which are caused by the patient rapidly moving the device during the measurement; therefore, it is necessary to isolate the intervals disturbed by noise, and then to eliminate them.

The second phase in signal preprocessing is about the detection of important points in the signal: an algorithm is used to recognize the distinct heart cycles of the BVP, then significant features in each cycle are identified, like specific maxima and minima; data about the time instants of the maxima and minima are later used in the classification of the patient.

4.3.1 Noise detection

As mentioned earlier, it is fundamental to suppress the interference caused by movement artifacts; any significant movement of the device on the patient's wrist can critically distort the acquisition (Figure 4.6); in order to counter that, accelerometric data collected by the device are analyzed.

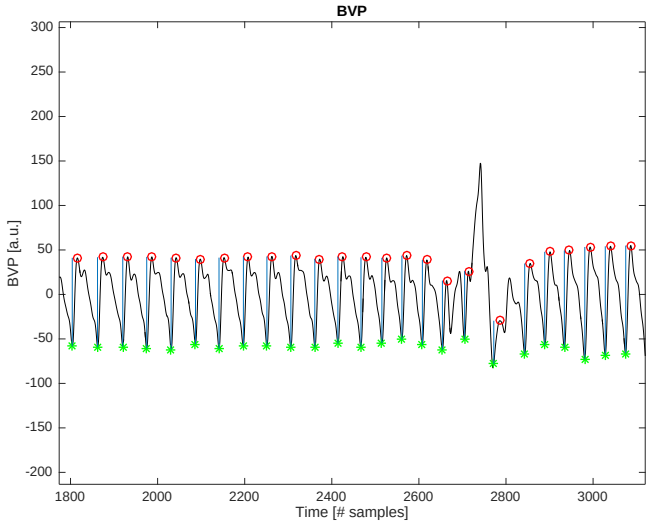

Figure 4.6: ***Disturbed signal.*** *Example of significant signal distortion due to movement noise in a healthy subject.*

The Empatica E4 wristband features a tri-axial accelerometer, which operates synchronously with the photoplethysmograph employed for blood volume pulse recording. Since signal distortion is proportional to the mobility of the device (Figure 4.7), data from the accelerometer are used to decide which signal portions have to be discarded.

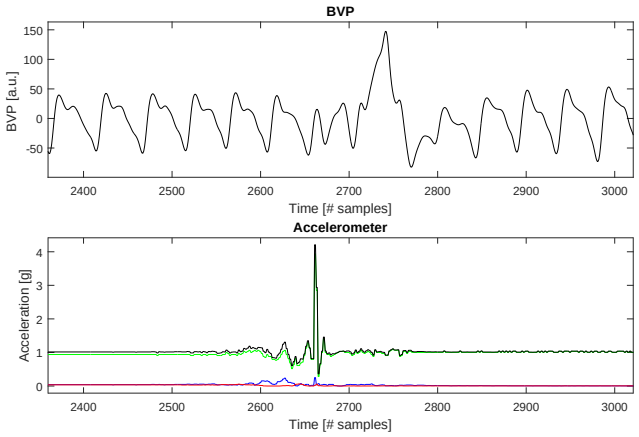

Figure 4.7: ***Disturbed signal and accelerometric data.*** *The noise distortion in the signal (above) is plotted together with accelerometer data (below), each colored line shows the acceleration on one of the three axes of the accelerometer, while the black line shows the norm of the acceleration; it can be seen that the distortion in the BVP signal happens right after a significant acceleration has been recorded.*

To operate an automatic cleansing of the acquisition it is established that, when acceleration is too high, the signal interval is classified as disturbed and then cleared.

In order to evaluate the global movement in a three-dimensional space, the norm of the accelerations on the three axes is computed (the black line in Figure 4.7, below), and the deviation from the acceleration of gravity g is calculated. The absolute value of the deviation is then compared to a threshold, and when it is exceeded, the algorithm classifies the signal as disturbed by noise; the signal interval identified is then zero padded, in this way the acquisition disturbed by noise is substituted with flat signal segments.

The absolute value of the deviation from g above which the signal is considered distorted is set empirically, choosing a value low enough to trigger the detection of significant distortions, and also high enough to ignore the intervals which are only slightly affected by noise. The threshold is set to $0.07g$.

4.3.2 Peak detection

The second step of signal processing is the detection of systolic peaks and diastolic minima in the blood volume pulse recording.

The BVP is a deterministic quasi-periodic signal, which means it has a generally recognizable shape that is repeated from the beginning to the end, in a similar way as the typical ECG signal; for each cycle, we can identify significant points in time, which represent different moments of the cardiac cycle (Figure 4.8).

An algorithm was developed in order to automatically identify such characteristic points of the signal. The diastolic minima can be classified as the local minima which are found at the ends of a complete cycle, while the systolic peaks are identified as the first and generally highest maxima of each cardiac cycle.

The first step of the algorithm is the detection of the diastolic minima; to find them, a 1-D convolution is performed between the BVP signal and a kernel; the kernel is a mono dimensional vector which extends in time for 0.3594 seconds and has the same function as an averaging filter, thus acting on the signal as a low-pass filter.

After the convolution, a smoothed version of the original BVP is obtained (Figure 4.9, below), the shape of which shows distinct waves for each cardiac cycle in the original signal. Cutting the high frequency content allows a better discrimination of the end of every cycle: each wave is limited by

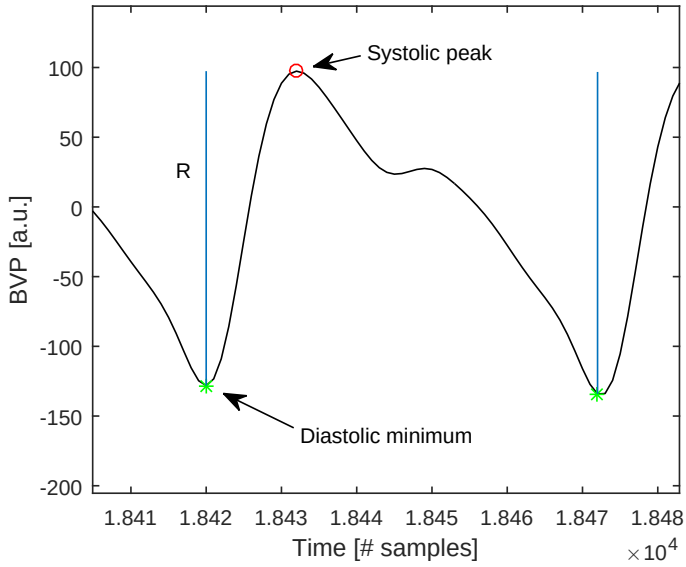

Figure 4.8: ***Peak detection.*** *The BVP signal is shown with highlighted peaks and minima, labeled after their equivalent in the pulse pressure signal; the systolic peak is associated to the contraction phase of the cardiac cycle, while the diastolic minimum is linked to the refill of the heart; they represent opposite phases of the cycle.*

two low regions at both sides, so in order to locate them the algorithm searches for local minima; after this process, the algorithm searches for the lowest minimum in the original signal in a 0.2 seconds neighborhood of every minimum previously detected in the filtered signal; the new time instants that are found represent the diastolic minima (Figure 4.9, above).

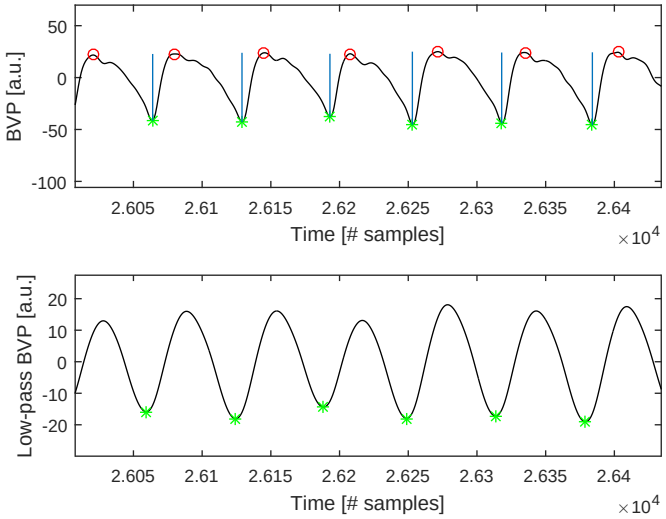

Figure 4.9: ***Diastolic minima detection.*** *The bottom figure shows the low-pass signal in which minima can be better identified; the true diastolic minima are found later in the original signal above, by searching the lowest point in a short time interval centered in the minimum of the filtered signal.*

To automatically locate the systolic peaks, first the algorithm searches and saves every local maximum in the BVP signal, then, using the information of all the diastolic minima previously found, it identifies as a systolic peak the first local maximum after each diastolic minimum, with the restriction that there can be only one peak for every cycle (Figure 4.9, above); all the other local maxima previously found are discarded.

4.3.2.1 Inter-systolic intervals

An important information which is obtained from knowing the time instants of each systolic peak is the inter-systolic interval (ISI). This value represents the time interval between one systolic peak and the previous one, and it can be compared to the better known RR interval, which is obtained in the electrocardiogram; this interval gives us information about the heart rate of the subject from beat to beat.

By knowing the ISIs, it is possible to study their progression in time and relative statistical features, such as the variance, and correlate them to a pathological heart function; many of the diagnostic indexes in literature are based solely on the ISI or on other data derived from it.

4.3.2.2 Inter-diastolic intervals

The inter-systolic intervals are not always a robust method to quantify the heart rate [13]: the automatic recognition of the systolic peak can be erratic when wave morphology is not very clear (Figure 4.10), as a consequence the ISI series obtained becomes unreliable, making it necessary to use other approaches for heart rate estimation.

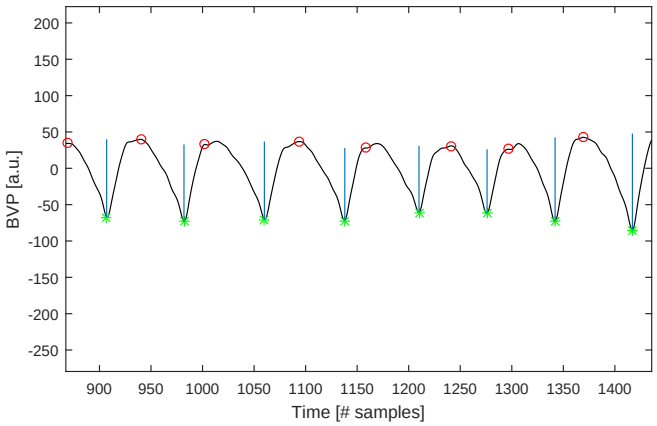

Figure 4.10: ***Variability of the sistolic peak.*** *With certain acquisitions, the shape of every heart cycle is not definite, making identification of the systolic peak unclear; from wave to wave, the BVP peak is shifted in time.*

Another possible marker of each heart cycle is the diastolic minimum: it indicates the beginning of every period, is more stable than the systolic peak and it is easily recognizable even when BVP waves are distorted (Figure 4.10).

From the diastolic minima, it is possible to calculate the inter-diastolic intervals, in the same way as the ISIs are obtained; the inter-diastolic intervals, from now on simply referred to as *intervals* (I), can be used to evaluate the heart rate exactly like the ISIs series, with the advantage of being a more stable measure; as a consequence, in this study it was decided to employ the I, instead of the ISIs as a mean of heart rate estimation.

4.3.2.3 Additional information

Other information is also calculated and memorized for each heart cycle: along with the time of the systolic peak and diastolic minimum and the inter-systolic and inter-diastolic interval with respect to the previous beat, the algorithm also saves the BVP values of the systolic peak and dias-

tolic minimum and calculates the delta between the two, which in the pulse pressure signal would represent the pulse pressure of the beat (Figure 4.11).

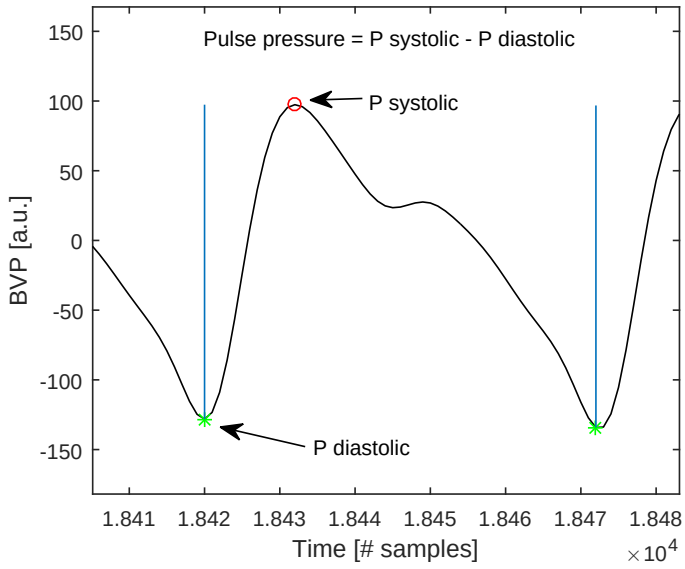

Figure 4.11: ***BVP Characteristics.*** *In the blood pressure signal, pulse pressure for a certain beat is calculated as the delta between systolic and diastolic pressure.*

Chapter 5

Measures and results

This chapter describes the calculation of diagnostic indexes, which are later used by a decision making system to classify the patient's health status.

5.1 Spectral analysis

Spectral analysis has not been consistently performed in clinical AF assessment because of the difficulty to interpret the huge number of spectral peaks [22]. In this study, instead, the very absence of clear peaks in the pathological signal is used to discriminate between NSR and AF patients. The spectral analysis is performed on both the BVP signal and the intervals series.

5.1.1 BVP spectral analysis

The analysis of the power spectrum yields many information about the BVP signal. The operation uses the matlab function *plomb*, which produces the Lomb-Scargle power spectral density (PSD) estimate of a signal; the choice to use the Lomb-Scargle PSD estimate is due to the fact that this method can handle a signal in which interruptions are present, such as the BVP we are analyzing, in which there are missing samples after the previous elimination of noisy periods (Figure 5.1).

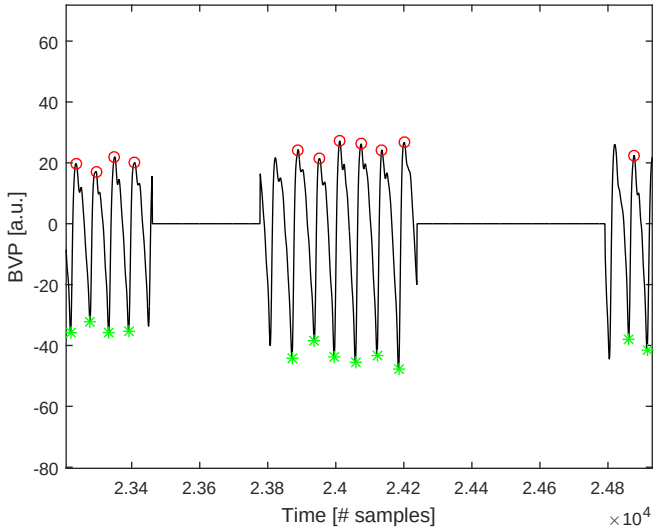

Figure 5.1: ***Signal example.*** *The BVP signal is zero padded in the periods disturbed by movement noise, such regions are empty and do not contain any information, therefore the PSD estimation must be performed with a method that can analyze discontinuous data, such as the Lomb-Scargle PSD estimate.*

The BVP of a healthy individual generally is a predictable and repetitive signal, thus the expected signal for a healthy subject is quasi-periodic and, consequently, has a frequency content concentrated in a few frequencies, mainly around the heart rate and its harmonic; instead, the signal from an AF patient is expected to be much more irregular, with a power spectrum spreading on many different frequencies.

An example is shown in Figure 5.2: the subject affected by atrial fibrillation (Figure 5.2, left) has a much broader frequency distribution than the healthy subject (Figure 5.2, right).

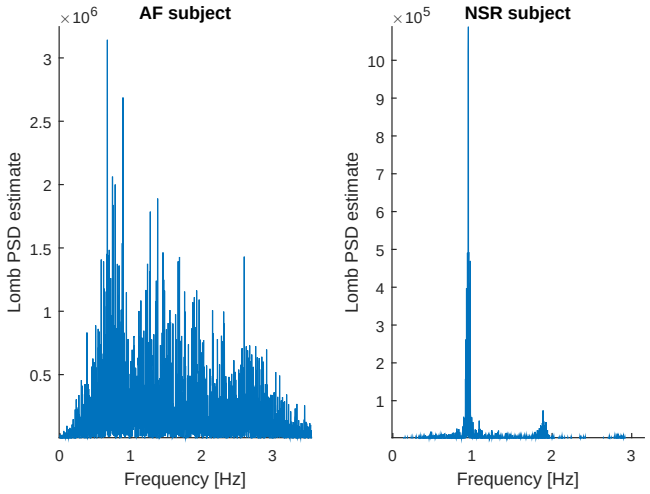

Figure 5.2: ***Power spectra comparison.*** *The PSD of BVP signal in a subject with normal sinus rhythm (right) is mainly focused around the heart rate, while the typical AF patient (left) has a wider PSD distribution.*

In order to quantify this information from the PSD graphs into a single diagnostic index, we calculate the *peak density* (PD) parameter.

The *peak density* is computed as the ratio between the integral of the PSD in a band around the dominant frequency peak (f_D) and the overall PSD of the signal:

$$PD = \frac{\int_{f_D-\Delta f}^{f_D+\Delta f} S_{BVP}(\omega)\,\mathrm{d}\omega}{\int_0^{f_S} S_{BVP}(\omega)\,\mathrm{d}\omega} \tag{5.1}$$

where $S_{BVP}(\omega)$ is the PSD of the BVP signal, Δf= 6.1 mHz and f_S is the sampling frequency.

This parameter is a rather simple way to understand whether the spectrum is broad or narrow around the dominant peak. The distribution of this index in our population is shown in Figure 5.3; higher values are observed for healthy subjects; this happens because their spectra are generally highly focused around the heart rate, while the power spectrum for AF subjects is much wider due to the signal irregularity.

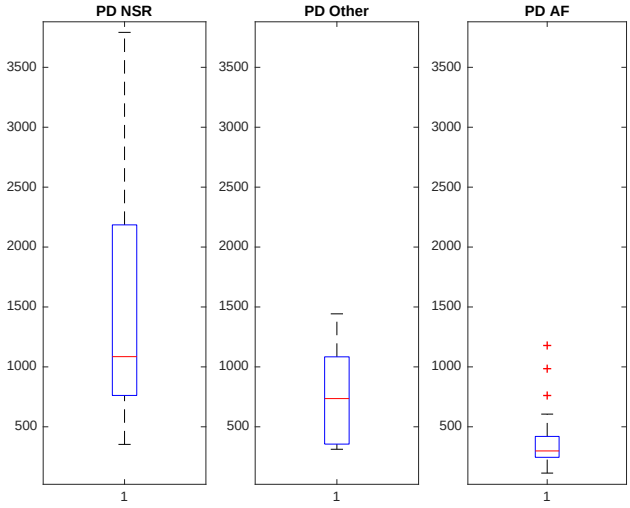

Figure 5.3: ***Spectral analysis boxplot.*** *Distribution of the peak density index for the three classes of subjects.*

Although this index shows correlation to the health status of the patient, it is rather influenced by the presence of white noise in the signal: the effect of such disturbance causes the same effect on the PSD as the presence of AF phenomena, broadening the frequency content of the signal.

For subjects affected by other arrhythmias, the PD index shows intermediate values.

5.1.2 Intervals spectral analysis

The power spectral density (PSD) of the RR intervals is a widely known technique of analysis in the study of the ECG signal: the power spectrum of the RR-time sequence, or tachogram, is characterized by spectral peaks in different frequency bands, each one correlated to the influence of the autonomic nervous system.

This work is based on BVP recordings so the PSD of the inter-diastolic intervals is studied, rather than that of the RR-time sequence; the generation of the interval series is computed in the aforementioned peak detection section (paragraph 4.3.2).

Before spectral estimation, the time sequence of the intervals is interpolated with a 4 Hz time resolution (Figure 5.4).

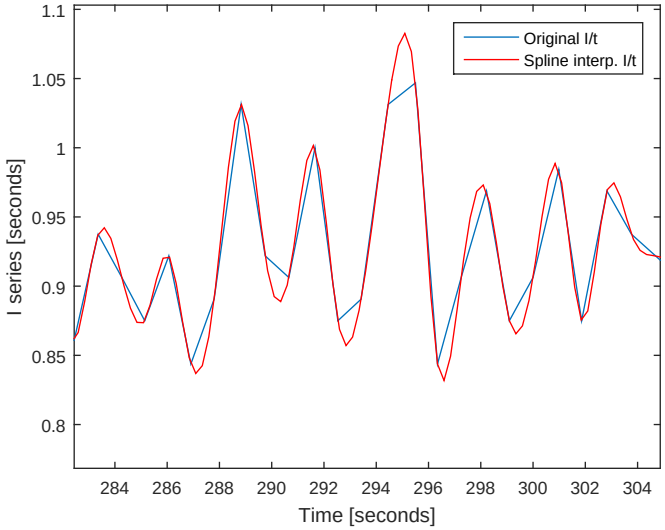

Figure 5.4: ***Original intervals sequence and interpolation.*** *Comparison between the original intervals time sequence, and the spline interpolation with 4 Hz frequency; the interpolation is performed because it improves the classification capability of the index.*

After obtaining the interpolated version of the series, the algorithm calculates the PSD through the matlab function *plomb*, using the time sequence with 4 Hz resolution. For BVP spectral analysis, the choice to use the Lomb-Scargle PSD estimate is requested to handle missing samples during the previously zero padded noisy periods (Figure 5.5).

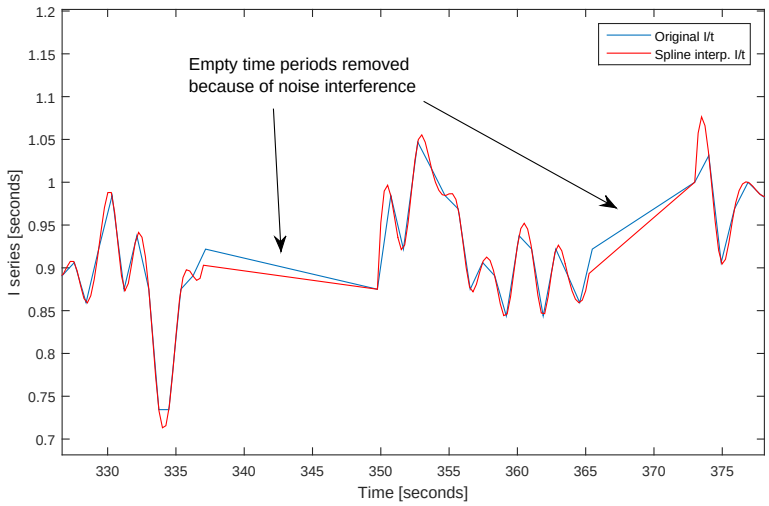

Figure 5.5: ***Interval series with empty periods.*** *The interval series and its interpolated version include empty periods, those are the previously zero-padded zones corrupted by movement noise; the PSD must be therefore calcolated with a method capable of PSD estimation of discontinuous data, in our case we employed the Lomb-Scargle PSD estimate.*

After performing the Lomb spectral estimate, the integral of the PSD for all frequencies is evaluated (i.e. the total power), this index is called $PSDsum$:

$$PSDsum = \int_0^{f_S} S_{series}(\omega)\,\mathrm{d}\omega \tag{5.2}$$

where $S_I(\omega)$ is the PSD of the interval sequence and f_S is the sampling frequency.

By comparing the results for healthy subjects and for people affected by atrial fibrillation, one observes that the former tend to have lower values (Figure 5.6).

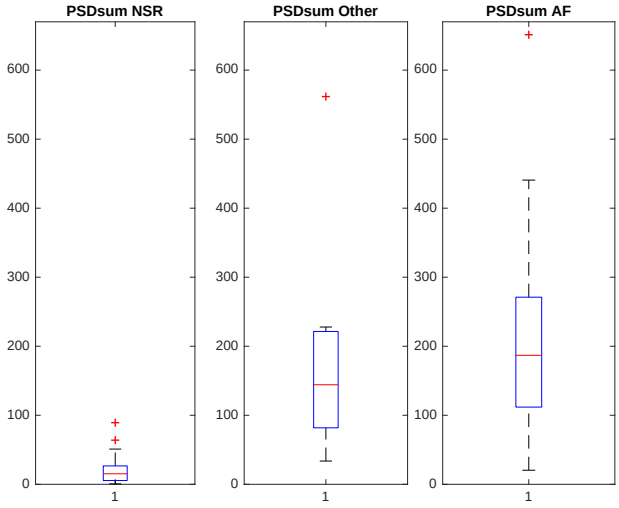

Figure 5.6: ***Intervals spectral analysis boxplot.*** *Distribution of the intervals PSD sum for the three classes of subjects.*

Those results can be explained considering the related concept of variance: since the PSD describes how the signal variance is distributed along the frequency spectrum, it is reasonable to expect higher values for patients affected by atrial fibrillation, since the distribution of the intervals is much more irregular than that of a physiological subject.

5.2 Time domain indexes

Time domain parameters allow the study of intervals' variability. In clinical practice, it is possible to support AF diagnosis by calculating statistical parameters on the RR series, such as the standard deviation (SD), root mean square of successive differences (RMSSD), coefficient of variation (CV), percentage of successive differences greater than 50 ms (pNN50) and the AF evidence by Sarkar et al. [30] [22].

5.2.1 Standard deviation

The standard deviation (SD) of the intervals is a straightforward index to quantify the variation of the heart rate, therefore it provides a simple way to determine whether the patient's heart has a regular or irregular (arrhythmic) behavior. The SD is computed as in equation (3.8).

This index shows low values for healthy subjects and higher values for AF

subjects, with intermediate values for subjects affected by other arrhythmias (Figure 5.7).

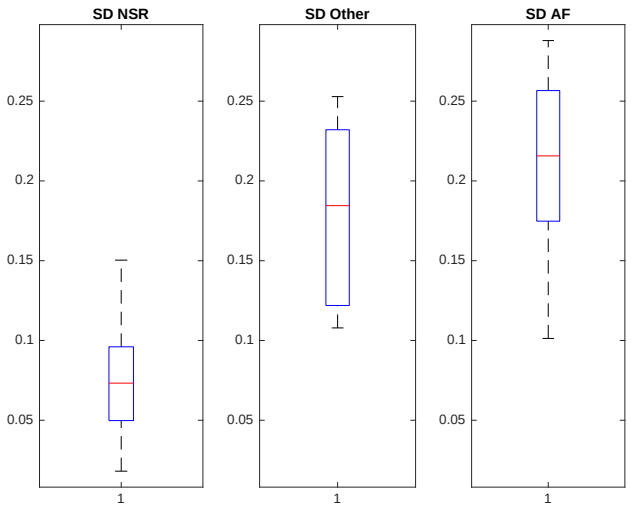

Figure 5.7: ***SD boxplot.*** *Distribution of the SD for the three classes of subjects.*

5.2.2 Root mean square of successive differences

Another index used to evaluate heart variability is the root mean square of successive differences (RMSSD) of the intervals; this quantity is defined as the square root of the mean of the squares of the differences between adjacent intervals.

The RMSSD is well known in clinical practice, and is generally applied to ECG recordings, where it is calculated for the RR intervals, as shown in equation (3.9).

One issue with the use of the RMSSD is that it is inversely proportional to the heart rate, which is not a constant value for every patient. In order to remove this bias, another index is computed, called normalized root mean square of successive differences (nRMSSD), equal to the RMSSD divided by the mean of the interval series.

$$nRMSSD = \frac{RMSSD}{\overline{I}} \tag{5.3}$$

The boxplots of the RMSSD and nRMSSD are depicted respectively in Figure 5.8 and Figure 5.9.

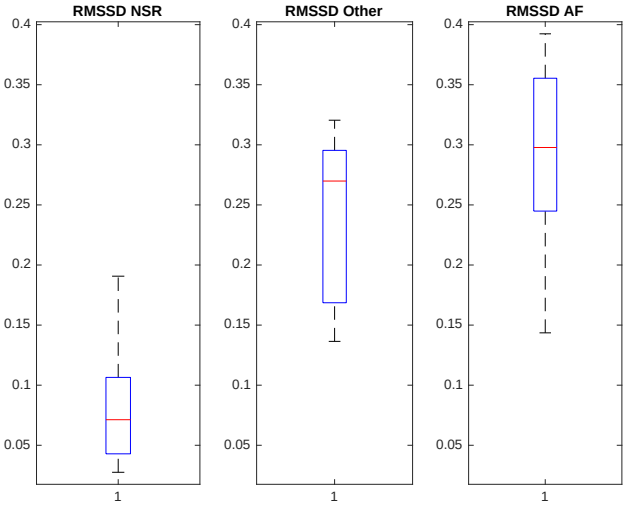

Figure 5.8: ***RMSSD boxplot.*** *Distribution of the RMSSD for the three classes of subjects.*

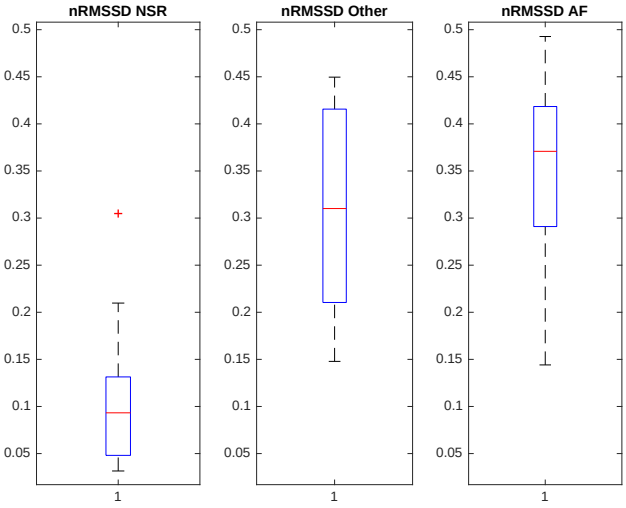

Figure 5.9: ***nRMSSD boxplot.*** *Distribution of the nRMSSD for the three classes of subjects.*

5.2.3 Coefficient of variation

The coefficient of variation (CV) is derived from the standard deviation, and is calculated by dividing SD by the absolute value of the mean, as in

equation (3.10).

The CV is calculated on the distribution of the intervals, as a normalization of the SD, in the same way as the nRMSSD is a normalized version of the RMSSD.

The CV boxplots depicted in Figure 5.10 show similar values between the classes of AF patients and subjects affected by other arrhythmias, meaning this index does not discriminate these conditions very well, while the values for healthy subjects are generally lower.

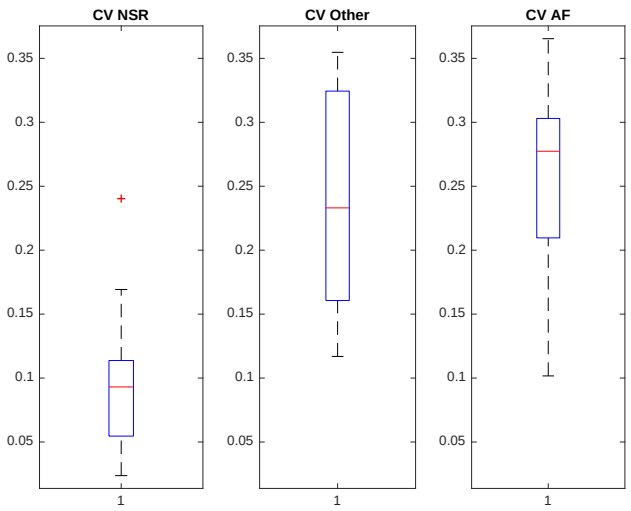

Figure 5.10: ***CV boxplot.*** *Distribution of the CV index for the three classes of subjects.*

5.2.4 pNN50

pNN50 is calculated as the percentage of differences of successive intervals (I) greater than 50 ms:

$$pNN50 = \frac{\#[successive\ \delta I > 50\ ms]}{\#successive\ \delta I} \tag{5.4}$$

Higher values of pNN50 show high variability between intervals, a typical condition of AF plethysmographic signals.

The pNN50 boxplots for the three different classes show little overlapping between NSR and AF patients, while the values obtained for the class of patients suffering from other arrhythmias are pretty much superimposed to the other two, meaning this index alone cannot accurately classify this condition (Figure 5.11).

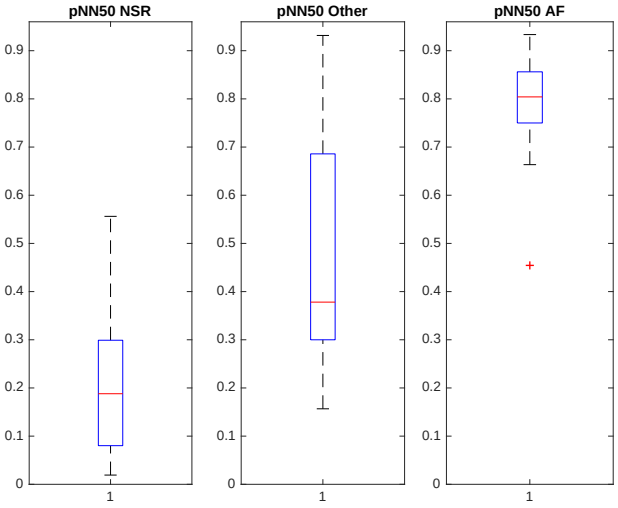

Figure 5.11: ***pNN50 boxplot.*** *Distribution of the pNN50 index for the three classes of subjects.*

5.2.5 AF evidence

The AF evidence is an index specialized in the detection of atrial fibrillation phenomena; it was originally developed by Sarkar at al. [30] and in this work has been adapted to the analysis of the PPG signal.

The original AF evidence was computed on signals which were 2 minutes long, while the BVP signals analyzed in this study are usually longer, even after the subtraction of signal periods disturbed by noise; thus it was decided to evaluate the AF evidence on a portion of 2 minutes out of the whole acquisition.

In order to isolate this period, an algorithm searches the whole BVP signal for a section with no noise at least 2 minutes long; if it exists, then the index is calculated on such period, otherwise several noiseless portions of the signal are attached together, starting from the longest, until we reach a total duration of 2 minutes.

The index is based on the distribution of the deltas of the intervals (I), i.e. the time difference between subsequent I; for every interval, two deltas are calculated: one with respect to the following interval ($DeltaI_i = I_{i+1} - I_i$), and the other with respect to the previous interval ($DeltaI_{i-1} = I_i - I_{i-1}$), therefore we obtain two deltas for every interval.

The obtained deltas are then represented in a Lorenz plot, with $DeltaI_i$ value on the X axis and $DeltaI_{i-1}$ value on the Y axis, for every I (Fig-

ure 5.12).

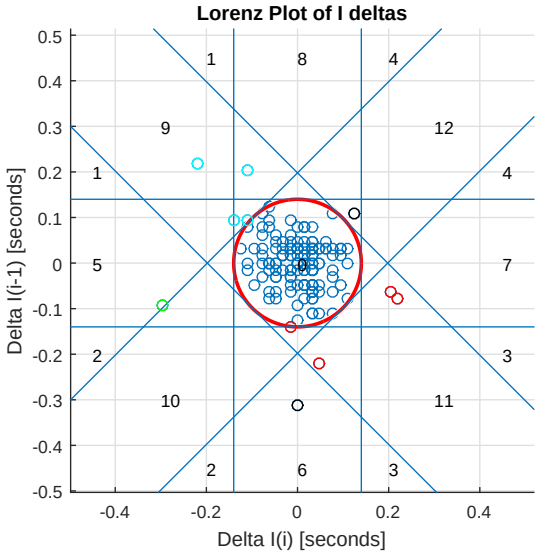

Figure 5.12: ***Lorenz plot distribution.*** *Every couple of I deltas [$DeltaI_i$, $DeltaI_{i-1}$] is represented on the Lorenz plot, the lines represent separate regions used to classify different heart beats.*

The circumference at the center of the graph represents the *NSRmask*, that is the circle inside which every pair of $[DeltaI_i; DeltaI_{i-1}]$ is considered physiological; the radius of the *NSRmask* is set at 140 ms.

If one dot on the graph falls outside the *NSRmask* boundaries, then it is pathological; there are 12 segments outside the *NSRmask*, delimited by straight lines (Figure 5.12); every segment includes a particular type of delta I. Every dot, or pair of deltas, that falls inside the *NSRmask* lowers the AF evidence index, while every dot belonging to one of the 12 outside segments is correlated to heart arrhythmia.

To compute the AF evidence, the first step is the automatic classification of each dot on the graph into one of the 12 segments, or inside the *NSRmask*; if one point falls inside two segments simultaneously (for example if it is located at the intersection between 7 and 11, near the *NSRmask*), then it is assigned to the segment with highest priority (segments 6, 7, 9, 11 have higher priority than segments 5, 8, 10, 12, and diagonal segments have higher priority than horizontal and vertical segments).

After this assignment, the B array is calculated: B is a 12 by one vector, where B_n indicates the number of different points included in segment n of the Lorenz plot, therefore if more points are identical, they are counted only

once in B; the probability to have two identical points is not null, since we have a limited time resolution of 15.625 milliseconds.

After obtaining B, the algorithm calculates vector P; P is also 12 cells long and P_n indicates how many points are found in segment n of the Lorentz plot, including repetitions (unlike B_n which only counts distinct points).

Before calculating the AF evidence, there are some intermediate indexes to be evaluated: the premature atrial contraction evidence ($\mathcal{L}_{PE}$) and the irregularity evidence ($\mathcal{L}_{IE}$); their calculation is identical to the original version, and is explained in equations (3.4) and (3.1).

The last index prior to AF evidence calculation is NSR count, which increases proportionally to the regularity of the patient's heart beat; the original version of this index, developed by Sarkar, is calculated as the total sum of points located in the histogram bin identified in the origin of the axes, that is the total of $[DeltaI_i; DeltaI_{i-1}]$ with a distance from the origin inferior to 40 ms.

In this analysis, it was found that very few points would fit into this small zone around the origin, even for healthy patients with regular heart rate; this is because the noise in the BVP signal introduces small distortions, even in the signal periods less affected by movement artifacts, and because it is much harder to have closely similar subsequent intervals than in an ECG signal. Consequently, it would be more representative to count the points located into the *NSRmask*, which is a slightly wider area (*NSRmask* radius=140 ms), and includes all the subsequent intervals that are sufficiently alike.

Finally, with all the previously collected indexes, the algorithm can proceed to the calculation of the AF evidence ($\mathcal{L}_{AFE}$), as in equation (3.5) with the difference that, in our case, $\mathcal{O}$ is not the number of points in the bin containing the origin, but is substituted by the NSR count.

The AF evidence is computed in a much different way with respect to other indexes, meaning the information content it carries is complementary to the other analyses. Higher values are observed for AF patients, lower values for healthy subjects and intermediate values for patients suffering from other arrhythmias; there is no overlapping between values of NSR and AF classes (Figure 5.13).

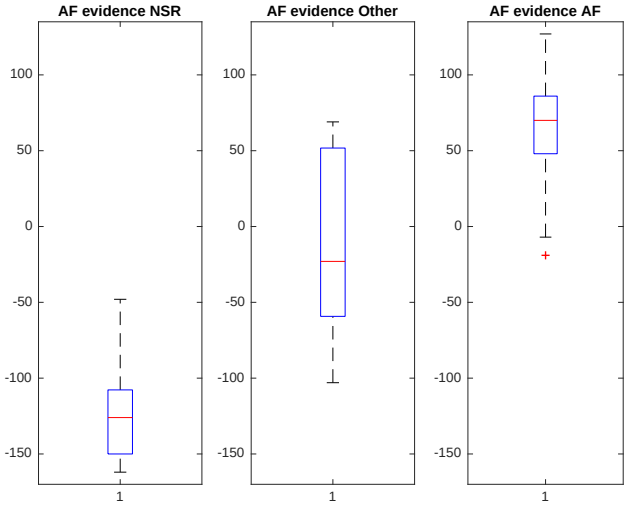

Figure 5.13: ***AF evidence boxplot.*** *Distribution of the AF evidence for the three classes of subjects.*

5.3 Nonlinear indexes

Nonlinear indexes are the result of algebraic equations in which the output values are not directly proportional to the input, but are obtained through nonlinear transformation. The indexes include the sample entropy and normalized Shannon entropy.

5.3.1 Sample entropy

Sample entropy (SampEn) is a modified version of approximate entropy. For a given embedding dimension m, tolerance r and number of data points N, SampEn is defined as the negative logarithm of the probability that, if two sets of simultaneous data points of length m have distance $< r$, then two sets of simultaneous data points of length $m+1$ also have distance $< r$.

Our analysis evaluated the sample entropy of the intervals, as an index of the complexity of their distribution; we set a tolerance value of 0.15 times the standard deviation of the series and an embedding dimension of 2.

The SampEn index assumes diverse values for the separate classes of healthy and AF patients: SampEn is lower for subjects with a normal sinus rhythm and higher for subjects affected by AF; as for patients affected by other arrhythmias, their SampEn indexes appear to be even lower than those of healthy subjects (Figure 5.14).

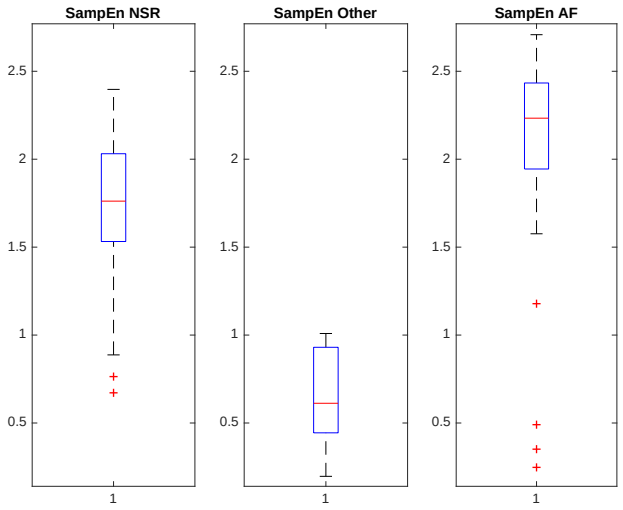

Figure 5.14: ***SampEn boxplot.*** *Distribution of the SampEn for the three classes of subjects.*

5.3.2 Normalized Shannon entropy

Shannon entropy (ShEn) characterizes the uncertainty of a statistical distribution and increases proportionally to the presence of randomness sources. It can be calculated through equation (3.14).

In this analysis, we calculate the Shannon entropy of the statistical distribution of the intervals, which are sampled with a time resolution of 1/64 seconds, and therefore represent a finite number of variables, even though they serve as numerical measurements.

The Shannon entropy index is then normalized by dividing it by the logarithm of the number of intervals (I) detected; this is performed since ShEn tends to increase with the dimension of the the dataset of variables.

$$Normalized\ ShEn = \frac{ShEn}{log(\#I)} \tag{5.5}$$

Normalized Shannon entropy (nShEn) values for the different classes of patients show a definite overlapping between all three types of subjects, therefore this index alone is not sufficient to operate a good classification (Figure 5.15).

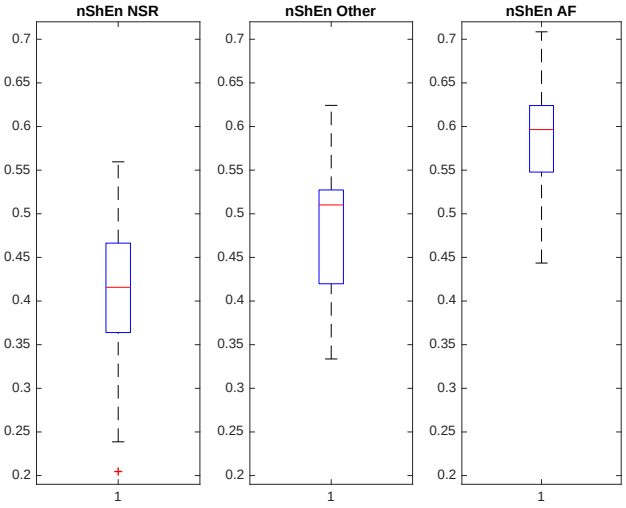

Figure 5.15: ***nShEn boxplot.*** *Distribution of the normalized Shannon entropy for the three classes of subjects.*

5.4 Shape analysis

The majority of indexes introduced up to this point are focused on the variability of time intervals between subsequent heart beats. In this section, instead, a new category of indexes based on the morphology of BVP is proposed. This category includes the normalized wave deviation, the detection of multi-peak waves and two-peak waves and the *shape similarity* index.

5.4.1 Normalized wave deviation

The difference between the systolic peak and diastolic minimum (Figure 5.16), from now on referred to as R, is an intuitive descriptor of the shape of every heart cycle; in order to evaluate the variation of this morphological feature, the median absolute deviation (MAD) of its distribution was computed; the index obtained was named wave deviation (WD):

$$WD = MAD(R) = median(\sum_{n=1}^{N} |R_n \ - \ median(R)|) \tag{5.6}$$

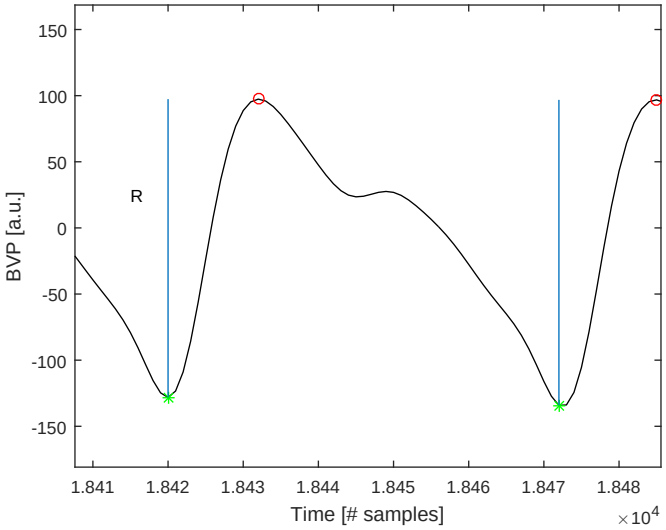

Figure 5.16: ***The R value.*** *Variability in wave shapes can not be noticed by indexes based on the intervals, which only consider the timing of the signal; if AF or other arrhythmias influence the excursion of R, the WD will be sensitive to this change.*

It is worth noting that R and the overall signal amplitude can change even for the same subject, depending on how the wristband is located during the measurement protocol: the looseness of the device on the patient's arm, together with the position where it is applied along the wrist, can significantly change the signal intensity during the acquisition.

In order to take this variation into account, the WD is normalized by dividing it for the median R:

$$nWD = \frac{WD}{median(R)} \tag{5.7}$$

As an index of morphological variability, the normalized WD gives us information not correlated to other indexes of time variability, like the RMSSD or AF evidence; by comparing the results obtained in different classes of patients however, this index does not seem to operate a very good distinction between them: the values for AF and healthy subjects are superimposed, and the range for the other arrhythmias is very wide (Figure 5.17).

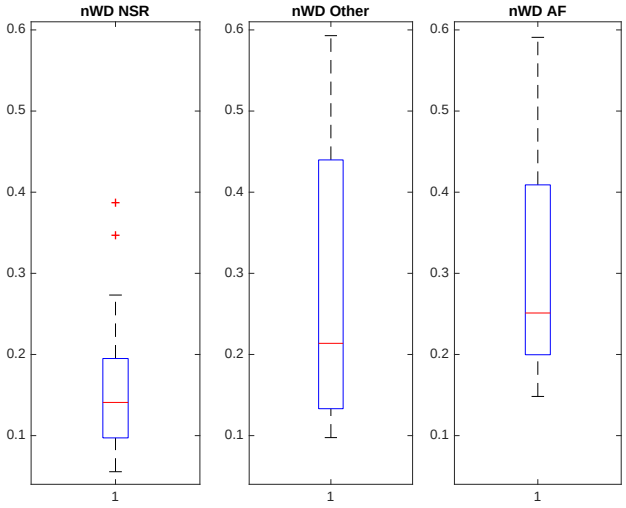

Figure 5.17: ***Normalized WD boxplot.*** *Distribution of the normalized WD for the three classes of subjects.*

5.4.2 Multi-peak waves

By observing several BVP measurements of AF patients, an occasional morphological pattern was noticed. This pattern seems to be more rare in healthy subjects: after one beat, the signal experiences a certain offset, and the subsequent heart cycles show a much smaller excursion between the maximum and minimum of each wave; this shape lasts for about three cycles, then the signal comes back to normality (Figure 5.18); this phenomenon was labeled as a multi-peak wave (MPW).

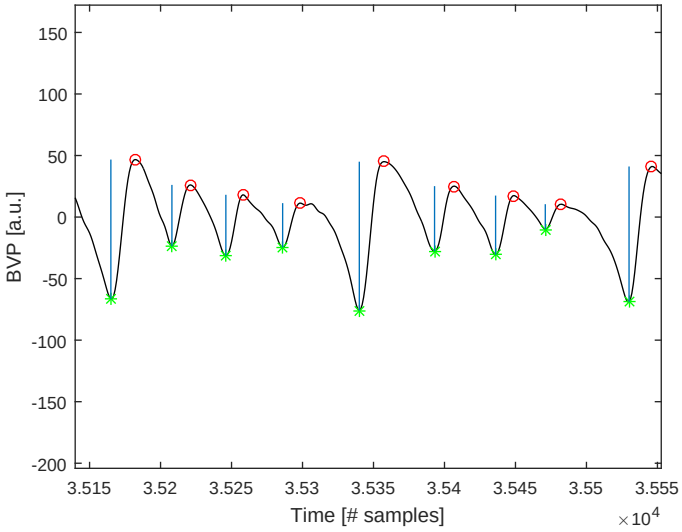

Figure 5.18: ***Multi-peak waves' identification.*** *A multi-peak wave is composed of a series of waves where from the second to the last the signal experiences a certain offset, and wave amplitude becomes smaller.*

A simple algorithm was developed in order to identify this pattern automatically; the software detects the event when the maximum-minimum range for one wave is much broader than in the subsequent one, and the diastolic minimum of the next wave is offset higher than half the excursion of the current wave. If those conditions are satisfied, the event is labeled as a MPW if at least one of the following cases occurs: either the second next wave has its diastolic minimum on a high offset too, or the inter-diastolic intervals between the three waves are similar enough.

After identifying all the MPWs, the percentage of MPWs over the total number of waves is computed:

$$MPW\ [\%] = \frac{\#\ MPWs\ detected}{\#\ waves} \tag{5.8}$$

The results confirm the higher concentration of MPWs for AF patients, while this pattern is observed very occasionally in healthy patients and the median number of MPWs detected in healthy patients is zero (Figure 5.19); despite this, the index is not able to discriminate values for all the three classes, since even for AF patients the total count of MPWs is sometimes as low as that of healthy subjects; this could be either due to the infrequent presence of the MPWs phenomenon, even in people affected by atrial fibrillation, or to the imprecision of the algorithm used for MPWs detection.

Patients affected by other arrhythmias show a wide range of values for this index, with a median value in between those of the other two categories.

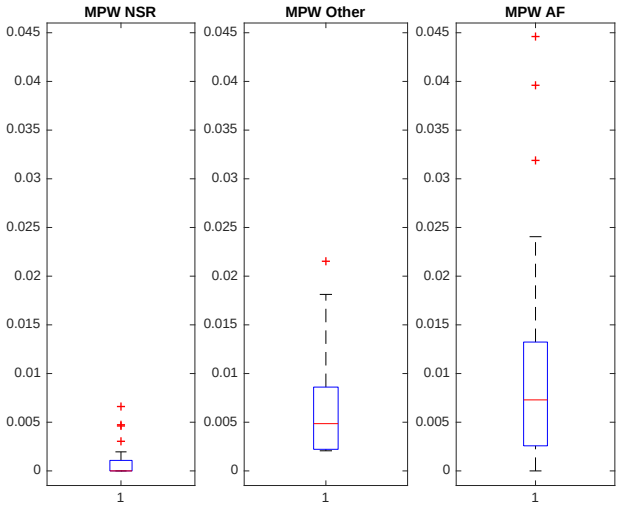

Figure 5.19: ***MPW boxplot.*** *Distribution of the MPW index for the three classes of subjects.*

5.4.3 Two-peak waves

Another typical shape is often recognized in AF patients: on certain occasions, at end of a heart cycle, the new one starts before the completion of the previous one, therefore the diastolic minimum of the next wave is on a higher offset, but unlike multi-peak waves, it lasts for one cycle only, then the signal proceeds normally (Figure 5.20).

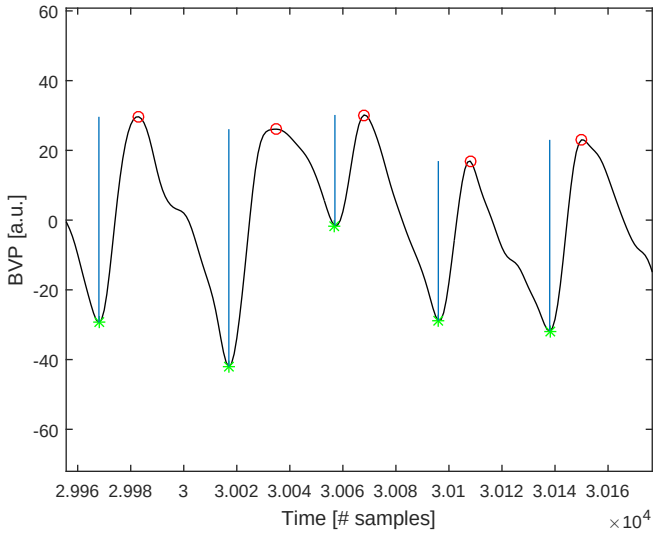

Figure 5.20: ***TPW shape.*** *This feature of the BVP signal is labeled as a two-peak wave (TPW), it consists of two subsequent waves where the second one starts before the completion of the first.*

This phenomenon, observed frequently in arrhythmic patients, was named two-peak waves (TPWs), since it appears like two waves from two separate heart cycles are merged into a single one.

An algorithm was developed to automatically detect this pattern in the signal; for every heart cycle, a TPW is identified when the following conditions are verified: the starting minimum of the current wave (A) and the ending minimum of the next wave (C) must be on a similar level and the alpha angle, obtained by linking minima A, B and C (Figure 5.21), has to be smaller than an empirical threshold set to 90.72 degrees (meaning that the first wave is ascending and the second wave is descending, creating a sharp corner in the middle).

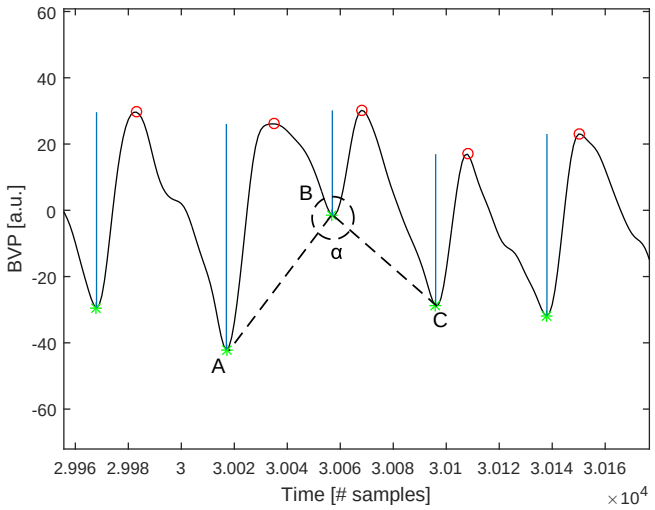

Figure 5.21: ***TPW shape and alpha angle.*** *The algorithm automatically identifies a TPW when the alpha angle, obtained by linking minima A, B and C, is smaller than 90.72 degrees.*

If the previous conditions are met, the current cycle is identified as the start of a TPW; the total number of TPWs is then counted, in order to obtain an index from this procedure, then the total count is normalized, as for the MPWs, dividing it by the sum of waves analyzed in the process.

$$TPW\ [\%] = \frac{\#\ TPWs\ detected}{\#\ waves} \tag{5.9}$$

The distribution of the TPWs index (Figure 5.22) shows common values between the three classes: even though AF patients tend to have more TPWs, on some occasions those phenomena occur only a few times during the whole acquisition; some healthy subjects also show a TPWs count higher than zero, this is likely due to the signal distortion caused by interfering noise. With such distribution, the TPWs index alone cannot be used as a discriminant for the patients' health condition.

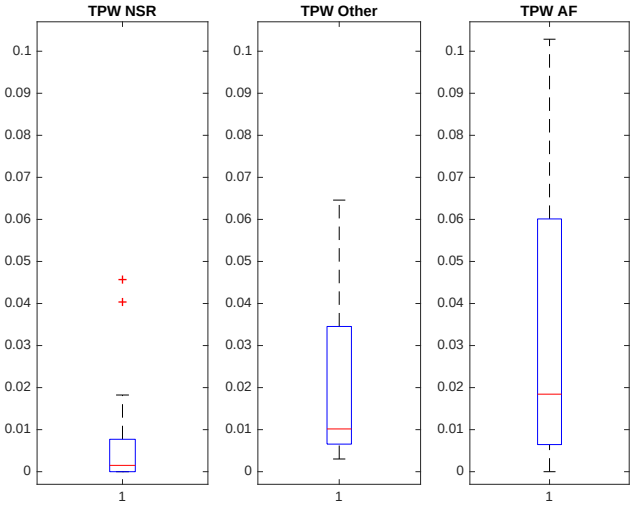

Figure 5.22: ***TPWs boxplot.*** *Distribution of the TPW index for the three classes of subjects.*

5.4.4 Shape similarity

In addition to the previously described morphological analyses, an investigation is conducted to evaluate the variability of the BVP waves of every heart cycle, by studying their entire shape, not only the values of minima and maxima as considered, for instance, in the MPW and TPW indexes. The index proposed by Faes et al. [14] for quantifying the organization of single bipolar electrograms recorded in human atria during AF, based on wave morphology similarity, was implemented and adjusted for a BVP signal. The algorithm compares each pair of waves in the signal and finds an index of their similarity, by using the dot product between the two waves.

Each wave can be considered as a 1-D array of BVP values in a time window, extending from the diastolic minimum at the beginning of the heart cycle for a fixed length; such length is calculated as the mean duration of the inter-diastolic intervals t. To compare all waves with one another, the algorithm performs a dot product between the arrays.

The dot product is an operation that, when performed on two different n-dimensional vectors, returns a 1-dimensional value proportional to the modules of the two vectors and to the cosine of the angle between them.

Since the t-samples long arrays of BVP wave values can be considered as t-dimensional vectors, the dot product between the two is indicative of the cosine of the angle between the vectors. Before performing the dot

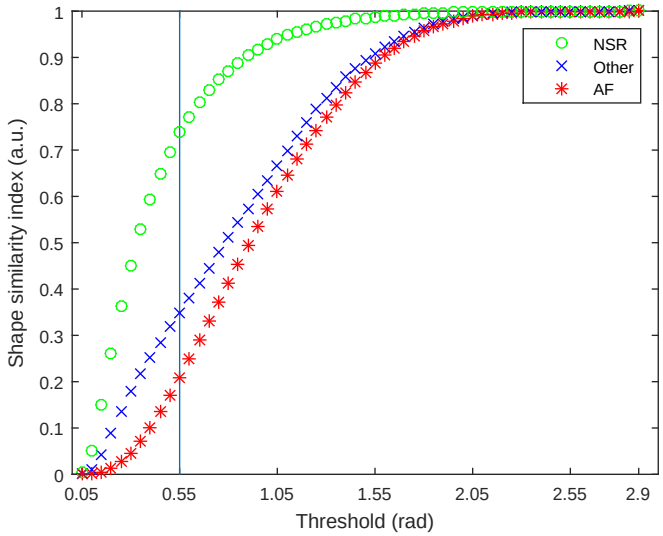

Figure 5.23: ***Comparison between different thresholds.*** *Average values of the shape similarity for each of the three target classes calculated as a function of the threshold. The best discrimination between the average values was obtained for a threshold of 0.55, as indicated by the vertical line.*

product, each array is divided by its norm as in equation (3.15), therefore the output of the dot product is independent from the moduli and depends only on the cosine of the angle. Consequently, the dot product values are higher for similar waves, because the angle between them is closer to zero; this property allows us to consider the dot product as an index of waves' similarity. After performing the dot product, the arccosine operand is used to convert the dot product into angle, which will be smaller for more similar waves (equation (3.16)).

The aforementioned operation is iterated to calculate the similarity between each pair of waves, thus for a signal with N heart cycles, $N(N-1)/2$ comparisons are performed. At such point, all the wave similarities are compared to a threshold, which was set to 0.55 radians: all waves with a smaller cosine angle are considered similar, while all angles above such threshold classify the waves as different. An index called *shape similarity* is computed out of this comparison, as the fraction of waves in the signal which have an angle of difference inferior to the threshold of 0.55 radians, as in equation (3.17). The threshold was chosen comparing the average value of the *shape similarity* index for each target class in function of the threshold and selecting the value that provided a greater discrimination between the classes, as depicted in Figure 5.23.

The *shape similarity* index has a range of values between 0 and 1, with generally lower values for AF patients and higher for normal subjects (Figure 5.24); this can be explained because heart cycles present a much more variable behavior in AF patients, and the respective BVP waves follow the same irregularity.

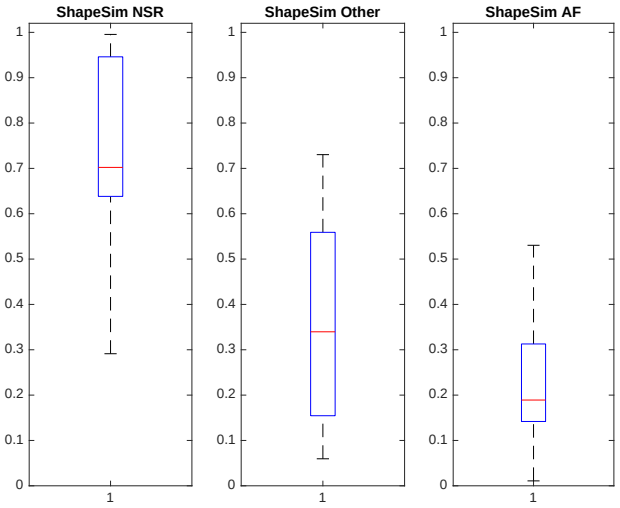

Figure 5.24: ***Shape similarity boxplot.*** *Distribution of the shape similarity index for the three classes of subjects.*

To obtain a more comprehensive examination from this analysis, two more indexes are computed: the median (*MedianArc*) and the mode (*ModeArc*) of the angle of the dot product, calculated for all waves. This values are instead higher for patients suffering from AF, while lower for subjects with normal sinus rhythm (Figure 5.25 and Figure 5.26).

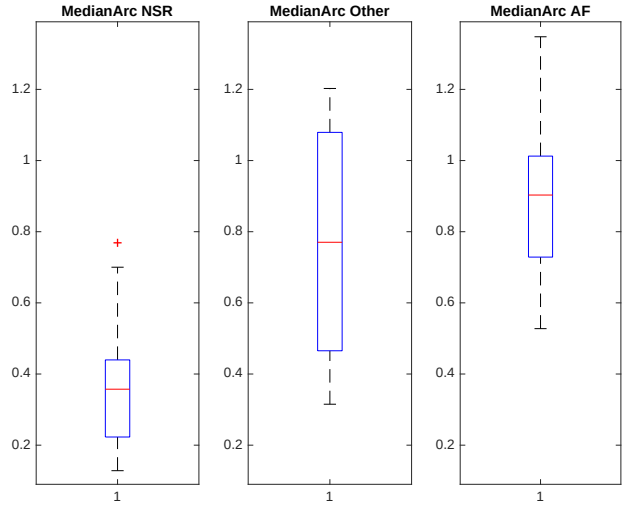

Figure 5.25: ***Boxplot of the median of the dot product angle.*** *Distribution of the median of the dot product angle for the three classes of subjects.*

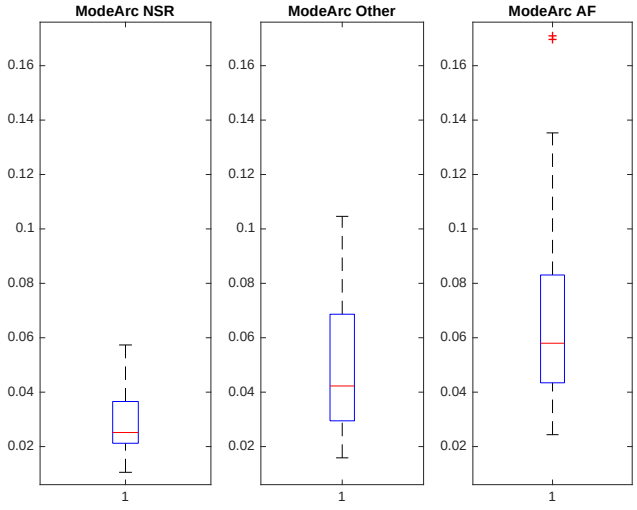

Figure 5.26: ***Boxplot of the mode of dot product angle.*** *Distribution of the mode of the dot product angle for the three classes of subjects.*

Chapter 6

Classification and results

In the previous chapter several diagnostic indexes have been analyzed and their classification capability was illustrated. Unfortunately, univariate analysis can not discriminate very well between the categories of NSR, AF and other arrhythmias, because the values of single variables overlap. Therefore a multivariate analysis could be a more appropriate solution to this problem. This chapter is divided in two sections: the first section analyzes the correlation between different indexes and their information content, while the second one focuses on the implementation of an automatic classification method based on a support vector machine.

6.1 Correlation between indexes

For an optimal outcome of multivariate analysis, it is fundamental to know the existing relationships between different indexes: for instance, if two or more indexes are correlated, using them simultaneously is a redundant operation which can negatively affect the efficiency of the classification process.

There is a strong correlation between many indexes, this is especially evident for those based on the study of the intervals. From a theoretical point of view, the standard deviation (SD) is correlated to the PSD power (parameter PSDsum) since the latter is a descriptor of the variance of the intervals distributed over the frequency spectrum. The correlation between the two indexes is not linear, mainly due to the fact that the PSD is linked to the variance, which is equal to the standard deviation squared, therefore a quadratic relationship can be expected (Figure 6.1). Given this correlation, the PSDsum index does not add significant information to the standard deviation in our analysis.

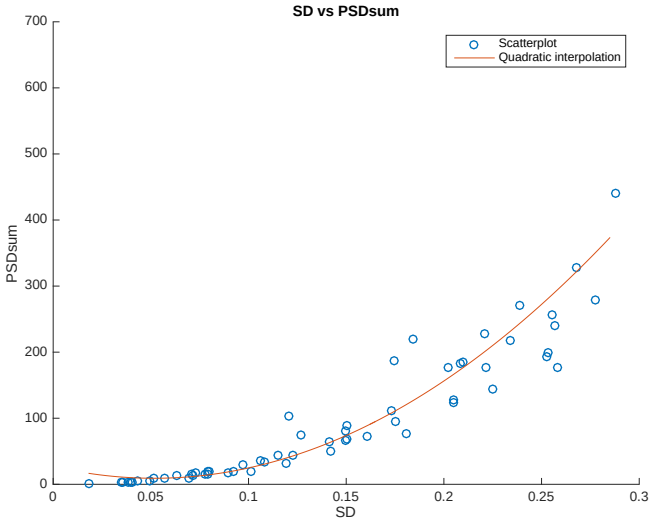

Figure 6.1: ***Correlation between SD and PSDsum.***

The RMSSD index also shows a strong linear correlation to the standard deviation (Figure 6.2), meaning they are in fact two representations of the same variance: RMSSD is the square root of the mean of the squares of the successive differences between adjacent intervals, while SD is the square root of the mean of the squared deviations of the intervals from their average value, so their formula only differs in the type of the deviations, that are in one case between successive intervals and in the other between each interval and the average one.

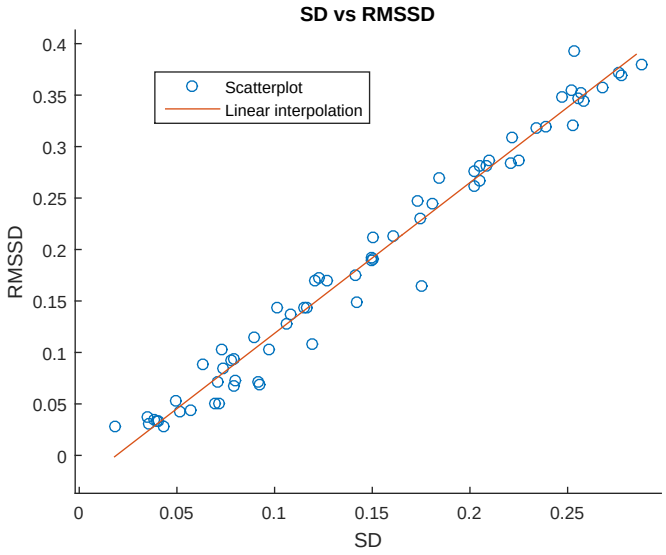

Figure 6.2: ***Correlation between SD and RMSSD.***

A strong correlation can also be expected between the nRMSSD and the CV (Figure 6.3), in the exact same way as the RMSSD and SD are correlated: in fact the nRMSSD and CV are both divided by the same mean value.

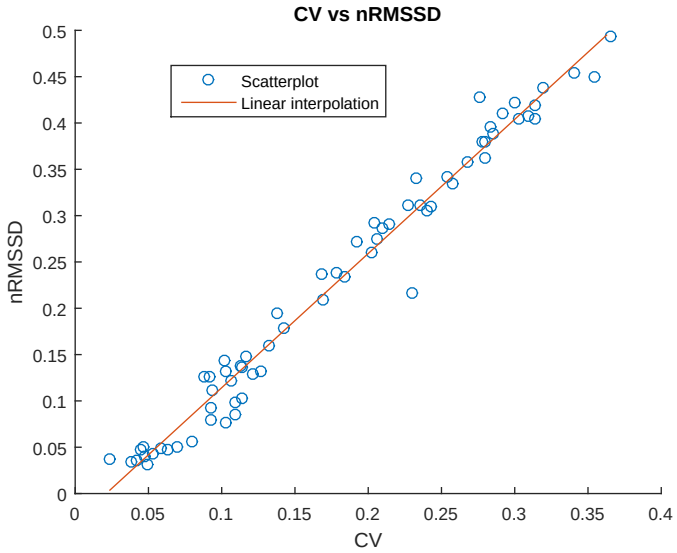

Figure 6.3: ***Comparison between nRMSSD and CV.***

When we compare intervals based indexes with other families of indexes instead, the correlation is very weak, meaning they are not a redundant

representation of the same features.

The SampEn index expresses a measure of heart rate variability, and generally it increases proportionally to the complexity of a physiological time-series signal, yet there is little correlation between SampEn and, for instance, the nRMSSD (Figure 6.4); consequently, the SampEn index adds different information to the classification algorithm, helping the categorization into target classes.

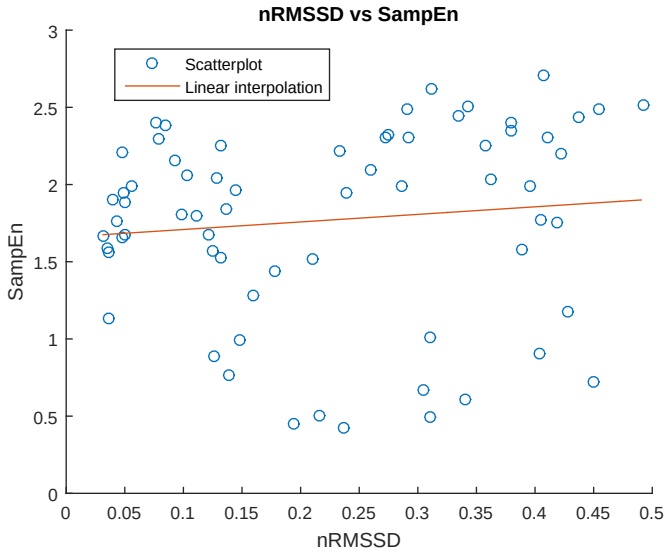

Figure 6.4: ***nRMSSD and SampEn comparison.***

Indexes falling in the category of shape analysis can be expected to have little correlation to other categories of indexes, since their calculation is based on BVP signal shapes instead of on the intervals. However, it can be shown that, by comparing the shape analysis indexes with the nRMSSD, a strong linear correlation appears. The linear correlation coefficient between the nRMSSD and the shape similarity index is equal to -0.9290 (Figure 6.5), while for the derived indexes of the median and mode of the dot product angle (introduced in section 5.4.4) the coefficients of linear correlation to the nRMSSD are 0.9250 and 0.7099 respectively.

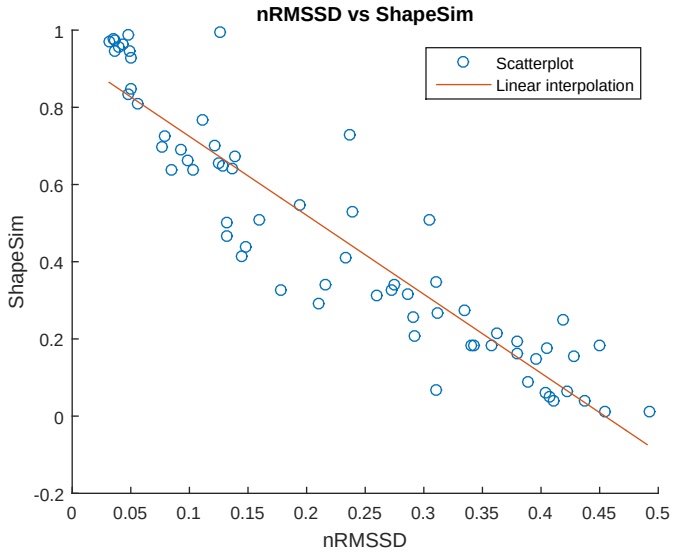

Figure 6.5: ***nRMSSD versus shape similarity.*** *The linear correlation coefficient is equal to -0.9290.*

There are lower linear correlation coefficients between the nRMSSD and other shape analysis indexes: values are equal to 0.6621 for the nRMSSD and the normalized wave deviation (nWD), 0.6280 between nRMSSD and the multi-peak waves (MPW) and 0.4948 between nRMSSD and two-peak waves (TPW).

6.2 Support vector machine

A support vector machine (SVM) is a decision-making method which takes into account multiple indexes to operate an automatic classification into several target classes, and is capable of solving problems of great dimensions [36]; SVMs perform the identification of archetypal examples, called *support vectors*, which are representative of target classes, and are used to classify observations into one or more categories.

In a multivariate analysis based on a number n of indexes, every observation, or patient in our case, is represented as a *n-dimensional* vector; each vector can be seen as the coordinates of a point in *n-dimensional* space, therefore the classification of every subject is computed by the SVM as a problem of spatial separation between *n-dimensional* points. The algorithm operates a partition between those points through the use of a hyperplane of separation, that is an item used to separate the observations of different classes; for example, if we have to distinguish between two categories on

the basis of two indexes, the hyperplane of separation can be visualized as a straight line delimiting two separated regions, each representative of one category (Figure 6.6).

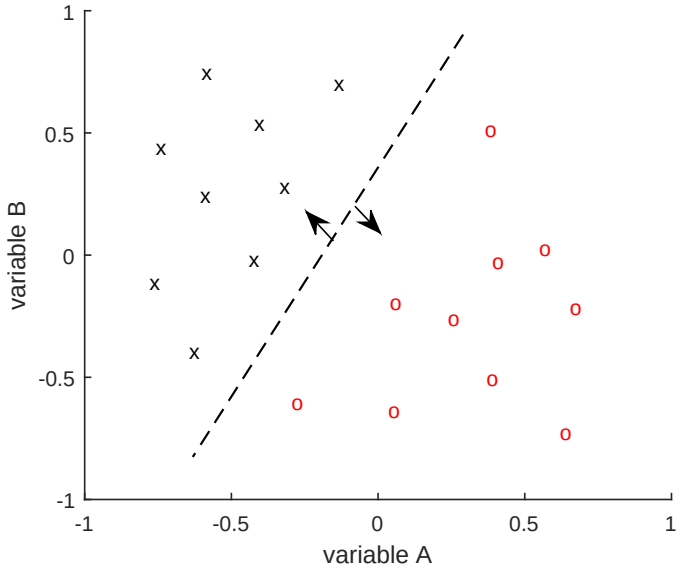

Figure 6.6: ***SVM classification in 2D space.*** *The classification between two categories is calculated by the SVM as a problem of space separation, in this case the distinction between* x *and* o *classes is seen as the separation of dots in the 2D plane using a straight line.*

For a correct use of the SVM, a preliminary operation is the normalization of the indexes: each vector is composed by many parameters, with heterogeneous origin and different ranges of values; parameters with greater excursions tend to have a bigger weight in the decision process; thus, in order to ensure that every parameter has the same relevance in the classification, each index is assigned a normalized value between zero and one, where zero is assigned to the lowest value measured for the index, and one is assigned to the maximum, with intermediate values in between; exceptionally high or low values, also called outliers, are given normalized values that are lower than zero or higher than one.

The SVM is an example of supervised learning, thus the algorithm goes through a training phase prior to its use in classification problems: the SVM is trained on a collection of data from several patients, each one already labeled as NSR, AF or suffering from other arrhythmias; this prior categorization is performed by an expert operator, in our case a cardiologist.

To evaluate the performance of the SVM, the *leave one out* cross-validation

method was employed: the SVM is trained on all the patients from the full dataset, except for one; the remaining subject has to be classified into AF, NSR or "other arrhythmia" class. The procedure is repeated for every patient of the full dataset, then the classification accuracy is computed as the ratio between the correct categorizations and the total number of the subjects.

There are several typologies of SVM that can be employed, in this analysis the *multisvm* function [26] for multiclass support vector machine was used: an algorithm inspired to the original Matlab SVM function which, unlike its original counterpart, can also operate multiclass categorization.

6.2.1 Indexes reduction

In the previous chapters, 16 different indexes have been described; some of those share similar information, enlarging the dimension of the dataset without adding new knowledge. Thus, a reduction in the number of indexes (attributes) could lead to a better efficiency of the classification algorithm, a simplification of the analysis and a potential improvement of the final separation accuracy. In this thesis two methods for indexes reduction have been tested: PCA and wrapper method.

6.2.1.1 PCA

The principal component analysis (PCA) is a method to simplify data, widely used in multivariate analysis; the aim of PCA is to reduce the initial number of variables into a smaller number of variables obtained as a linear combination of the original ones, without losing information. Being $\mathbf{X}$ the data matrix after standardization, and $\mathbf{V}=\mathbf{X}'\mathbf{X}$ the covariance matrix of the attributes, the PCA derives n orthogonal vectors (principal components) from the n original attributes. The strength of the PCA is that a subset of q principal components, with $q < n$, has an equivalent information content of the original dataset. Thus the n original attributes are projected in a lower dimensional space with the same explicative capacity [36]. The principal components are calculated in an iterative process. The first component is obtained by solving an optimization problem and is the component that explains the maximum percentage of variance of the data. The first component is computed as:

$$\mathbf{p}_1 = \mathbf{X}\mathbf{u}_1 \tag{6.1}$$

where $\mathbf{u}_1$ is the eigenvector associated with the maximum eigenvalue λ_1 of $\mathbf{V}$. The other principal components are calculated solving similar optimization

problems, adding the orthogonality condition between every component. At the end of the iterative process, n principal components are computed from the n eigenvectors sorted for non increasing eignevalues $\lambda_1 \geq \lambda_2 \geq ... \geq \lambda_n$. Thus the principal components are n orthogonal (and therefore non-correlated) vectors, sorted for a relevance indicator expressed by the correspondent eigenvalue. The variance of the principal component $\mathbf{p}_j$ is $\mathrm{Var}(\mathbf{p}_j)=\lambda_j$ so an index I_q measuring the percentage of variance expressed by the first q components can be computed as:

$$I_q = \frac{\lambda_1 + \lambda_2 + ... + \lambda_q}{\lambda_1 + \lambda_2 + ... + \lambda_n} \tag{6.2}$$

The PCA was performed on the full dataset of patients and indexes. The new dataset obtained projecting the original dataset in the new dimensional space was used to train the SVM and to classify all the subjects through a *leave one out* method. The performance of the classifier was evaluated for different numbers of principal components, from 1 to 16. In Table 6.1 the classification accuracy obtained for different numbers of principal components taken into account is displayed, together with the relative percentage of explained variance. The best accuracy is 90% and occurs when the first 12 principal components are considered, for an explained variance of 99.91%.

# PCs	1	2	3	4	5	6	7	8
Acc [%]	50	48.57	75.71	84.29	87.14	82.86	81.43	81.43
I_q[%]	50.61	76.36	82.71	87.72	91.37	94.52	96.72	98.21
# PCs	9	10	11	12	13	14	15	16
Acc [%]	85.71	87.14	85.71	90	84.29	85.71	82.86	81.43
I_q[%]	98.80	99.34	99.71	99.91	99.98	99.99	100	100

Table 6.1: ***Classification accuracy for number of principal components included.*** *The classification accuracy obtained through a* leave one out *procedure is displayed for an increasing number of principal components considered and their relative percentage of explained variance.*

6.2.1.2 Wrapper method

The choice of the most relevant indexes is performed through the wrapper method, a process often used in feature selection problems [36]: the decision-making algorithm is repeated, every time using a different subset of attributes; at every iteration, the classification accuracy is calculated and

finally, when all the combinations have been tested, the ones providing the best results are selected.

In this analysis, the SVM was given all the possible sets of indexes, thus, for 16 indexes, $2^{16} - 1$ combinations were tested; to calculate the classification accuracy of each combination, a *leave one out* procedure has been performed.

The distribution of the classification performance for all the combinations of indexes is shown in Figure 6.7.

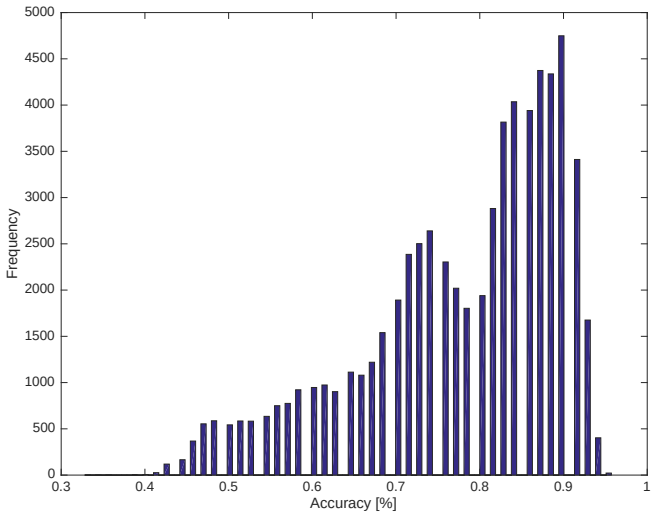

Figure 6.7: ***Distribution of SVM classification accuracy.*** *The hystogram displays the classification accuracies obtained using different combinations of indexes.*

As shown, the results of the SVM can vary greatly depending on the indexes it is trained on, going from a minimum accuracy of 32.86% of one case to a maximum of 95.71% obtained by 22 combinations; as for the statistical distribution of the accuracy, the median is equal to 81.43%, with a mean of 77.65% and a mode of 90%. The accuracy obtained by the SVM trained on all indexes is equal to 88.57%, greatly inferior to the accuracy of the best cases. Out of the optimum 22 combinations, 16 produce also the best sensitivity to the AF class, 96.67%, making them the preferred ones. The sets of indexes that achieved the best performance are reported in Table 6.2.

																% Ind
SD	1	1	1				1	1	1			1		1		1	56.25
RMSSD		1				1	1	1			1	1	1	1	1	1	62.5
nRMMSD	1	1		1		1	1	1			1	1	1	1	1	1	75
pNN50	1	1	1	1	1	1	1	1	1	1	1	1	1	1	1	1	100
CV					1	1	1			1			1	1	1	1	50
SampEn	1	1	1	1	1	1	1	1	1	1	1	1	1	1	1	1	100
nShEn	1	1	1	1	1	1	1	1	1	1	1	1	1	1	1	1	100
ShapeSim	1																6.25
MedianArc		1				1	1	1			1	1	1	1	1	1	62.5
ModeArc			1	1	1				1	1							31.25
AF evidence	1	1	1	1	1	1	1	1	1	1	1	1	1	1	1	1	100
PD																	0
nWD											1	1	1	1			25
MPW						1	1								1	1	25
TPW																	0
PSDsum								1	1	1	1	1	1	1	1	1	56.25
Tot Ind	7	8	6	6	6	9	10	9	7	7	9	10	10	11	10	11	

Table 6.2: ***Sets of indexes with best classification accuracy and sensitivity.*** *This table shows the best 16 combinations of indexes (columns). For each combination, the indexes (rows) taken into account are marked with 1 in the correspondent box. At the end of each column the number of indexes considered for each combination is specified. At the end of each row the frequency of appearance for each index in all the 16 combinations is indicated.*

Four indexes have been used in all the 16 best cases: pNN50, SampEn, AF evidence and nShEn, constituting an essential set of indexes for a good classification performance. Instead, the *peak density* (PD) and the TPW are never used, while the ShapeSim index appears only in one case: thus these indexes don't exhibit any additional information for the algorithm or even confuse the classification procedure.

For each combination, we analyzed the confusion matrix obtained at the end of the *leave one out* method. The columns of the matrix indicate the true health status of every subject, while the rows indicate the category in which the patient is classified by the SVM; therefore, the diagonal elements represent the correct classifications. For the 16 best combinations, two typologies of confusion matrix were obtained multiple times, displayed in Table 6.3 and Table 6.4.

	NSR	Other	AF
NSR	31	1	0
Other	0	7	1
AF	0	1	29

Table 6.3: ***Confusion matrix A.*** *Confusion matrix obtained in 10 of the 16 best combinations of indexes. NSR=normal sinus rhythm, AF=atrial fibrillation and "other" stands for other typologies of arrhythmia. The columns of the matrix indicate the true health status of every subject, while the rows indicate the category in which the patient is classified by the SVM.*

	NSR	Other	AF
NSR	30	1	0
Other	1	8	1
AF	0	0	29

Table 6.4: ***Confusion matrix B.*** *Confusion matrix obtained in 6 of the 16 best combinations od indexes. NSR=normal sinus rhythm, AF=atrial fibrillation and "other" stands for other typologies of arrhythmia. The columns of the matrix indicate the true health status of every subject, while the rows indicate the category in which the patient is classified by the SVM.*

In both A and B matrices the sensitivity, that is the ratio between the number of AF identified by the SVM and the total number of AF subjects, is 96.67%, while the specificity to NSR class was 100% in ten cases and 96.77% in the other combinations; specificity to "other arrhythmia" class was 77.78% in ten cases and 88.89% for the remaining six combinations.

Chapter 7

Discussion

The photopletismographic BVP signal can hold valuable information about the patient's health condition; in this thesis, it was attested that the impact of AF or other arrhythmias on blood pressure is evident, and such information content can be extracted through the use of specific algorithms. Many diagnostic indexes employed in this analysis are based on algorithms which assess the inter-beat variability, such as the nRMSSD, AF evidence or the Sample entropy, which are used for diagnostic evaluation on the ECG signal; the reason why those methods, originally conceived for ECG analysis, are equivalently applied to the BVP signal, is that the BVP signal is the result of the mechanical contraction of the heart, which in turn is due to the electrical activity recorded by a ECG system. Thus, BVP and ECG are directly related and some main features of the ECG have an equivalent in the BVP, for instance the RR sequence can be compared to the intervals sequence obtained from the BVP signal. One of the main differences in extracting inter-beat series between the ECG and BVP signal is the type of noise which influences the measure: the BVP signal can experience serious distortions due to the movement of the patient, compromising the signal to noise ratio up to rendering the acquisition useless; since the sensor employed is placed on the patient's wrist, a lot of disturbance can be expected, and the quality of the measurement can be highly influenced by the steadiness and cooperation of the subject.

In this thesis, the capability of the diagnostic indexes to estimate the wellness of the subject is shown, in both cases of univariate and multivariate analysis. In the following sections, the main results are discussed.

7.1 Univariate classification

Univariate SVM classification can, in some cases, roughly discriminate between healthy and arrhythmic subjects, however the results for single indexes alone do not achieve good classification performances.
A good indicator of the classification capability of each index is the degree of overlap among the distribution of the parameters' values among classes, which can be observed in the respective boxplots (chapter 5). Unfortunately, even the best indexes can assume similar values between different target classes, especially if patients with other arrhythmias are taken into account: in this class of patients, the values of many indexes are overlapped with both those of AF and NSR subjects, therefore it is impossible to clearly discriminate between them.

In univariate analysis, nRMMSSD, RMSSD and CV offer the best accuracy, respectively 82.85%, 81.43% and 80%. By observing the confusion matrices (Table 7.1, Table 7.2 and Table 7.3), however, it is obvious that the high level of accuracy is obtained exclusively due to to their good separation between AF and NSR values, while the "other" class is often assigned to the wrong category; the overall accuracy is still high (around 80%) because of the limited number of "other" patients.

	NSR	Other	AF
NSR	30	3	1
Other	0	1	2
AF	1	5	27

Table 7.1: ***nRMSSD confusion matrix.*** *Confusion matrix obtained for the univariate analysis based on nRMSSD. NSR=normal sinus rhythm, AF=atrial fibrillation and "other" stands for other typologies of arrhythmia. The columns of the matrix indicate the true health status of every subject, while the rows indicate the category in which the patient is classified by the SVM.*

	NSR	Other	AF
NSR	30	4	2
Other	0	1	2
AF	1	4	26

Table 7.2: ***RMSSD confusion matrix.*** *Confusion matrix obtained for the univariate analysis based on RMSSD. NSR=normal sinus rhythm, AF=atrial fibrillation and "other" stands for other typologies of arrhythmia. The columns of the matrix indicate the true health status of every subject, while the rows indicate the category in which the patient is classified by the SVM.*

	NSR	Other	AF
NSR	30	3	3
Other	0	1	2
AF	1	5	25

Table 7.3: ***CV confusion matrix.*** *Confusion matrix obtained for the univariate analysis based on CV. NSR=normal sinus rhythm, AF=atrial fibrillation and "other" stands for other typologies of arrhythmia. The columns of the matrix indicate the true health status of every subject, while the rows indicate the category in which the patient is classified by the SVM.*

Instead, by looking at the best specificity to the "other" class, the most efficient indexes are ShapeSim ad AF evidence, which recognize 6 "other" patients out of 9, followed by PD, MedianArc, nWD and SampEn. These indexes don't allow a good identification of AF patients (AF sensitivity goes from 0% to 20% for these 4 indexes), but are decent detectors for other arrhythmias only. In conclusion, no single index can reach an accurate classification for all the target classes, but together they can complete the classifier's capability; thus, multivariate classification was carried out.

7.2 Multivariate classification

In multivariate analysis, the SVM considers many variables simultaneously in the decision making process. Using more indexes together allows the SVM to combine their classification ability, obtaining potentially better results. On the other side, using more indexes than necessary can lead to an inefficient complexity that could even confuse the algorithm, worsening the accuracy. Indeed, in section 6.2 we saw that using many indexes combined

improves the accuracy (95.71% for the best combinations achieved by the wrapper method versus 82.85% obtained in the best case of univariate analysis), however using all of them is counterproductive (88.57% of accuracy using all 16 indexes).

The best accuracy of 95.71%, together with the best AF sensitivity of 96.67%, was obtained in 16 combinations, shown in Table 6.2. Four indexes appeared in all the 16 combinations: pNN50, SampEn, nShEn and AF evidence. SampEn and AF evidence are two indexes that presented a good specificity to the other arrhythmia class in univariate analysis, while nShEn is a quantitative measure of uncertainty, thus able to underline the unpredictable behavior of the intervals series during AF; indeed nShEn had a 75.71% accuracy in univariate analysis, with 90% AF sensitivity. pNN50 is a measure of variability with low values of accuracy (54.28%) and AF sensitivity (30%) in univariate analysis, still, used with other indexes, helps significantly the classification. Three combinations out of 16 used a minimum number of 6 indexes. In addition to the 4 already described, ModeArc, that is a morphology based index, was included in all these 3 combinations, together with another time variability parameter: either SD, nRMSSD or CV. This trend is present in each of the 16 combinations: aside from the 4 always present indexes, at least one parameter is morphology based and one is an index of heart variability in the time domain.

Chapter 8

Limitations and future work

The final SVM for AF detection has an optimal value of accuracy (95.71%) for the dataset acquired in this analysis. As we previously considered, the main difficulty of this classification is the discrimination of the patients suffering from other arrhythmias from the AF and NSR classes; there are many possible strategies in which we could improve the diagnostic capability of our system, in this section we will discuss some of our proposals.

The creation of specific indexes for the detection of other arrhythmias should be considered: every one of such indexes should be used for the detection of a specific heart arrhythmia, and a good starting point for the creation of this detectors could be the Lorenz plot of the interval deltas, which is employed in the AF evidence index: the Lorenz plot of the deltas of arrhythmic patients shows generally distinct distributions (as depicted in Figure 3.6), and a dedicated algorithm could identify those distributions, associating each case to a specific arrhythmia.

Concerning the impact of the low number of cases in the other arrhythmias class on the global results, it is worth noting that it may lead to a bias in the overall accuracy: out of all the 70 subjects composing our dataset, only 9 of them are affected by other arrhythmias; in fact, if the SVM maximizes the discrimination between AF and NSR, but completely fails to recognize the other arrhythmia category, an overall good accuracy of $\frac{70-9}{70} = 87\%$ is still obtained; therefore, a dataset in which subjects are equally distributed between the three categories could bring results that equally weight the importance of each target class. In addition to that, a comparable number of subjects between target classes could prevent the training procedure of the SVM from being biased towards the most frequent AF and NSR categories.

Furthermore, even though the best SVM combinations actually manage to correctly classify between 78% and 89% of the other arrhythmias (as

shown in Table 6.3 and Table 6.4), this results are possibly achieved mainly thanks to the SampEn index, which assumes much lower values for this class in comparison with the other two (as depicted in Figure 5.14); however, due to our limited number of acquisitions for this category, this efficient discrimination could be occasional, either because those few values are all influenced from external causes or because the arrhythmias we recorded are all quite similar, with a comparable effect on the SampEn. Again, only a more extended dataset could help us understand the true classification capability of the SVM for this class.

A current limitation of our dataset is that age is not uniform among target classes. In this study, the mean age of healthy patients (33.83 years) is inferior than the mean age of patients suffering from other arrhythmias (67.33 years) and even more inferior than the mean age of AF patients (76.25 years). Also, the subjects' gender is unequally distributed among classes: all subjects in the other arhythmias class are male.

Another possible enhancement is in the method used to assess the classification performance of the SVM: in our work, we evaluate the SVM accuracy through a *leave one out* approach, which was employed because of the limited number of recorded signals, especially for the number of patients suffering from other arrhythmias; however, it would be better to instruct the classifier on a definite training set of patients, and then to assess the classification accuracy with a different test set.

A different aspect which could benefit from some improvement is a regulation in the noise affecting our signal: our signals were often disturbed by movement noise, which in some cases obliged us to discard even more than 20% of the whole acquisition; for a better quality of the signal, it could be useful to implement different measurement protocols, for example by acquiring data while the subject is asleep and immobile, and also to require a new acquisition if the current one is too disturbed.

Finally, as for a possible application of our work, it could be practical to employ the final decision-making software as part of an application embedded in a wristband for physiological signals monitoring; by providing such device with the diagnostic capability of the software, it would be possible to identify AF occurrences in paroxysmal subjects. The implementation of this software would also allow a preliminary screening on the asymptomatic population, without the need to employ medical personnel on a vast scale; in addition to that, a real-time version of the diagnostic software would be able to alert the user, for instance by triggering an alarm, whenever the manifestation of AF is detected, so that the subject could seek medical treatment before his/her conditions worsen.

Bibliography

[1] O. Abdallah and A. Bolz, *Adaptive filtering applications*, in Adaptive Filtering by Non-Invasive Vital Signals Monitoring and Diseases Diagnosis, L. Garcia, ed., InTech, 2011.

[2] A. ahangir, V. Lee, P. A. Friedman, J. M. Trusty, D. O. Hodge, S. L. Kopecky, D. L. Packer, S. C. Hammill, W.-K. Shen, and B. J. Gersh, *Long-term progression and outcomes with aging in patients with lone atrial fibrillation: A 30-year follow-up study*, Circulation, 115 (2007), pp. 3050–3056.

[3] R. Alcaraz and J. J. Rieta, *A review on sample entropy applications for the non-invasive analysis of atrial fibrillation electrocardiograms*, Biomedical Signal Processing and Control, (2010).

[4] R. Alcaraza and J. J. Rietab, *Nonlinear synchronization assessment between atrial and ventricular activations series from the surface ECG in atrial fibrillation*, Biomedical Signal Processing and Control, (2013).

[5] M. A. Allessie, W. J. E. P. Lammers, F. I. M. Bonke, and J. Hollen, *Experimental evaluation of Moe's multiple wavelet hypothesis of atrial fibrillation*, In Cardiac Electrophysiology and Arrhythmias, (1985), pp. 265–276.

[6] E. Anter, M. Jessup, and D. J. Callans, *Atrial fibrillation and heart failure: Treatment considerations for a dual epidemic*, Circulation, 119 (2009), pp. 2516–2525.

[7] V. Barbaro, P. Bartolini, G. Calcagnini, and F. Censi, *Extraction of physiological and clinical information from intra-atrial electrograms during atrial fibrillation: review of methods*, Ann. Ist. Super. Sanità, 37 (2001), pp. 319–324.

[8] V. Barbaro, P. Bartolini, G. Calcagnini, S. Morelli, A. Michelucci, and G. Gensini, *Automated classification of human atrial fibrillation from intraatrial electrograms*, Pacing Clin Electrophysiol, 23 (2000), pp. 192–202.

[9] E. J. Benjamin, P. A. Wolf, R. B. D'Agostino, H. Silbershatz, W. B. Kannel, and D. Levy, *Impact of atrial fibrillation on the risk of death*, Clinical Investigation and Reports, (1998).

[10] C.-C. Chang and C.-J. Lin, *Libsvm: A library for Support Vector Machines*, ACM Transactions on Intelligent Systems and Technology, 2 (2011), pp. 27:1–27:27.

[11] S. S. Chugh, R. Havmoeller, K. Narayana, D. Singh, M. Rienstra, E. J. Benjamin, R. F. Gillum, Y.-H. Kim, J. H. McAnulty, Z.-J. Zheng, M. H. Forouzanfar, M. Naghavi, G. A. Mensah, M. Ezzati, and C. J. Murray, *Worldwide epidemiology of atrial fibrillation: A global burden of disease 2010 study*, Circulation, 129 (2014), pp. 837–847.

[12] R. Colloca, *Implementation and testing of atrial fibrillation detectors for a mobile phone application*, Master's thesis, Politecnico di Milano, 2012.

[13] M. Elgendi, *On the analysis of fingertip photoplethysmogram signals*, Current Cardiology Reviews, 8 (2012), pp. 14–25.

[14] L. Faes, G. Nollo, R. Antolini, F. Gaita, and F. Ravelli, *A method for quantifying atrial fibrillation organization based on wave-morphology similarity*, IEEE Transactions on Biomedical Engineering, 49 (2002), pp. 1504–1513.

[15] V. Gokana, C. Phua, and G. Lissorgues, *Automatic detection of atrial fibrillation using RR interval from ECG signals*, in The 15th International Conference on Biomedical Engineering, J. Goh, ed., vol. 43 of IFMBE Proceedings, Springer International Publishing, 2014, pp. 215–218.

[16] M. Haïssaguerre, P. Jaïs, D. C. Shah, A. Takahashi, M. Hocini, G. Quiniou, S. Garrigue, A. Le Mouroux, P. Le Métayer, and J. Clémenty, *Spontaneous initiation of atrial fibrillation by ectopic beats originating in the pulmonary veins*, New England Journal of Medicine, 339 (1998), pp. 659–666.

[17] S. Hargittai, *Is it possible to detect atrial fibrillation by simply using RR intervals?*, Computing in Cardiology, (2014).

[18] J. Jalifea, O. Berenfelda, and M. Mansourb, *Mother rotors and fibrillatory conduction: a mechanism of atrial fibrillation*, Cardiovascular Research, 54 (2002), pp. 204–216.

[19] K. T. Konings, C. J. Kirchhof, J. R. Smeets, H. J. Wellens, O. C. Penn, and M. A. Allessie, *High-density mapping of electrically induced atrial fibrillation in humans*, Circulation, 89 (1995), pp. 1665–80.

[20] J. Lee, B. A. Reyes, D. D. McManus, O. Mathias, and K. H. Chon, *Atrial fibrillation detection using an iPhone 4S*, IEEE Transactions on Biomedical Engineering, 60 (2013).

[21] S. Lévy, M. Maarek, P. Coumel, L. Guize, J. Lekieffre, J.-L. Medvedowsky, and A. Sebaoun, *Characterization of different subsets of atrial fibrillation in general practice in France: The ALFA study*, Circulation, 99 (1999).

[22] L. Mainardi, L. Sörnmo, and S. Cerutti, *Understanding Atrial Fibrillation: The Signal Processing Contribution*, Morgan & Claypool, 2008.

[23] V. Markides and R. J. Schilling, *Atrial fibrillation: classification, pathophysiology, mechanisms and drug treatment*, Heart, 89 (2003).

[24] M. Masè, L. Faes, R. Antolini, M. Scaglione, and F. Ravelli, *Quantification of synchronization during atrial fibrillation by Shannon entropy: validation in patients and computer model of atrial arrhythmias*, Physiological Measurement, 26 (2005), p. 911.

[25] G. Mines, *On dynamic equilibrium in the heart*, The Journal of Physiology, 46 (1913), pp. 349–383.

[26] A. Mishra, *Multi Class Support Vector Machine*. Matlab Central-File Exchange, October 2011.

[27] G. Moe and J. Abildskov, *Atrial fibrillation as a self-sustaining arrhythmia independent of focal discharge*, American Heart Journal, (1959).

[28] T. M. Munger, L.-Q. Wu, and W. K. Shen, *Atrial fibrillation*, Journal of Biomedical Research, 28 (2014), pp. 1–17.

[29] J. S. Richman and J. R. Moorman, *Physiological time-series analysis using approximate entropy and sample entropy*, American Journal of Physiology - Heart and Circulatory Physiology, 278 (2000), pp. H2039–H2049.

[30] S. Sarkar, D. Ritscher, and R. Mehra, *A detector for a chronic implantable atrial tachyarrhythmia monitor*, IEEE Transactions on Biomedical Engineering, 55 (2008), pp. 1219–1224.

[31] C. E. Shannon, *A mathematical theory of communication*, The Bell System Technical Journal, 27 (1948), pp. 379–423, 623–656.

[32] E. Z. Soliman, M. M. Safford, P. Muntner, Y. Khodneva, F. Z. Dawood, N. A. Zakai, E. L. Thacker, S. Judd, V. J. Howard, G. Howard, D. M. Herrington, and M. Cushman, *Atrial fibrillation and the risk of myocardial infarction*, JAMA Internal Medicine, 174 (2014), pp. 107–114.

[33] T. Tamura, Y. Maeda, M. Sekine, and M. Yoshida, *Wearable photoplethysmographic sensors—past and present*, Electronics, 3 (2014), pp. 282–302.

[34] V. Tuzcu, S. Nas, T. Börklü, and A. Ugur, *Decrease in the heart rate complexity prior to the onset of atrial fibrillation*, Europace, 8 (2006), pp. 398–402.

[35] C. R. Vasamreddy, D. Dalal, J. Dong, A. Cheng, D. Spragg, S. Z. Lamiy, G. Meininger, C. A. Henrikson, J. E. Marine, R. Berger, and H. Calkins, *Symptomatic and asymptomatic atrial fibrillation in patients undergoing radiofrequency catheter ablation*, Journal of Cardiovascular Electrophysiology, 17 (2006), pp. 134–139.

[36] C. Vercellis, *Business intelligence*, McGraw-Hill, 2006.

[37] J. L. Wells, R. B. Karp, N. T. Kouchoukos, W. A. MacLean, T. N. James, and A. L. Waldo, *Characterization of atrial fibrillation in man: Studies following open heart surgery*, Pacing and Clinical Electrophysiology, 1 (1978), pp. 426–438.

[38] M. C. Wijffels, C. J. Kirchhof, R. Dorland, and M. A. Allessie, *Atrial fibrillation begets atrial fibrillation: A study in awake chronically instrumented goats*, Circulation, 92 (1995), pp. 1954–1968.

[39] P. A. Wolf, R. D. Abbott, and W. B. Kannel, *Atrial fibrillation as an independent risk factor for stroke: the Framingham Study*, Stroke, 22 (1991).

[40] www.empatica.com, *Empatica website.*

[41] www.healthline.com, *Atrial fibrillation by the numbers: Facts, statistics, and you.*

[42] A. Yamada, J. Hayano, S. Sakata, A. Okada, S. Mukai, N. Ohte, and G. Kimura, *Reduced ventricular response irregularity is associated with increased mortality in patients with chronic atrial fibrillation*, Circulation, 102 (2000), pp. 300–306.

[43] P. D. Ziegler, J. L. Koehler, and R. Mehra, *Comparison of continuous versus intermittent monitoring of atrial arrhythmias*, Heart Rhythm, 3 (2006), pp. 1445–1452.

[44] M. Zoni-Berisso, F. Lercari, and T. C. . S. Domenicucci, *Epidemiology of atrial fibrillation: European perspective*, Clinical Epidemiology, (2014).